Performance Analysis of EGC and MRC Receivers over Fading Channels with Phase Estimation Error and Co-channel Interference

A

Thesis Submitted

in Partial Fulfillment of the Requirement

for the Degree of

DOCTOR OF PHILOSOPHY

By

G. ARUNA

to the

DEPARTMENT OF ELECTRONICS AND ELECTRICAL ENGINEERING

INDIAN INSTITUTE OF TECHNOLOGY GUWAHATI

GUWAHATI - 781039, ASSAM, INDIA

December, 2012

Certificate

This is to certify that the thesis entitled "**Performance Analysis of EGC and MRC Receivers over Fading Channels With Phase Estimation Error and Co-channel Interference**", submitted by **G.ARUNA** (06610211), a research scholar in the *Department of Electronics and Electrical Engineering, Indian Institute of Technology Guwahati*, for the award of the degree of **Doctor of Philosophy**, is a record of an original research work carried out by him under my supervision and guidance. The thesis in my opinion has reached the standard needed for submission. The results embodied in this thesis have not been submitted to any other University or Institute for the award of any degree or diploma.

Dated:

Guwahati.

Pravas Ranjan Sahu
Associate Professor
Dept. of Electronics and Electrical Engineering
Indian Institute of Technology Guwahati
Guwahati - 781039, Assam, India.

Acknowledgements

First and foremost, I feel it as a great privilege in expressing my deepest and most sincere gratitude to my supervisor Dr. Pravas Ranjan Sahu, for his excellent guidance. His kindness, dedication, friendly accessibility and attention to detail have been a great inspiration to me. My heartfelt thanks to my supervisor for the unlimited support and patience shown to me. I would particularly like to thank for all his help in patiently and carefully correcting all my manuscripts.

I am also very thankful to my doctoral committee members Prof. Dr. R. Bhattacharjee, Dr. Rohit Sinha and Dr. A. Rajesh for sparing their precious time to evaluate the progress of my work. Their suggestions have been valuable. I would also like to thank other faculty members for their kind help carried out during my academic studies. I am grateful to all the members of the research and technical staff of the department without whose help I could not have completed this thesis. My special thanks to Mr. Sanjib Das, for maintaining an excellent computing facility and helping in various computing techniques useful for the research work.

Thanks go out to all my friends at ISPL Laboratory. They have always been around to provide useful suggestions, companionship and created a peaceful research environment.

My friends at IITG made my life joyful and were constant source of encouragement. Among my friends, I would like to extend my special thanks to Padam Priyal, for being so caring and encouraging me. I also specially thank Josephine for all her help and support. My work in this remote place definitely would not be possible without their love and care that helped me to enjoy my new life in this IITG.

My deepest gratitude goes to my husband and parents for their continuous love and support throughout my studies. I extend my deepest gratitude for my son for his unlimited sacrifices for what I have accomplished so far.

Finally, I believe this research experience will greatly benefit my career in the future.

G. Aruna

This work is dedicated to

My Family

Abstract

Signals transmitted through wireless medium undergo several distortion due to various atmospheric effects. As a result, received several copies of the original signal with random attenuation and phases causes the net received signal strength to fluctuate with time causing fading. Fading causes degradation in the performance of communication systems relative to the performance in additive white Gaussian (AWGN) channels. As the fading environment experienced by a mobile user keeps on changing, the channel experienced by the user can be characterized by multipath fading, shadow fading, or a mixture of the both. Some known fading models are Hoyt, Nakagami-m, Nakagami-q, Generalized Gamma (GG), Generalized-K (K_G), $\eta-\mu$ and $\kappa-\mu$ fading channels.

Effect of fading can be reduced by implementing diversity combining techniques in receivers in which received copies of the original signal, are processed together to generate a resultant signal whose rate of fluctuation becomes less compared to that of individual signal copies. Known basic diversity combining techniques are selection combining (SC), maximal ratio combining (MRC) and equal gain combining (EGC). To obtain best performance from diversity combiners it is required to accurately estimate the instantaneous amplitude and phase of each signal copy. Under ideal conditions, the performance improvement obtained through MRC is better than that of EGC which is better than that of SC, compared to systems without diversity combining. In practice, the received carrier phase is estimated using a first order phase locked loop (PLL). Due to the presence of thermal noise in the phase estimation circuit the estimated parameters may not be accurate and hence degradation in the receiver performance is obvious.

To maximize system capacity, mobile communication systems reuse frequency in cell clusters which causes co-channel interference (CCI) resulting in further degradation in receiver performance. Thus, phase estimation error and CCI are two issues of practical importance in mobile communications. Hence, an investigation on the performance of mobile communication systems using diversity combining is necessary to know the amount of performance the practical systems can provide in the presence of both phase estimation error and CCI.

In literature, analysis of diversity combining receivers in the presence of both phase estimation error and CCI has not received enough attention. This analysis is challenging since it involves handling of 'desired signal with phase estimation error' and CCI signals which could be received through paths having different fading distributions. The performance analysis of the system in the presence of phase estimation error, CCI and AWGN is certainly complex.

In this thesis work, the performance of EGC and MRC combining receivers is analyzed over Hoyt, Nakagami-*m*, Composite (Generalized gamma and Generalized K) and non-homogeneous fading channels ($\eta-\mu$ and $\kappa-\mu$) with phase estimation error and CCI with a focus to obtain mathematical expressions, wherever possible, for different performance measures such as average signal to noise ratio (SNR), outage probability and average bit error probability (ABEP). Numerical evaluation of analytically obtained performance measures is plotted and the effect of various system parameters on the performance is studied. Obtained results are verified with simulation results and compared with available results in literature for some special cases.

Contents

List of Figures **xiii**

List of Tables **xiv**

List of Acronyms **xv**

List of Symbols **xvii**

1 Introduction **1**

1.1 Cellular Communication System 1

1.2 Causes of Performance Degradation 2

1.2.1 Fading 2

1.2.2 Phase Estimation Error 19

1.2.3 Co-channel Interference 19

1.3 Literature survey 20

1.4 Motivation 23

1.5 Problem Formulation 24

1.6 Thesis Contribution 24

1.7 Thesis Organization 25

2 System Model and Analysis Methods **26**

2.1 System Model 26
2.2 Gaussian Assumption for Cochannel Interference 28
2.3 Performance Analysis Methods 29
2.3.1 Probability Density Function Based Method 29
2.3.2 Moment Generation Function Method 30
2.3.3 Applying Padè Approximation Method for Analysis of EGC Receiver . . . 31
2.3.4 Characteristic Function Based Method 33

3 Performance of EGC Receiver 34

3.1 ABEP Analysis for Dual-EGC 36
3.1.1 ABEP Evaluation Method 38
3.1.2 Correlated Hoyt Fading Channels 38
3.1.3 Composite and Non-homogeneous Fading Channels 46
3.1.4 Independent Nakagami-*m* Fading Channels 55
3.2 Performance of Dual-EGC in Nakagami-*m* Fading - PDF Based Approach 62
3.2.1 Probability Density Function of Output SINR 62
3.2.2 Outage Probability 63
3.2.3 Average Bit Error Probability 64
3.2.4 Numerical and Simulation Results 64
3.3 Outage of *L*-EGC over Composite Fading Channels 69
3.3.1 Output Signal-to-Interference Ratio 69
3.3.2 Outage Probability of Output SIR 70
3.3.3 Numerical and Simulation Results 71
3.4 Performance of $L-$EGC in Nakagami-*m* Fading with Phase Error and AWGN Only - PDF Based Approach 78
3.4.1 Output SNR 78
3.4.2 Probability Density Function of Output SNR, γ_{egc} 79

3.4.3 Outage Probability of Output SNR 79
3.4.4 Average Bit Error Probability of Output SNR 79
3.4.5 Numerical and Simulation Results 80
3.5 Summary 83

4 MRC Receiver in Nakagami-*m* Channels **84**
4.1 PDF of MRC Output SINR 85
4.2 Outage Probability of MRC Output SINR 86
4.3 Average Symbol Error Probability 87
4.4 Numerical and Simulation Results 88
4.5 Summary 101

5 Conclusions and Future Work **102**
5.1 Future Work 103

Appendix **104**

A Derivation of Expressions **104**
A.1 Demodulated Signal at the EGC Output 104
A.2 Output SINR of EGC Receiver 105
A.3 Joint Moments of Correlated Hoyt Fading Channels 107
A.4 Derivation of Joint Moments of GG RVs 108
A.5 Derivation of Joint Moments of Generalized-*K* RVs 109
A.6 Derivation of EGC Output SINR in Asynchronous Case 110
A.7 Derivation of $\mathrm{E}_U\{e^{-jn\omega_0\sqrt{\gamma_{th}U}}\}$ 111
A.8 Derivation of PDF of $\gamma_{egc} = \left(\sum_{l=1}^{L}\sqrt{\gamma_l}\cos(\psi_l)\right)^2$ 112
A.8.1 Derivation of Outage Probability of EGC 115
A.8.2 Derivation of Average Bit Error Probability 116

A.9 Derivation of γ_{egc} with Phase Error and CCI - PDF Based Approach 117
A.9.1 Derivation of PDF of γ_{egc} 117
A.9.2 Derivation of Outage Probability of EGC 118
A.10 Output SINR of MRC Receiver 120
A.10.1 Derivation of PDF of x in Section 4.1 121
A.10.2 Derivation of PDF of γ_{mrc} 122
A.10.3 Derivation of Outage Probability of MRC 123
A.10.4 Derivation of ASEP of MRC 124
A.11 Padé Approximation 125
A.12 Padé Approximation Coefficients in the Numerical Evaluation of Equation 2.8 for GG Fading Channels 127
A.13 Padé Approximation Coefficients in the Numerical Evaluation of Equation 2.8 for K_G Fading Channels 128
A.14 Padé Approximation Coefficients in the Numerical Evaluation of Eq. 2.8 for Nakagami-m Fading Channels 129
A.15 List of Formulas 129

Publications **138**

List of Figures

1.1 Cell geometry with seven clusters (A to G) and co-channel cells. A_d is the desired user's cell and A_i are cochannel users' cells. 2

1.2 A typical mobile communication channel 3

1.3 PDF of Rayleigh random variable. 8

1.4 PDF of Nakagami-m random variable. 8

1.5 PDF of Hoyt random variable. 9

1.6 PDF of Rician random variable. 9

1.7 PDF of Weibull random variable 10

1.8 PDF of Generalized-Gamma random variable 11

1.9 PDF of K_G random variable with $m = 1$ 12

1.10 PDF of K_G random variable with $k = 2.5$ 12

1.11 PDF of $\kappa - \mu$ random vairable for $\mu = 0.5$ 14

1.12 PDF of $\kappa - \mu$ variable for $\kappa = 1$. 14

1.13 PDF of $\eta - \mu$ random variable with $\mu = 0.6$ 15

1.14 PDF of $\eta - \mu$ random variable with $\eta = 0.5$ 15

1.15 Block diagram showing principle of operation of MRC. 17

1.16 Block diagram showing principle of operation of EGC. 18

2.1 Desired and CCI signal in cellular communication system. A_d is the desired user's cell and A_is are cochannel cells. 27

3.1 ABEP in correlated Hoyt fading channels with varying N and ρ. 41
3.2 Effect of q on ABEP in correlated Hoyt fading channels. 42
3.3 Effect of m_i on ABEP in correlated Hoyt fading channels. 42
3.4 ABEP in correlated Hoyt fading channels with varying $\bar{\gamma}_i$. 43
3.5 Comparison of ABEP of in correlated Hoyt fading channels with and without CCI. 43
3.6 ABEP in correlated Hoyt fading channels with varying ρ 44
3.7 ABEP in correlated Hoyt fading channels with $N = 6$ and $N = 7$. 44
3.8 ABEP in GG fading channels with $\sigma_\psi = 2^\circ, 8^\circ$, m_g=1, $\beta_g = 2$, varying N and ρ. . . 49
3.9 ABEP in GG fading channels with $\sigma_\psi = 2^\circ, 8^\circ$, β_g = 2 and varying m_g. 50
3.10 ABEP in GG fading channels with $\sigma_\psi = 2^\circ, 8^\circ$, m_g = 1, $\beta_g = 2$ and varying m_i. . . 51
3.11 ABEP in GG fading channels with $\sigma_\psi = 2^\circ, 8^\circ$, m_g = 1,$\beta_g = 2$ and varying $\bar{\gamma}_i$. . . . 52
3.12 ABEP in K_G fading channels with $\sigma_\psi = 2^\circ, 8^\circ$ and varying ρ, N. 52
3.13 ABEP in K_G fading channels with $\sigma_\psi = 2^\circ, 8^\circ$ and varying m_k. 53
3.14 ABEP in $\eta - \mu$ fading channels with $\sigma_\psi = 2^\circ, 8^\circ$ and varying N and μ. 53
3.15 ABEP in $\kappa - \mu$ fading channel with $\sigma_\psi = 2^\circ, 8^\circ$, $\kappa = 0$ and varying μ. 54
3.16 ABEP in independent Nakagami-m fading channels with $\sigma_\psi = 2^\circ$, 8°, $m = 1$, m_i=1 and $\bar{\gamma}_i = 1$ dB with varying N. 59
3.17 ABEP in independent Nakagami-m fading channels with $\sigma_\psi = 2^\circ$,8°, $N = 6$ and $\bar{\gamma}_i$ =1 dB with varying m and m_i. 60
3.18 ABEP in independent Nakagami-m fading channels with varying $\bar{\gamma}_i$. 60
3.19 Comparison dual-EGC in Nakagami-m fading channels for synchronous and asynchronous cases. 61
3.20 Outage probability in Nakagami-m fading channels with $\sigma_\psi = 2^\circ, 12^\circ$ and varying N. 65
3.21 Outage probability in Nakagami-m fading channels with $\sigma_\psi = 2^\circ, 12^\circ$ varying m, m_i. 66
3.22 Outage probability in Nakagami-m fading channels with $\sigma_\psi = 2^\circ, 12^\circ$ $\gamma_{th} = 1$ dB and varying N. 66

3.23 Outage probability in Nakagami-m fading channels with $\sigma_\psi = 2^\circ, 12^\circ$ and varying γ_i. 67

3.24 ABEP in Nakagami-m fading channels with $\sigma_\psi = 2^\circ, 12^\circ$ and varying N. 67

3.25 ABEP in Nakagami-m fading channels with $\sigma_\psi = 2^\circ, 12^\circ$ and varying m. 68

3.26 ABEP in Nakagami-m fading channels with $\sigma_\psi = 2^\circ, 12^\circ$ and varying γ_i. 68

3.27 Outage probability in GG fading with $\sigma_\psi = 2^\circ, 8^\circ$, $N = 1$, $m_g = 1$ and $\beta_g = 2$. . . . 73

3.28 Outage probability in GG fading with $\sigma_\psi = 2^\circ, 8^\circ$, $L = 1$, $m_g = 1$ and $\beta_g = 2$. . . . 73

3.29 Outage probability in GG fading with $\sigma_\psi = 2^\circ, 8^\circ$, $L = 2$ and $N = 1$. 74

3.30 Outage probability in GG fading with $\sigma_\psi = 2^\circ, 8^\circ$, $L = 2, 4$ and $N = 1$. 74

3.31 Outage probability in GG fading channels with $\sigma_\psi = 2^\circ, 8^\circ$, $L = 2$, $N = 1$, $m_g = 1$ and $\beta_g = 2$. 75

3.32 Outage probability in K_G fading channels with $\sigma_\psi = 2^\circ, 8^\circ$, N=1, m_k= 1 and β_k =1. 75

3.33 Outage probability in K_G fading channels with $\sigma_\psi = 2^\circ, 8^\circ$, L=2, m_k= 1 and β_k =1. 76

3.34 Outage probability in K_G fading channels with $\sigma_\psi = 2^\circ, 8^\circ$, $L = 2$ and $N = 1$. . . . 76

3.35 Outage probability in K_G fading channels with $\sigma_\psi = 2^\circ, 8^\circ$, $L = 1$ and $N = 1$. . . . 77

3.36 Outage probability in Nakagami-m fading channels with $\sigma_\psi = 2^\circ, 12^\circ$. 81

3.37 Outage probability in Nakagami-m fading channels with $\sigma_\psi = 2^\circ, 12^\circ$. 81

3.38 ABEP in Nakagami-m fading channels with $\sigma_\psi = 2^\circ, 12^\circ$. 82

4.1 Outage probability of L-MRC receiver in Nakagami-m fading channels for $N = 1$, $m = 1$, $m_i = 1$ and $\bar{\gamma} = 1dB$. 90

4.2 Outage probability of L-MRC receiver in Nakagami-m fading channels for $N = 1$, $m = 1$, $m_i = 1$ and $\bar{\gamma} = 1dB$. 91

4.3 Outage probability of L-MRC receiver in Nakagami-m fading channels with L = 4, m = 1, $m_i = 1$, $\bar{\gamma} = 1dB$ and $\bar{\gamma}_i = 1dB$. 92

4.4 Outage probability of L-MRC receiver in Nakagami-m fading channels for L = 4, N=1, $\bar{\gamma} = 1$ and $\bar{\gamma}_i = 1dB$. 93

4.5 Outage probability of L-MRC receiver in Nakagami-m fading channels with L = 4, N=1, m = 1, $m_i = 1$ and $\bar{\gamma} = 1dB$. 94

4.6 ASEP of L-MRC receiver in Nakagami-m fading channels with N=1, m = 1, $m_i = 1$ and $\bar{\gamma}_i = 1dB$. 95

4.7 Outage probability of L-MRC receiver in Nakagami-m fading channels with N=1, m = 1, $m_i = 1$ and $\bar{\gamma}_i = 1dB$. 96

4.8 ASEP of L-MRC receiver in Nakagami-m fading channels with N=1, m = 1, $m_i = 1$ and $\bar{\gamma}_i = 1dB$. 97

4.9 ASEP of L-MRC receiver in Nakagami-m fading channels with L=4, m = 1, $m_i = 1$ and $\bar{\gamma}_i = 1dB$. 98

4.10 ASEP of L-MRC receiver in Nakagami-m fading channels with N=1, L=4, $\bar{\gamma}_i = 1dB$. 98

4.11 ASEP of L-MRC receiver in Nakagami-m fading channels with N=1, L=8, $m = 1$ and $m_i = 1$. 99

4.12 ASEP of L-MRC receiver in Nakagami-m fading channels with N=1, m = 1, $m_i = 1$, $\bar{\gamma}_i = 1$ and L=8. 100

List of Tables

3.1 ABEP in correlated Hoyt fading channels with varying N, σ_ψ at $\bar{\gamma} = 5$ dB. 41

3.2 ABEP in correlated Hoyt fading channels with varying N, ρ, σ_ψ 45

3.3 ABEP in GG fading channels with varying N, ρ and σ_ψ. 51

3.4 ABEP in K_G fading channels with varying N, ρ and σ_ψ 51

3.5 ABEP in Nakagami-m fading channels varying N, σ_ψ for $\bar{\gamma} = 10$ dB. 58

List of Acronyms

ABER	Average bit error rate
ASER	Average symbol error rate
AWGN	Additive white Gaussian noise
ASEP	Average symbol error probability
ASINR	Average **SINR**
ABEP	Average bit error probability
ASEP	Average symbol error probability
ASNR	Average **SNR**
BER	Bit error rate
BPSK	Binary phase-shift-keying
CF	Characteristic function
CDF	Cumulative distribution function
CCI	Co-channel interference
dB	Decibel
EGC	Equal gain combiner
GG	Generalized Gamma
LOS	Line of sight
***L*–MRC**	*L*- branch **MRC**
***L*–EGC**	*L*- branch **EGC**

MRC	Maximal ratio combiner
MGF	Moment generating function
PDF	Probability density function
PSK	Phase-shift-keying
RMS	Root mean square
RV	Random variable
SEP	Symbol error probability
SC	Selection combiner
SNR	Signal to noise ratio
SINR	Signal to interference plus noise ratio

List of Symbols

$F_A(\cdot;\cdot;\cdot;\cdot)$	Appell hypergeometric function
$\bar{(\cdot)}$	Statistical average
$\binom{a}{n}$	Binomial coefficient
$B(\cdot,\cdot)$	Beta function
${}_1F_1(\cdot,\cdot;\cdot)$	Confluent hypergeometric function
$E[\cdot]$	Expectation operator
$exp(\cdot)$	Exponential operator
$erf(\cdot)$	Gaussian error function
$erfc(\cdot)$	Gaussian complementary error function
$\forall$	For all
${}_2F_1(\cdot,\cdot;\cdot;\cdot)$	Hypergeometric function
$\Gamma(\cdot)$	Gamma function
$G(\cdot)$	Meijer's G-function
$\nu(a,x) = \int_0^x t^{a-1}e^{-t}dt$	Lower incomplete gamma function
$\Gamma(a,x) = \int_x^\infty t^{a-1}e^{-t}dt$	Upper incomplete gamma function
${}_rF_s\left[\begin{matrix} a_1 & a_2 & \dots & a_r \\ b_1 & b_2 & \dots & b_s \end{matrix} z\right] = \sum_{n=0}^{\infty} \frac{(a_1)_n(a_2)_n\dots(a_r)_n}{(b_1)_n(b_2)_n\dots(b_s)_n} z^n$	Generalized hypergeometric function

γ_{sc}	Output SNR of SC receiver
γ_{egc}	Output SNR of EGC receiver
γ_{mrc}	Output SNR of MRC receiver
$I_0(\cdot)$	Modified Bessel function of first kind and order zero
$I_v(\cdot)$	Modified Bessel function of first kind and order v
$\in$	Set membership
$\Im\{\cdot\}$	Operator of imaginary part
$K_v(\cdot)$	Modified Bessel function of second kind and order v
$\ln(\cdot)$	Natural logarithm
$\log_{10}(\cdot)$	Logarithm with base 10
$\lvert\cdot\rvert$	Absolute value or modulus
$\mathrm{Max}(\cdot,\cdot,\ldots,\cdot)$	Maximum
$Q_M(\cdot,\cdot)$	Marcum Q-function
$\prod_{i=1}^{n}$	Product of n terms
$(x)_n$	Pochhammer's symbol
$Q(\cdot)$	Gaussian $Q-$ function
$\Re\{\cdot\}$	Real-part operator
σ_ψ	Root mean square phase error
$\sum_{i=0}^{n}$	Summation of n terms
t	Time
τ	Time delay
$var[\cdot]$	Variance operator

Chapter 1

Introduction

1.1 Cellular Communication System

In mobile cellular communications, the entire geographic area is divided into small areas of identical geometry called cells [1]. Each cell is assigned a set of channels (frequencies) for communication from the total number of channels available within the allocated band of frequencies. The total number of cells (M) to which the total number of available channels are assigned is called a *Cluster* of M cells. Use of cluster provides the benefit to increase spectral efficiency and traffic carrying capacity in cellular communication system. To maximize the capacity of the system, the clusters are repeated at a minimum distance from a reference cluster [1, 2]. This makes it possible to reuse the same channels within the total area of operation resulting in enhancement of spectral efficiency and the cluster size decides how closely the frequencies are reused. The cells operating with the same frequencies are called *Co-channel cells*. Figure 1.1 shows the cell geometry in which seven cells (A-B-C-D-E-F-G) form a cluster which are repeated. The desired user's cell is denoted as A_d and $A_i s$ are the co-channel cells. For the purpose of analysis the geometry of cells is chosen to be a hexagon with M number of cells within one cluster which satisfies the relation $M = i^2 + ij + j^2$, where i and j are non negative integers.

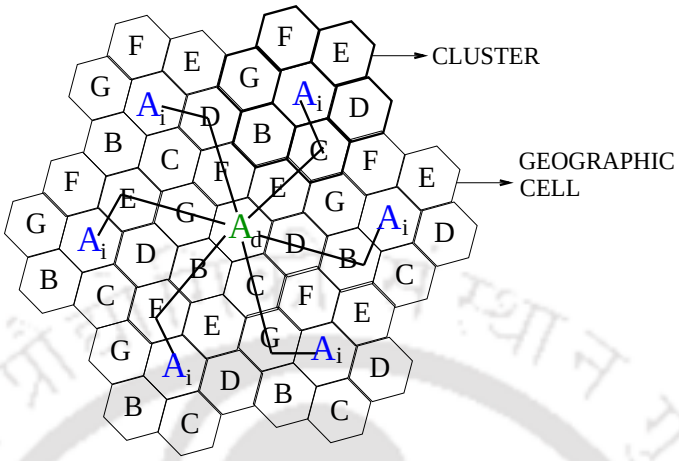

Figure 1.1: Cell geometry with seven clusters (A to G) and co-channel cells. A_d is the desired user's cell and A_i are cochannel users' cells.

1.2 Causes of Performance Degradation

There are a number of factors which may corrupt the signals propagating in the mobile communication channels. This results in the degradation of performance of mobile communication systems. Some factors which are significant among various factors responsible for performance degradation are discussed below.

1.2.1 Fading

Communication signals transmitted through wireless medium come across several natural and man-made obstructions. All physical phenomena that are observed in a typical mobile communication channel are shown in Fig. 1.2. Due to the presence of different objects in the path between transmitter and receiver, the transmitted signal takes multiple paths to reach the receiver. Hence many copies of the original signal gets generated, called *multipath waves*. These multipath waves arriving at the receiver combine vectorially to form the resultant signal which varies widely in amplitude over a short duration of time. The rapid fluctuations of the amplitude of the received radio signal over a short period of time or travel distance is called *fading*. Performance of a receiver in the presence of fading becomes poor when compared to the performance in an additive white Gaussian noise

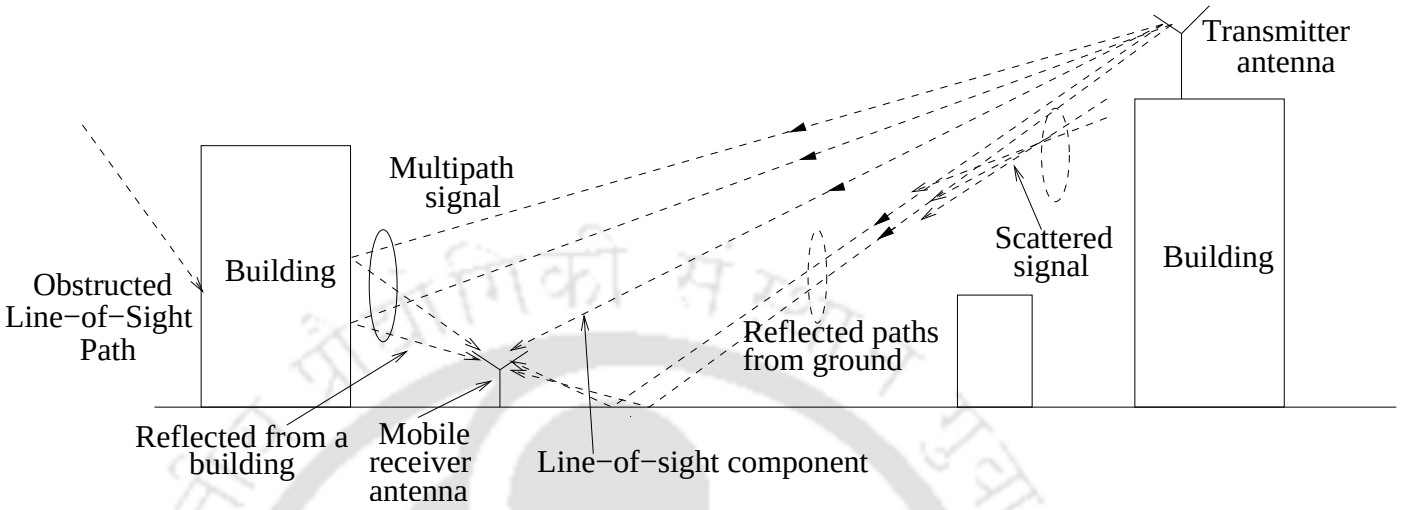

Figure 1.2: A typical mobile communication channel

(AWGN) channel.

Depending on the characteristics of the channel, fading can be of different types such as small-scale fading and large scale fading. Depending on the signal parameters such as bandwidth, symbol period, and the channel parameters such as root mean square (RMS) delay spread, and doppler shift, different signals undergo different kinds of fading.

Small Scale Fading

In urban areas, there will be no line of sight path between transmitter and receiver. Due to the presence of high rise man-made structures severe diffraction loss of signal occurs resulting in many destructed copies of the original signal besides multiple reflections from various objects. Due to the constructive and destructive effects of multipath waves summing at various points in space, a mobile receiver can pass through several fades in a small period of time. Hence, even over a short duration of time or short distance, the fluctuation of the amplitude of the received signal is severe. This is called small scale fading.

Large Scale Fading

The variation of the received mean signal strength for an arbitrary transmitter receiver separation distances is called large scale fading. Large scale fading estimates the entire radio coverage area of a transmitter. As the mobile moves away from the transmitter over much larger distances, the mean signal strength will gradually decrease.

Large scale fading is more relevant to the issues such as cell-site planning. Small scale multipath fading is more relevant to the design of reliable and efficient communication systems.

Multipath Channel Parameters

Coherence Bandwidth

Coherence bandwidth (B_c) is the range of frequencies over which two frequency components have a strong potential for amplitude correlation. In other words, it is defined as the range of frequencies over which the channel is considered flat, meaning that the range of frequencies over which the channel passes all the frequency components with approximately equal gain and linear phase. Coherence bandwidth describes the frequency invariance of the channel [1]. The coherence bandwidth of a channel can be determined from the formula.

$$B_c = \begin{cases} \frac{1}{50\sigma_\tau}, & \text{if frequency correlation function is above 0.9} \\ \frac{1}{5\sigma_\tau}, & \text{if frequency correlation function is above 0.5} \end{cases}$$

, where σ_τ is the RMS delay spread.

Doppler Spread

The measure of frequency shift in the received signal w.r.t the transmitted signal is called doppler spread. The range of frequency components of the received signal is called doppler spectrum. If a pure sinusoidal tone of frequency f_c is transmitted the received signal spectrum will have the components in the range of $f_c - f_d$ to $f_c + f_d$ where f_d is the doppler shift [1].

Coherence Time

Coherence time (T_c) is the statistical measure the time duration over which the channel impulse response is invariant. In other words, coherence time is the time duration over which two received signals have a strong potential for amplitude correlation. The coherence time is related to maximum doppler shift f_m by $T_c = \frac{9}{16\pi f_m}$ [1].

Types of Small Scale Fading

Depending on the relation between the signal parameters (bandwidth B_s and symbol period T_s) and the channel parameters (RMS delay spread σ_τ and doppler spread B_d), fading can be classified into different types as mentioned below:

Based on Multipath Time Delay Spread:

Based on the multipath Time delay spread, fading can be of two types viz. flat fading and frequency selective fading.

Flat Fading

When the bandwidth of the channel is greater than the bandwidth of the signal, the received signal will undergo flat fading. Since the channel bandwidth is greater, it can pass all the signal components without any distortion. When the radio channel has a constant gain and linear phase response over a bandwidth which is greater than the bandwidth of the signal, the signal undergoes flat fading. Mathematically, this fading condition can be expressed as $B_s << B_c$ and $T_s >> \sigma_\tau$ [1].

Frequency Selective Fading

If the channel has a constant gain and linear phase response over a bandwidth less than the signal bandwidth then the signal will undergo frequency selective fading. Different frequency components of the signal will undergo different amount of fading. Mathematically, this fading condition can be expressed as $B_s >> B_c$ and $T_s << \sigma_\tau$ [1].

Based on Doppler Spread:

Based on the doppler spread the fading can be of two types: Fast fading and Slow fading.

Fast Fading

If the channel impulse response changes rapidly within one symbol duration of the signal then the channel fading is known as fast fading. It means, the coherence time of the channel is smaller than the symbol duration. In practice, fast fading occurs only for very low data rates. A signal undergoes fast fading for the condition $T_s >> T_c$ and $B_s << B_d$ [1].

Slow Fading

If the channel impulse response changes at a rate much slower than the transmitted signal then the signal will undergo slow fading. In frequency domain, if the doppler spread of the channel is much smaller than the bandwidth of the baseband signal then the signal undergoes slow fading. Mathematically, it can be shown as $T_s << T_c$ and $B_s >> B_d$ [1].

Fading Channel Statistics

Rayleigh Fading

Ralyleigh distribution is used to model the multipath fading without line of sight (LOS) path. This distribution typically agrees with experimental data for mobile communication systems where no LOS path exists between the transmitter and receiver antennas. It also applies to the propagation of signal being reflected and refracted through the troposphere and ionosphere and to ship-to-ship radio links. The probability density function (PDF) of a Rayleigh distributed random variable (RV) can be given as [3]

$$f_\alpha(\alpha) = \frac{2\alpha}{\Omega} exp\left(-\frac{\alpha^2}{2\Omega}\right), \qquad \alpha \geq 0, \tag{1.1}$$

where $\Omega = E[\alpha^2]$ is the average power of the received signal envelope α. Rayleigh distribution can be also modeled as the magnitude of complex Gaussian RV $X + jY$, where X and Y are two

independent and identically distributed (i.i.d) Gaussian RVs with zero mean and equal variance. Figure 1.3 shows the Rayleigh PDF for different values of Ω.

Nakagami-m Fading

Nakagami derived the m-distribution as an approximate distribution for the square root of sum of "square of n independent Gaussian random variables," where $m = n/2$. The distribution, for $m = 1$ corresponds to Rayleigh fading while $m > 1$ corresponds to a fading having severity less compared to Rayleigh and $m < 1$ corresponds to a fading with severity more compared to Rayleigh [4]. The Nakagami-m distribution is a generalized distribution of the multipath propagation. It gives best fit to land-mobile, indoor-mobile multipath propagation and scintillation of ionospheric radio links [3]. The PDF of Nakagami-m distributed RV is given as [3]

$$f_{\alpha}(\alpha) = 2\left(\frac{m}{\Omega}\right)^{m} \frac{\alpha^{2m-1}}{\Gamma(m)} exp\left(-\frac{m\alpha^2}{\Omega}\right), \alpha \geq 0, \tag{1.2}$$

where $\Omega = E[\alpha^2]$, $m = \frac{\Omega^2}{E[\alpha^2 - \Omega^2]} \geq \frac{1}{2}$ is the Nakagami-m fading parameter and $\Gamma(\cdot)$ is the Gamma function. For $0.5 < m \leq 1$ fading severity is high which occurs due to the scintillation in the ionospheric radio links, $m = 1$ denotes multipath fading with no LOS component and $m > 1$ denotes fading with less severity. As a limiting case when $m \to \infty$, the Nakagami-m fading channel converges to a nonfading AWGN channel. Figure 1.4 shows the Nakagami-m PDF for different values of m.

Hoyt Fading

The PDF of the Hoyt distribution is given by [3]

$$f_{\alpha}(\alpha) = \frac{(1+q^2)\alpha}{q\Omega} \exp\left(\frac{(1+q^2)^2\alpha^2}{4q^2\Omega}\right) I_0\left(\frac{(1-q^4)\alpha^2}{4q^2\Omega}\right), \alpha \geq 0, \tag{1.3}$$

where $q \in (0,1)$ is the fading parameter. For $q = 0$ the distribution becomes one sided Gaussian and for $q = 1$, it corresponds to Rayleigh distribution. Figure 1.5 shows the Hoyt PDF for different

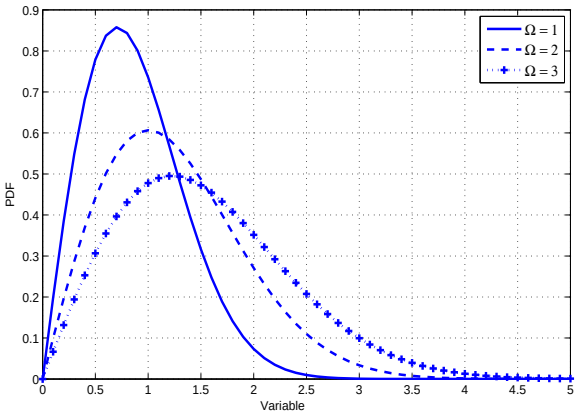

Figure 1.3: PDF of Rayleigh random variable.

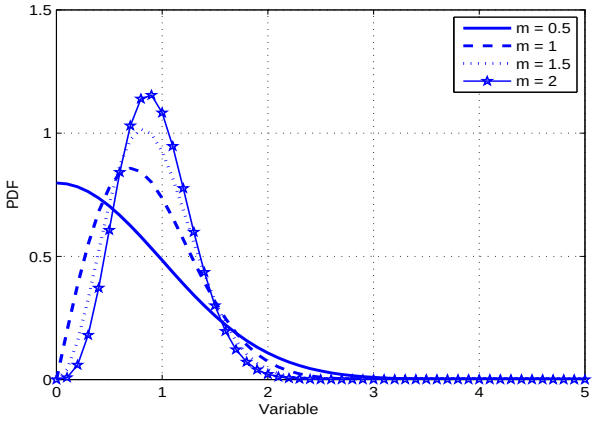

Figure 1.4: PDF of Nakagami-*m* random variable.

values of q.

Nakagami-n (Rician) Fading

The Nakagami-n distribution is also known as the Rice distribution. It is often used to model multipath propagation consisting of one strong LOS component and many random weak components. The PDF of Rician distribution is given as [3, (2.15)]

$$f_\alpha(\alpha) = \frac{2(1+n^2)e^{-n^2}\alpha}{\Omega} \exp\left(-\frac{(1+n^2)\alpha^2}{\Omega}\right) I_0\left(2n\alpha\sqrt{\frac{1+n^2}{\Omega}}\right), \alpha \geq 0, \tag{1.4}$$

where $n \in (0,\infty)$ is the Nakagami-n fading parameter. This parameter is related to the Rician K factor by $K = n^2$ which corresponds to the ratio of the power of the LOS component to the average power of the scattered component. The Nakagami-n distribution spans the range from Rayleigh fading $(n = 0)$ to no fading $(n = \infty)$. This type of fading is typically observed in the first resolvable LOS paths of micro-cellular urban and suburban land to mobile, picocellular indoor and factory environments. It also applies to the dominant LOS path of satellite and ship-to-ship radio links. Ricean distribution can be modeled as $\alpha = |X + jY|$, where X and Y are two independent identical Gaussian RVs with nonzero mean and variance Ω. Figure 1.6 shows the Rician PDF for different values of n.

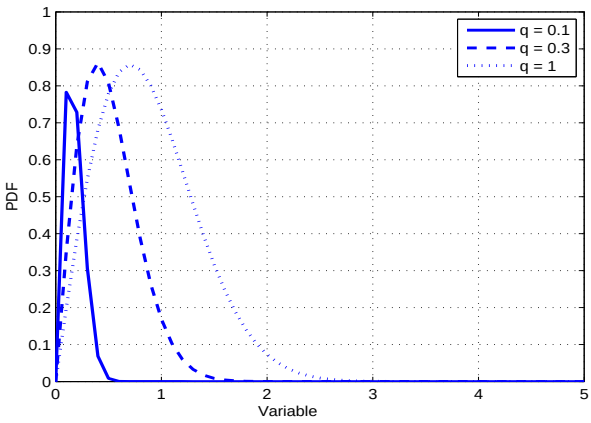

Figure 1.5: PDF of Hoyt random variable.

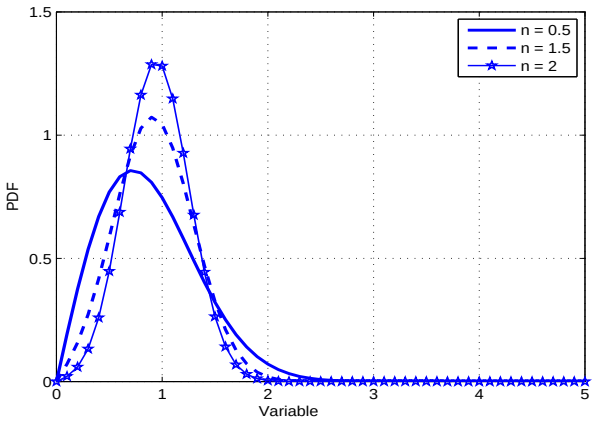

Figure 1.6: PDF of Rician random variable.

Weibull Fading

The Weibull fading model considers a multipath wave propagating in a non-homogeneous environment. The PDF of Weibull fading is given by [3, (2.27)]

$$f_{\alpha}(\alpha) = \beta \left(\frac{\Gamma\left(1+\frac{2}{\beta}\right)}{\Omega} \right)^{\beta/2} \alpha^{\beta-1} exp\left[-\left(\frac{\alpha^2}{\Omega} \Gamma\left(1+\frac{2}{\beta}\right) \right)^{\beta/2} \right], \alpha \geq 0, \tag{1.5}$$

where $\beta \in (0,\infty)$ is the Weibull fading parameter and $\Omega = E[\alpha^2]$. Weibull PDF simplifies to Rayleigh PDF for $\beta = 2$ and to an exponential distribution for $\beta = 1$ [3]. Weibull distribution is used to characterize the mobile radio systems operating in the frequency range of 800/900 MHz in indoor and outdoor environments. Weibull distribution can be modeled as $\alpha = (X^2 + Y^2)^{1/\beta}$, where X and Y are independent zero mean Gaussian RVs with variance Ω. Figure 1.7 shows the Weibull PDF for different values of β.

Composite Fading

The channel characteristics between transmitter and receiver changes constantly as the mobile user travels in different environments where the surrounding objects are not stationary. As a result, the channel can be characterized by multipath fading, shadow fading, or a mixture of both the cases [5].

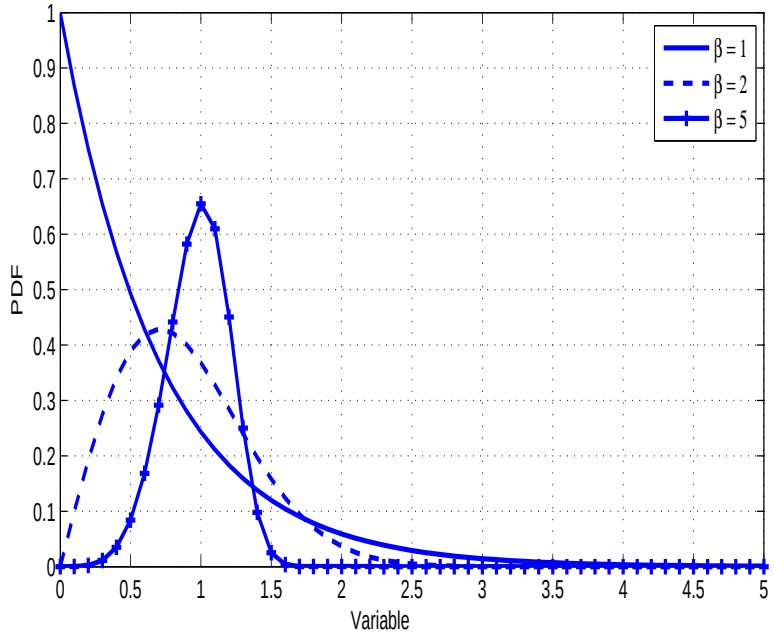

Figure 1.7: PDF of Weibull random variable

In some environments, such as congested downtown areas and land-mobile satellite systems with foliage and urban shadowing, the analysis of the channel model must include both multipath and shadow fading. Hence, it is widely accepted that radio propagation is characterized by both long-term fading and multipath fading. Several experimental measurement campaigns have shown that multipath fading and shadowing occur simultaneously [6]. Thus, in order to study such fading environments, a composite fading model must be considered. A relatively simple and versatile envelope distribution that generalizes many of the commonly used models for multipath and shadow fading is the generalized gamma distribution (GG).

Generalized-Gamma Fading

The GG distribution can be used to model the channel undergoing both severe and weak fadings. It is a versatile envelope distribution and it includes the Rayleigh, Nakagami and Weibull distributions as special cases and the lognormal distribution as a limiting case. The PDF of the generalized Gamma

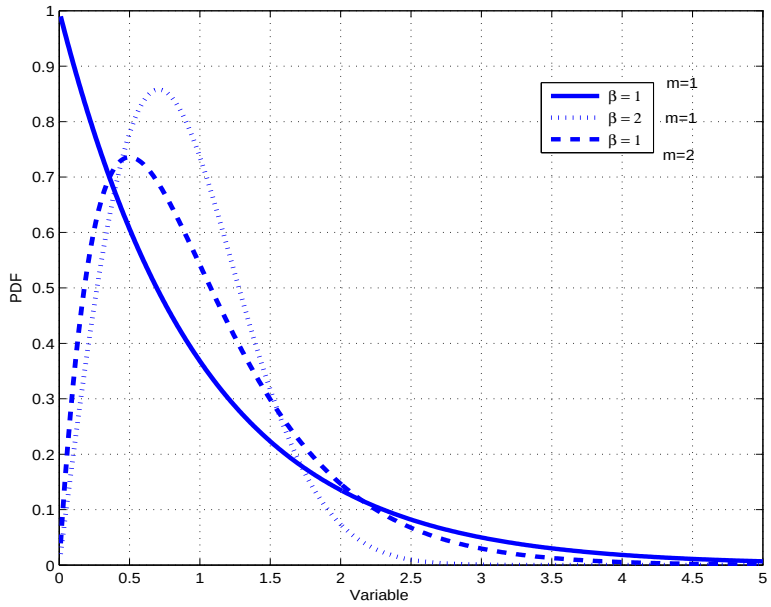

Figure 1.8: PDF of Generalized-Gamma random variable

fading is given by [7, 8].

$$f_{\alpha}(\alpha) = \frac{\beta_g \alpha^{m_g \beta_g - 1}}{(\Omega_g/m_g)^{m_g}\,\Gamma(m_g)} \exp\left(-\frac{m_g}{\Omega_g}\alpha^{\beta_g}\right), \alpha > 0, \tag{1.6}$$

where $\beta_g > 0$, $m_g \geq 1/2$ are parameters of fading severity, Ω_g is related to the average fading power as $E\left[\alpha^2\right] = (\Omega_g/m_g)^{2/\beta_g}\,\Gamma(m_g + 2/\beta_g)/\Gamma(m_g)$ [8]. The GG distribution approximates Rayleigh for $\beta_g = 2$ and $m_g = 1$, Nakagami-m for $\beta_g = 2$, and Weibull for $m_g = 1$ as special cases. In the limiting case as $\beta_g \to 0$ and $m_g \to \infty$, it becomes the lognormal PDF. Figure 1.8 shows the GG PDF for different values of m and β.

Generalized-K (K_G) Fading

The Nakagami-m-gamma distribution is also known as generalized K (K_G) distribution. It is a mixture of Nakagami-m and gamma distributions. In past, the K_G distribution was used for modeling electromagnetic scattering from the physical media such as optical scintillation through atmosphere, tropospheric propagation of radio waves and various types of radar clutters. Later on, this distribu-

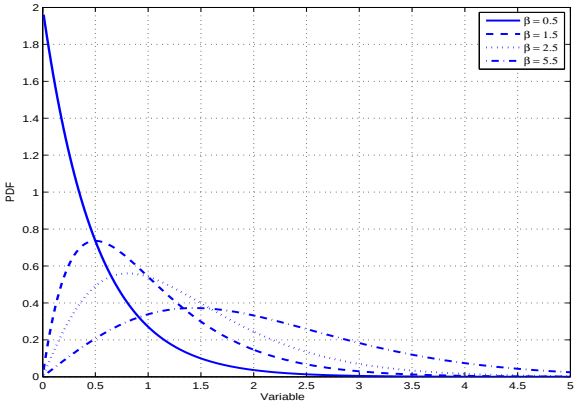

Figure 1.9: PDF of K_G random variable with $m = 1$

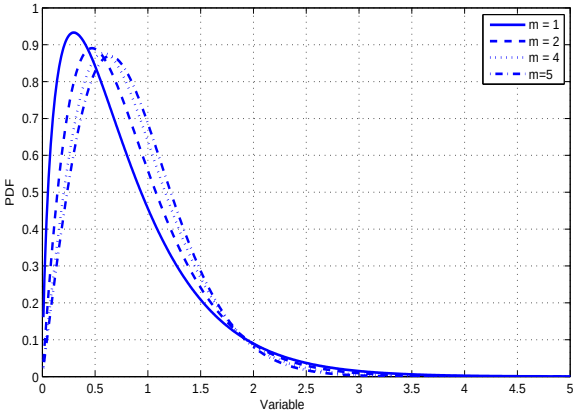

Figure 1.10: PDF of K_G random variable with $k = 2.5$

tion was used to model the composite fading channels. The PDF of K_G distribution is given by [9]

$$f_\alpha(\alpha) = \frac{4m_k^{(\nu+1)/2}\alpha^\nu}{\Gamma(m_k)\Gamma(\beta_k)\Omega_k^{(\nu+1)/2}} K_\lambda\left(2\left(\frac{m_k}{\Omega_k}\right)^{1/2}\alpha\right), \alpha > 0, \tag{1.7}$$

where $\lambda = \beta_k - m_k$, $\nu = m_k + \beta_k - 1$, m_k and β_k are the fading parameters of K_G distribution [9], $K_\lambda(\cdot)$ is the modified Bessel function of second kind and order λ [10, (8.407.1)] and $\Omega_k = E[\alpha^2]/\nu$ is the average fading power of K_G distribution. Since, K_G distribution is two parameter (m_k, β_k) model, by varying these parameters it is possible to get channels with different levels of fading and shadowing. For example, if $m_k = 1$ then Equation 1.7 simplifies to K distribution, for $\beta_k \to \infty$ Equation 1.7 can be approximated to Nakagami-m distribution and for $\beta_k \to \infty$ and $m_k \to \infty$ Equation 1.7 can be approximated to AWGN channel. Figures 1.9 and 1.10 show the K_G PDF for different values of m and β.

Non-homogeneous Fading

The fading models which are used to describe small scale fading such as Rayleigh, Nakagami-m, Rice, Hoyt distributions etc., assume that the channel is homogeneous. In practice, the surfaces are observed to be spatially correlated, which means that the channel is non-homogeneous [11]. The distributions used to model non-homogeneous fading channels are generalized n-distribution and

generalized q-distribution. They are applicable in the presence and the absence of LOS component respectively and are more appropriate for modeling practical fading channels. Mathematical description of these two models are difficult [12]. So, parameterized distributions such as $\kappa-\mu$ distribution and $\eta-\mu$ distributions are used to model this type of non-homogeneous channels which have functional similarities as that of generalized-n and generalized-q distributions, respectively [12]. These two models are explained below:

The $\kappa-\mu$ Fading

The $\kappa-\mu$ distribution is used to model small scale fading in the presence of LOS components in non-homogeneous fading channel. The PDF of $\kappa-\mu$ distribution is given by [11, 12]

$$f_{\alpha}(\alpha)=\frac{2\mu(1+\kappa)^{\frac{\mu+1}{2}}\alpha^{\mu}e^{-\frac{\mu(1+\kappa)}{\Omega}\alpha^2}}{\kappa^{\frac{\mu-1}{2}}\exp(\mu\kappa)\,\Omega^{\frac{\mu+1}{2}}}I_{\mu-1}\left[2\mu\sqrt{\frac{\kappa(1+\kappa)}{\Omega}}\alpha\right],\alpha>0,\kappa>0,\mu>0, \tag{1.8}$$

where $\Omega=E\left[\alpha^2\right]$, parameter $\kappa>0$ is defined as the ratio between the total power of dominant components and the total power of the scattered waves, μ denotes the number of multipath clusters and is related to other fading parameters as $\mu=\frac{E^2(\alpha^2)}{V(\alpha^2)}\frac{1+2\kappa}{(1+2\kappa)^2}$ and $I_v(\cdot)$ is the modified Bessel function of the first kind and v^{th} order [11, 12].

The $\kappa-\mu$ distribution can be used to model all well-known fading distributions by varying the fading parameters. Equation 1.8 simplifies to, Rice distribution for $\mu=1$, Nakagami-m distribution for $\kappa\to 0$, Rayleigh distribution for $\mu=1$, $\kappa\to 0$, and one-sided Gaussian distribution for $\mu=0.5$, $\kappa\to 0$ [11, 12]. Figures 1.11 and 1.12 show the $\kappa-\mu$ PDF for different values of μ and κ.

The $\eta-\mu$ Fading

The $\eta-\mu$ distribution is used to model the non-homogeneous small scale fading in the absence of LOS components. There are two formats of this type reported in the literature, both describe the channel with different parameters. In Format 1, parameter $\eta_{Format1}\in(0,\infty)$ is the ratio between the power of the in-phase components to the power of the quadrature phase components of each cluster

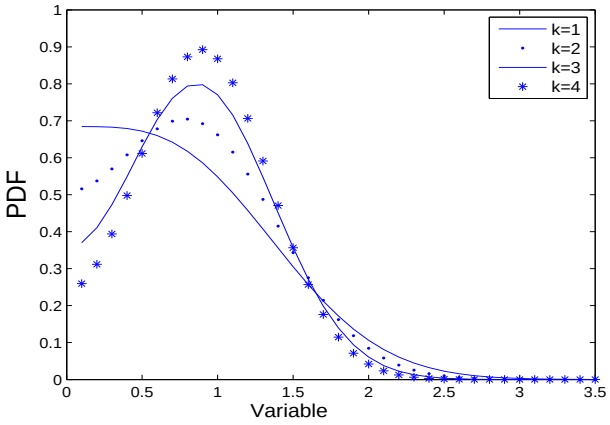

Figure 1.11: PDF of $\kappa-\mu$ random vairable for $\mu = 0.5$

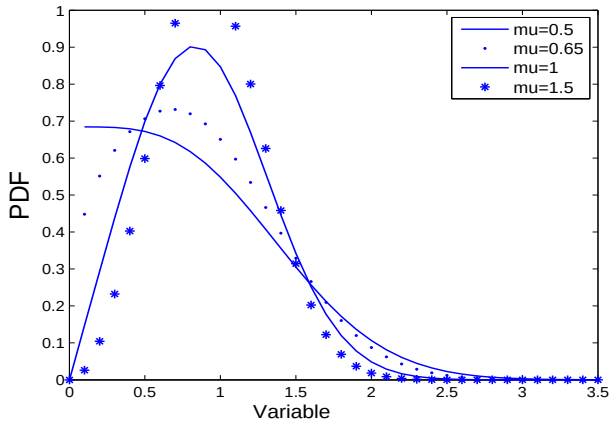

Figure 1.12: PDF of $\kappa-\mu$ variable for $\kappa = 1$.

of multipath. In Format 2, the parameter $\eta_{Format2}$ is ranging from -1 to 1, which is the correlation coefficient between the in-phase and quadrature components of each cluster of the multipath. Mathematically, it is possible to relate these parameters of Format 1 and Format 2 as $\eta_{Format2} = \frac{1-\eta_{Format1}}{1+\eta_{Format1}}$ and $\eta_{Format1} = \frac{1-\eta_{Format2}}{1+\eta_{Format2}}$. These two are related to other common parameters h and H of both the formats as in Format 1: $h = \frac{2+\eta^{-1}+\eta}{4}$, $H = \frac{\eta^{-1}-\eta}{4}$ and in Format 2: $h = \frac{1}{1-\eta^2}$, $H = \frac{\eta}{1-\eta^2}$. With the help of these two parameters the PDF of $\eta-\mu$ distribution is given as [11, 13]

$$f_\alpha(\alpha) = \frac{4\sqrt{\pi}\mu^{\mu+\frac{1}{2}}h^\mu\alpha^{2\mu}}{\Gamma(\mu)H^{\mu-\frac{1}{2}}\Omega^{\mu+\frac{1}{2}}}e^{-\frac{2\mu h}{\Omega}\alpha^2}I_{\mu-\frac{1}{2}}\left[\frac{2\mu H}{\Omega}\alpha^2\right], \alpha > 0, \mu > 0, \tag{1.9}$$

where μ is the half of the number of multipath clusters, which is related to other fading parameters as $\mu = \frac{E^2(\alpha^2)}{2V(\alpha^2)}\left[1+\left(\frac{H}{h}\right)^2\right]$.

The $\eta-\mu$ distribution is a two parameter model. By varying these parameters it can be approximated to other known models. In Format 1: Equation 1.9 simplifies to Hoyt distribution for $\mu = 0.5$ with Hoyt parameter $b = -\frac{1-\eta}{1+\eta}$ (or $q^2 = \eta$), one-sided Gaussian distribution for $\eta \to 0$ and $\eta \to \infty$, Rayleigh distribution for $\mu = 0.5$ and $\eta = 1$, Nakagami-m for $\mu = m$, $\eta \to 0$ or $\eta \to \infty$ [12]. In Format 2: Equation 1.9 simplifies to, Hoyt distribution for $\mu = 0.5$ with Hoyt parameter $b = -\eta$ (or $q^2 = \frac{1-\eta}{1+\eta}$), one-sided Gaussian distribution for $\eta \to \pm 1$, Rayleigh distribution for $\mu = 0.5$ and $\eta = 0$, Nakagami-m for $\mu = m$ and $\eta \to \pm 1$ [11, 13]. Figures 1.13 and 1.14 show the $\eta-\mu$ PDF for

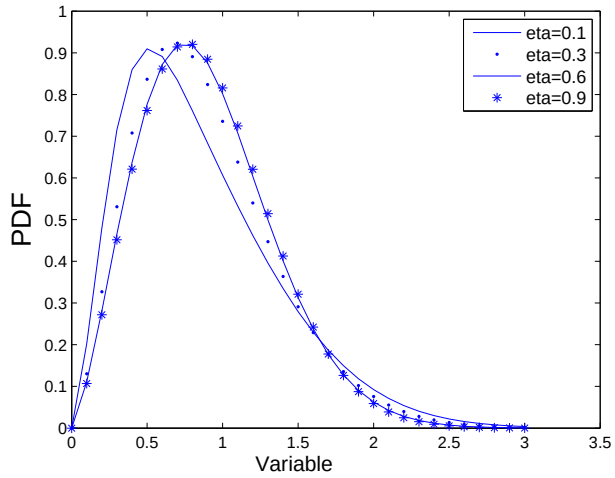

Figure 1.13: PDF of $\eta - \mu$ random variable with $\mu = 0.6$

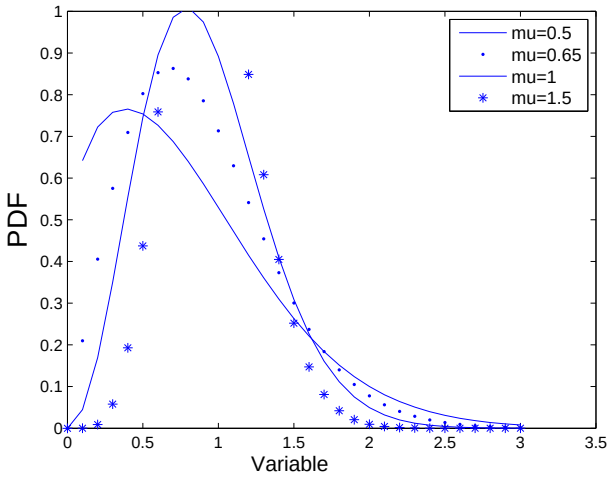

Figure 1.14: PDF of $\eta - \mu$ random variable with $\eta = 0.5$

different values of μ and η.

Fading Counter Measures

Diversity Combining

Diversity combining is a well known approach to mitigate the effect of fading in wireless channels. A diversity combining operation improves the receiver performance by processing preferably a number of statistically independent copies of the same information-bearing signal over two or more fading channels and combining these multiple replicas efficiently. The intuition behind this concept is to exploit the low probability of concurrence of deep fades in all the diversity channels at the same time, hence reduce the probability of error or outage. The possible ways by which independent fading signals can be obtained are enumerated below.

1. Spatial Diversity: By receiving signals from a source by different antennas placed sufficiently apart statistically independent fading signals can be received [2, 3, 14]. The minimum antenna spacing for a mobile unit can be at least half wavelength [2]. For a base station, which is stationary with elevated antennas, the required antenna spacing to receive independent faded

signals can be much wider than the mobile unit antenna spacings [2]. An experimental value of 30 to 50 wavelength for stationary receivers can restrict the correlation below 0.3 between faded signals is also reported in [14].

2. Frequency Diversity: Signal may be transmitted through different modulation frequencies which are sufficiently apart to induce independent fading channels. The minimum frequency separation should be at least the coherence bandwidth of the channel [15].

3. Time Diversity: The same information signal transmitted at different time intervals can be received as independent fading signals. The minimum time interval should exceed the coherence time of the channel [15].

4. Polarization Diversity: Independent fading path may also be realized by simultaneous horizontal and vertical polarizations transmission of signals [15].

5. Angle Diversity: Angle of arrival in case of beam forming antennas can also be used to generates independent fading channels [15].

6. Multipath Diversity: By resolving multipath components at different delays by using direct sequence spread spectrum signaling along with a RAKE receiver [2, 15].

The spatial diversity technique can be classified into the following types:

Selection and Switched Combining

In this technique all the branches are scanned and the branch having highest SNR is chosen for processing. It requires continuous monitoring of all receiving signals. The receiver performance improves with the number of branches. Basic requirement of this diversity technique is the number of branches should be more. The instantaneous SNR γ_{sc} at the output of a L-branch selection combiner can be given as $\gamma_{sc} = \max(\gamma_1, \gamma_2, \ldots, \gamma_L)$, where γ_is are the received input SNRs [2]. The

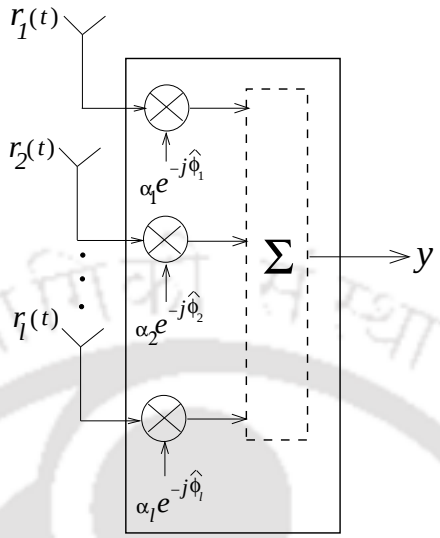

Figure 1.15: Block diagram showing principle of operation of MRC.

average signal-to-noise ratio (ASNR) of a selection combiner in a Rayleigh fading channel is given as [2, (6.9)] $\bar{\gamma}_{sc} = \bar{\gamma}_c \sum_{k=1}^{L} \frac{1}{k}$, where $\bar{\gamma}_c$ is the average received branch symbol energy to noise ratio.

Another diversity combining technique which is less complex than selection combining is the switched combiner (SWC) which scans through the diversity branches until it finds one branch having a SNR exceeding a specified threshold. This diversity branch is selected for processing and is used until its signal to noise ratio falls below a specified threshold and switches to other diversity branch when exceeds the thereshold. This diversity technique is also called switch-and-stay combining. This keeps switching mechanism always in control.

Maximal Ratio Combining

In maximal ratio combining (MRC), the diversity branches are weighted by their respective complex fading gains. The individual branch gains and their carrier phases are required to be estimated. The output SNR is equal to the sum of individual SNRs. It gives an optimum performance but the complexity is high. The average output SNR increases with the number of branches. Figure 1.15 shows the operation of MRC combiner. The output SNR of a L-branch MRC can be given as

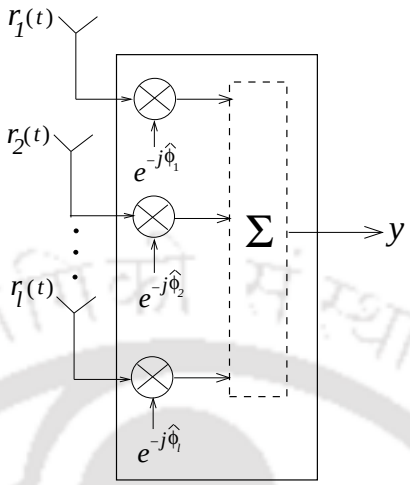

Figure 1.16: Block diagram showing principle of operation of EGC.

$\gamma_{mrc} = \sum_{k=1}^{L} \gamma_k$, where γ_k denotes the signal to noise ratio of individual branch [2, (6.22)].

Equal Gain Combining

In this technique, the diversity signals are received through a number of antennas as shown in Figure 1.16. The signal of individual branch is weighted by unity and all the branches are cophased with respect to one branch. The individual branch carrier phases are estimated for cophasing the respective branch signals. It is relatively less complex when compared to the implementation of MRC. Figure 1.16 shows the operation of EGC combiner where the received signal of the l^{th} branch is multiplied by $e^{-j\phi_l}$, where ϕ_l is the phase of the received signal. In this operation it is assumed that the phase ϕ_l is estimated by an additional circuit and the estimation is accurate. Subsequently, in the combiner the cophased outputs are algebraically added to obtain the combined signal at the output. The instantaneous output SNR of a L-branch EGC can be given as [2, (6.32)] $\gamma_{egc} = \frac{\alpha_{egc}^2}{2LP_n}$, where $\alpha_{egc} = \sum_{i=1}^{L} \alpha_i$, α_i is the fading amplitude of the i^{th} branch and P_n is the noise power per branch.

1.2.2 Phase Estimation Error

Signals transmitted in a wireless channel may undergo random phase shift depending on the propagation paths. In diversity combining the received signals at each combiner antenna may have different phase shifts. To have effective combining it is required to undo the phase shifting of the received signal [16]. Hence, it is required to estimate the phase of the received signals. But due to the presence of doppler spread in carrier frequency, thermal noise and other unwanted signals in the phase estimation circuit the estimated phase may not be accurate [16]. This inaccuracy in the phase estimation is called the phase estimation error. This phase error causes the performance of diversity combining receivers poor compared to ideal condition. When the carrier phase is estimated by a first order phase locked loop (PLL) the random phase error follows the Tikhonov distribution given by [16–18].

$$f_{\psi}(\psi) = \frac{\exp[\zeta\cos(\psi)]}{2\pi I_0(\zeta)}, |\psi| \leq \pi, \tag{1.10}$$

where ζ is the carrier recovery loop SNR and $I_n(\cdot)$ is the n^{th} order modified Bessel function of first kind. The root mean square (RMS) phase error $\sigma_{\psi_{l,s}}$ is related to the ζ as $\sigma_{\psi} \approx 1/\sqrt{\zeta}$. To ensure a satisfactory coherent reception, the RMS phase error in tracking the signal phase should lie within $6^{\circ} - 12^{\circ}$ [17].

1.2.3 Co-channel Interference

As discussed in the Section 1.1, the cells in a cellular system operating with the same frequency are called co-channel cells. The base stations of all co-channel cells are likely to transmit simultaneously. A desired mobile user in one of the co-channel cells receives signals from co-channel cells other than his own cell which are not meant for him. These unwanted signals are called co-channel interference (CCI). Due to the presence of CCI, the performance of the mobile receivers degrades. As fading cannot be avoided in mobile communication bands of frequencies, the performance further degrades due fading. There can be a wide variation of fading types as the signals from cochannel

cells travel different paths depending their location.

The above discussed three causes of receiver performance degradation i.e., fading, phase estimation error and CCI are main factors those occur in practical systems. Their combined effect affects the performance of receivers used for cellular mobile communications. To have effective mobile communication there is a need to design a receiver which can operate satisfactorily in the presence of these effects. In this thesis work, we analyze the outage and ABER performance of EGC and MRC diversity combining schemes in the presence of CCI and phase estimation error for different fading environments.

1.3 Literature survey

Phase Error:

Sagias and Karagiannidis studied the effect of phase error on the performance of dual branch EGC receivers in correlated Nakagami-*m* fading channels using moment generating function (MGF) and Padé approximation approach [19]. Najib and Prabhu presented the error probability of EGC receiver assuming imperfect carrier recovery due to the presence of random noise in carrier recovery loops [16]. Rhodes studied the detection loss due to imperfect carrier synchronization for coherent phase-shift-keying (PSK) communications. This detection loss was greater for quaternary PSK (QPSK) signaling than for the binary PSK (BPSK) case. It was shown that the use of offset QPSK instead of conventional QPSK modulation for a specified value of allowable detection loss requires almost 3 dB less SNR [20]. Smadi and Prabhu developed a new method to analyze the performance of partially coherent phase shift keying systems in EGC receiver [21].

Co-channel Interference:

Beaulieu and Adnan presented the performances of QPSK in the presence of CCI in both non-fading and fading environments. Two interference models were considered, in AWGN environment and in different flat fading environments [22]. Abu-Dayya and Beauleiu derived closed form ex-

pressions for outage probability in generalized Nakagami fading environment for EGC, MRC and SC diversity combining schemes [23]. Song *et.al.,* presented a new outage performance analysis for EGC receiver that are limited by CCI in Rayleigh fading [24]. In [25], the performance analysis of MRC receiver with imperfect channel estimation in the presence of CCI is presented. The channel coefficients and their estimates were assumed to be complex Gaussian distributed. Closed form expression for outage probability and average symbol error probability (ASEP) were presented. In [26] the effects of imperfect channel estimation on MRC receiver are examined with multiple cochannel interferer over Rayleigh fading channels. Velkov presented the second order statistics of EGC in the presence of CCI for Rayleigh fading channels by applying the characteristic function (CF) method and the Beaulieu series [27]. Shah and Haimovich presented the performance of MRC receiver in the presence of multiple CCI sources for Rayleigh or Rician fading channel. The interfering user signal was considered as Rayleigh [28]. Rahimzadeh derived the exact closed-form expressions for the BER of BPSK in Rayleigh fading channels of MRC receiver was presented in the presence of CCI and AWGN [29]. More recently, Paris and David derived exact closed-form expressions for the outage probability of Hoyt fading channels under CCI [30]. David *et. al.* derived exact closed-form expressions for the outage probability of MRC in $\eta - \mu$ fading channels with antenna correlation and CCI [31]. Aalo and Zhang studied the effect of CCI on the performance of digital mobile radio systems in a Nakagami fading channel. The performance of MRC diversity in the presence of multiple CCI interferes and AWGN were presented. Closed-form expressions were derived for the ABER and outage probability of both coherent BPSK systems. In [32], Leib and Pasupathy presented the study of vectors perturbed by Gaussian noise. In [33] Beaulieu and Cheng derived the BER of bandlimited BPSK and CCI environment for perfect coherent detection

Fading Channels:

Karagiannidis presented a moment based approach for the performance analysis of an L branch EGC receiver using Padé approximation method [34]. Mendes *et. al.*, derived expressions for moments and correlation coefficient of two Hoyt (Nakagami-q) signals [35]. Patel *et. al.,* presented

the performance of EGC receiver over correlated Nakagami-*m* fading with arbitrary *m* and unequal branch SNR's. Closed form expression for ABER for coherent binary modulation schemes were derived [36]. Zogas *et. al.,* presented the performance of EGC receiver over Hoyt and Rician fading channels using MGF and Padé approximation method. Exact closed-form expressions for the moments of the combiner output SNR were derived [37]. Karagiannidis *et. al.,* presented the performance of a dual branch EGC receiver over correlated Nakagami-*m* fading using the CF method. The performance was done for BPSK and coherent BFSK [38]. Nakagami-*m* distribution is a generalized distribution of the multipath propagation [4]. It often gives the best fit to land-mobile and indoor-mobile multipath propagation. Scintillation of ionospheric radio links is modeled by Nakagami-*q* distribution [39]. Hoyt derived the distribution functions and the cumulative distribution functions pertaining to the modulus and angle of the normal complex variate when the mean is zero and variance is different for the in phase and quadrature components of the normal complex variate [39]. In some environments, such as congested downtown areas and land-mobile satellite systems with foliage and urban shadowing, the analysis of the channel model must include both multipath and shadow fading. A relatively simple and versatile envelope distribution that generalizes multipath and shadow fading is the generalized gamma distribution (GG) [7]. In [7] Stacy introduced the *GG* distribution. The author had generalized the two parameter gamma distribution which includes Rayleigh, Nakagami-*m* and Weibull as the special cases and Log-normal as the limiting case. In addition to the *GG* distribution, generalized-$K(K_G)$ distribution is also a versatile distribution for the accurate modeling of the composite propagation consisting of multipath fading superimposed by lognormal shadowing [5]. The correlated bivariate generalized-$K(K_G)$ distribution is introduced and studied in [5]. The performance analysis of MRC, EGC, and SC over bivariate K_G fading channel were also presented. In the available small scale fading models such as Rayleigh, Nakagami-*m*, Rician and Hoyt the channel is assumed to be homogeneous. But in practice, the surfaces are observed to be spatially correlated, which means the channel is non-homogenous. The $\eta-\mu$ and $\kappa-\mu$ fading channels are the non-homogenous channels. Yacoub introduced the $\kappa-\mu$ distribution as a

generalized distribution and showed it includes the Rice and Nakagami-*m* distribution as the special cases [11]. Yacoub also presented two general fading distributions, the $\kappa - \mu$ distribution and the $\eta - \mu$ distribution and proposed fading models for the distributions [12]. Yacoub introduced the symmetrical $\eta - \mu$ distribution as a general distribution to describe the statistical variation of the envelope in the fast fading environment [13].

1.4 Motivation

In literature, the performance of all diversity receivers are analyzed assuming the estimated channel parameters are exact. Practical problems in the application of diversity receivers, such as phase error, timing error are not considered. Due to the presence of noise in the phase estimation circuit, the estimated phase is not exact resulting in phase estimation error or phase error. In literature, this problem of phase error has not been investigated in depth due to the complexity in deriving the statistics of output SNR of diversity receivers with phase error. The received signal at the array output of the diversity combiner becomes complicated due to phase error, meaning the detection of the phase results in a random variable instead of being zero as in the case when the estimated phase is assumed to be exact. The performance analysis of diversity receivers requires the knowledge of the closed form statistics of the output SNR of diversity receivers with phase error in addition to fading. So, the problem of phase error is considered for investigation in this thesis.

In addition to phase error, another practical problem that occurs in wireless communication is also analyzed which is the CCI. When the CCI occurs, the received signal itself becomes very complicated when compared to the non CCI case. Each antenna receives a signal which is interfered by N CCI users signal. In most of the cases, where CCI is dealt in literature two assumptions are made. Firstly, the fading environment is assumed to be only interference limited omitting the AWGN. When AWGN is considered, it becomes very difficult to solve the steps to reach the output signal-to-interference-plus-noise ratio (SINR) starting from the received signal which is already

complex in nature. Secondly, the CCI signals are assumed to be in perfect synchronization to the desired user. But practically both the cases cannot happen. In literature very few research work is presented on the performance analysis of diversity receivers with CCI considering both noise and asynchronous case of desired user and interfering user. So, all together in addition to fading, the problem of phase error, interference with AWGN are together considered for analysis. To be specific the performance analysis of EGC and MRC receivers are analyzed in the presence of phase error and CCI.

1.5 Problem Formulation

It is observed from the literature survey that the analysis of diversity combining receivers in the presence of both phase estimation error and CCI has not received enough attention. This analysis is challenging since it involves desired signal with phase estimation error with CCI signals which are received through paths having different fading distributions. For example, signals path from one cochannel cell to the desired user cell may follow Rayleigh distribution whereas from another cochannel it may be Nakagami-*m* distributed. In addition to the above two problems, if additive white Gaussian noise is considered the analysis becomes more complicated. With the above discussed issues many open problems can be formulated for analysis.

In this thesis work, it is proposed to analyze the performance of EGC and MRC combining receivers with phase estimation error and CCI over various fading channels. The focus is to obtain mathematical expressions, wherever possible, for performance measures such as ABEP, outage probability and average output SNR.

1.6 Thesis Contribution

In this thesis work, performance of EGC and MRC diversity combining receivers are analyzed with phase estimation error, CCI and AWGN. The contribution under EGC and MRC receivers categories

are as stated below:

1. Performance analysis of EGC receiver:
   (a) ABEP of dual EGC receiver over correlated Hoyt, Nakagami-*m* and 'composite and non-homogenous' fading channels.
   (b) Outage probability of *L*-EGC over Composite Fading Channels.
   (c) ABEP and Outage of *L*-EGC over Nakagami-*m* fading channels using PDF based approach.
2. Performance analysis of *L*-MRC receiver over Nakagami-*m* fading channels.

1.7 Thesis Organization

Chapter 2 describes the system model, for the EGC receiver performance measures and analysis techniques, and provides definitions of some useful notations to be used in subsequent chapters. Chapter 3 presents the ABEP and outage performance of EGC receiver with phase estimation error and CCI over correlated Hoyt fading channel, Composite fading channels and Nakagami-*m* fading channel. The performance analysis of EGC receiver over Nakagami-*m* fading channel using PDF method is also presented. Chapter 4 presents the performance analysis of MRC receiver with channel estimation error and CCI over Nakagami-*m* fading channels. Chapter 5 presents the conclusion of the thesis with a brief summary of the work presented. Besides, it introduces some research problems for future work.

Chapter 2

System Model and Analysis Methods

2.1 System Model

Let us consider a cellular communication system with hexagonal cell structure as shown in Figure 2.1. The desired user's cell is denoted as A_d and the cochannel cells are denoted as A_i. Number of cochannel cells vary with the cluster size of the cell under consideration. For the cluster size of seven shown in the figure there will be six cochannel cells. The users in A_i cells may transmit simultaneously while the users in A_d cell keep receiving their signals from base station, resulting in CCI at the desired user's receiver.

Let the desired user's signal is given as $s_s(t) = a_s g_T(t)$, where a_s is the data symbol corresponding to the desired user's information bit and $g_T(t)$ is the transmitter impulse response. The channel through which the desired user's signal propagates is assumed to be a fading channel with α_s as the fading amplitude. The CCI signal can be given as $s_i(t) = a_i g_T(t), i = 1, 2 \ldots, N$, where a_i is the data symbol corresponding to the information bit of the i^{th} interfering signal and N is the number of active CCI transmission. The data symbols a_s and a_i are assumed to take values ± 1 with equal probability. The channel between the i^{th} interfering transmitter output and the desired user's receiver input is assumed to be a fading channel with fading amplitude α_i. The fading amplitudes α_s and

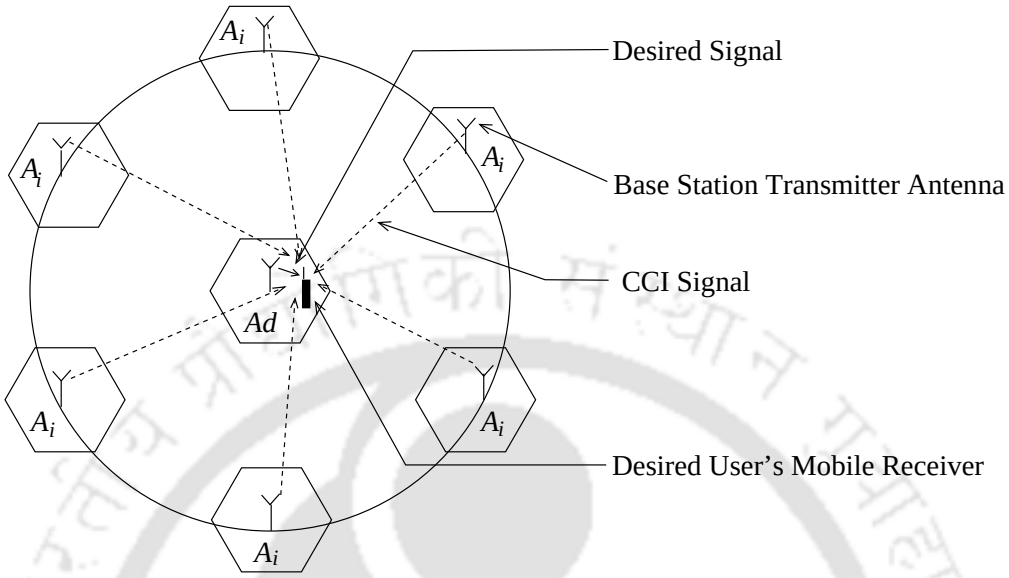

Figure 2.1: Desired and CCI signal in cellular communication system. A_d is the desired user's cell and A_is are cochannel cells.

α_is may not be from the same fading distribution as they are likely to be received through different propagation paths. The interfering users may transmit asynchronously with τ_i as the delay of the i^{th} interfering user's signal relative to the desired user's signal. For synchronous CCI, when all the interfering users transmit simultaneously with the desired user, $\tau_i = 0$.

For synchronous CCI, an EGC combiner gives an overestimation of the interference power whereas for the asynchronous CCI case the power estimation is exact [40, 41]. Interference power being an overestimation, the performance under synchronous assumption becomes poor compared to the performance of asynchronous case. Other way saying, the impairment caused by CCI to the desired user's signal is maximum, worst case, considering interferes as synchronous compared to asynchronous CCI users. As a fact, when all the interfering signals are half symbol duration delayed from the desired user, the impairment is minimum [41]. In [29], it can be seen that the interference power of synchronous CCI given as $\sum_{i=1}^{N} P_i$, whereas the interference power in the asynchronous case becomes a weighted sum of P_is where the weights are a function of involving delay τ_i of CCI signals [29, (2b)]. Similar discussion on the effect of interference power on synchronous and asynchronous cases are also presented in [24], [42], [43]. Assuming synchronous CCI, the received

signal at the desired user's receiver can be given as

$$r(t) = \alpha_s e^{j\phi_s} s_s(t) + \sum_{i=1}^{N} s_i(t)\alpha_i e^{j\phi_i} + n_s(t), \tag{2.1}$$

where ϕ_s is the phase of the desired user's received signal, ϕ_i is the phase of the signal received from the i^{th} CCI transmission and $n_s(t)$ is the AWGN with zero mean and power spectral density N_0.

To counter the effects of fading on the desired user's receiver performance we assume an L-branch EGC diversity combiner as discussed in Section 1.2.1 (Figure1.16) is implemented for receiving signals. Assuming the desired user's transmitter and N CCI users are transmitting asynchronously, the complex baseband received signal at the l^{th} antenna of the EGC over a symbol duration T can be expressed from the Equation 2.1 [19, 24]

$$r_l(t) = \alpha_{l,s} e^{j\phi_{l,s}} s_s(t) + \sum_{i=1}^{N} \alpha_{l,i} e^{j\phi_{l,i}} s_i(t-\tau_i) + n_{l,s}(t), l = 0, 1, 2, \ldots, L, \tag{2.2}$$

where $n_{l,s}(t)$ is the AWGN with zero mean and power spectral density N_0, and the RVs $\phi_{l,s}$ and $\phi_{l,i}$ are carrier phases.

2.2 Gaussian Assumption for Cochannel Interference

The interference term in Equation 2.2 is assumed to have a Gaussian distribution. The conventional form of the central limit theorem cannot be applied here because the interference term consists of independent, but not identically distributed terms . So, another form of the central limit theorem given by Cramer can be applied [25, 28, 44–46]. Cramer's central limit theorem states that the sum $X_1 + X_2 + \ldots + X_n$ of a large number of independent variables, is approximately normally distributed if

1. every component has a zero mean value;
2. every component has a finite variance $\sigma_i^2 = E[X_i^2]$;
3. $\sigma_i / s_n \longrightarrow 0$ and $s_n \longrightarrow \infty$, where $s_n = \sigma_1^2 + \ldots + \sigma_n^2$.

It can be shown that the interference component in Equation 2.2 satisfies these conditions, from the properties of the symbol a_i assumed in Equation 2.1 and hence can be assumed Gaussian to be Gaussian distributed [22, 28].

2.3 Performance Analysis Methods

Performance measures such as average output SNR, outage probability, average bit error probability (ABEP), amount of fading, level crossing rate etc. are used to compare the potential of different diversity combining techniques discussed in Section 1.2.1. Among these measures, the average output SNR, outage probability and ABEP are frequently used measures. As per the literature survey, a number of methods have evolved over the years to obtain these performance measures mathematically for different combining schemes. These methods can be broadly categorized under the following headings.

1. PDF based method.
2. Moment generation function based method.
3. Characteristic function based method.

2.3.1 Probability Density Function Based Method

Average Signal-to-Noise Ratio

The average signal to noise ratio (ASNR) is the most common performance measure of a communication receiver. Average SNR is defined as the statistical average of SNR over probability distribution of the fading and is given by [3, (1.1)]

$$\bar{\gamma} = \int_0^\infty \gamma f_\gamma(\gamma) d\gamma, \tag{2.3}$$

where $f_\gamma(\gamma)$ denotes the PDF of the received SNR γ.

Outage Probability

Outage probability (P_{out}) is an important performance measure of any communication receiver. It is defined as the probability that the output SNR falls below a certain threshold γ_{th}. Mathematically, it can be given as [3, (1.4)]

$$P_{out} = \int_0^{\gamma_{th}} f_\gamma(\gamma) d\gamma. \tag{2.4}$$

Average Bit Error Probability

The conditional average bit error rate (ABER) over the distribution of fading channel and is given by [3, (1.8)]

$$P_b(e) = \int_0^{\infty} P_b(e/\gamma) f_\gamma(\gamma) d\gamma, \tag{2.5}$$

where $f_\gamma(\gamma)$ is the PDF of SNR of the fading channel and $P_b(e/\gamma)$ is the conditional BER, depends on the type of modulation employed at the transmitter.

2.3.2 Moment Generation Function Method

If the PDF of the output SNR is not available or if it cannot be derived in an usable form then the MGF method can be used for the analysis of system performance. This method uses the MGF of combiner output SNR in the evaluation of ABEP. The method is discussed below:

ABER of a communication system in AWGN channel can be obtained from the useful expression given as [3, pp. 124]

$$P_e = \frac{1}{\pi} \int_0^{\pi/2} M_\gamma \left(-\frac{a^2}{2\sin^2\theta} \right) d\theta, \tag{2.6}$$

where a is a constant depends on the modulation scheme used for transmission and $M_\gamma(\cdot)$ is the MGF of the output SNR. The MGF of the output SNR can be given as $M_\gamma(s) \triangleq E\left[\exp(s\gamma)\right]$ [3] which can

be expressed by applying Taylor series to the exponential function as

$$M_{\gamma}(s) = \sum_{n=0}^{\infty} \mu_n \frac{s^n}{n!}, \tag{2.7}$$

where $\mu_n = \mathrm{E}[\gamma^n]$ is the n^{th} moment of γ.

Thus, an expression for ABER can be obtained by substituting Equation 2.7 in Equation 2.6 and solving the finite integral. Since the MGF expression in Equation 2.7 is an infinite power series, to obtain the sum the Pad*é* approximation method can be used. This method can express the infinite series as a rational function, called Pad*é* approximant, of polynomials of a specified order $N+1$ for the denominator and N for the numerator which can accurately approximate $M_{\gamma}(s)$. This requires only a finite number of moments to give approximate, but highly accurate, value of MGF. For such kind of rational functions, only a finite number of moments i.e., the first $(2N+1)$ order moments are needed in order to construct the approximated $M_{\gamma}(s)$ [34]. A discussion on Padé approximation is presented below. Further, the technique to obtain the approximated rational function is illustrated with an example in Appendix A.11.

2.3.3 Applying Padè Approximation Method for Analysis of EGC Receiver

Padè approximation is an useful mathematical tool which accurately approximates expressions involving infinite series and is used for the approximation of moment generating functions in literature [34, 47]. Performance analysis of EGC and MRC diversity receivers depend on the statistics of the combined SNR of all the branches at the antenna array output. Generally, it is difficult to obtain PDF of the output SNR [47]. Specifically, ABER and outage probability involves integration of the PDF of the output SNR and even if the PDF of output SNR is derived in closed form it becomes very difficult to numerically evaluate the ABER and outage expressions [47]. It is also mentioned that for the MGF method, Pade approximation approach is one accurate method to numerically evaluate performance of receivers [47]. More specifically, in literature, very important works on the ABER performance of EGC receiver was done using the *Padé* approximation [6,19,37,48]. The difficulty in

EGC receiver is more because the output SNR is the square of the sum of received signal amplitudes. Moreover, we have also considered the problem of phase estimation error, which further increases the complexity. Additionally, for different fading channels considered in the thesis work such as correlated Hoyt, generalized gamma and generalized-K, derivation of the PDF of the output SNR with phase error is not possible. So, the *Padé* approximation approach can be handy for numerical evaluation of the obtained expressions. Regarding accuracy, the *Padé* approximation method accurately approximates the MGF. A complete description of the *Padé* approximation method starting from the moment generating function is given in the thesis. An example to show the accuracy of the *Padé* approximation is also given in Appendix. Hence, the *Padé* approximation method is close to exact and approximates the MGF closely and hence it doesn't affect the performance analysis in large scale. The results are also cross checked with the simulation results for ensuring the accuracy. For binary phase shift keying (BPSK) modulation for which $a = \sqrt{2}$, the ABER expression in integral form can be given as

$$\overline{P}_e = \frac{1}{\pi} \int_0^{\frac{\pi}{2}} M_{\gamma_{egc}} \left(-\sin^{-2}(\theta) \right) d\theta, \tag{2.8}$$

which requires a numerical evaluation.

Average Output SNR: The average output SNR of a diversity combiner is given by [3, (1.3)]

$$\bar{\gamma} = \frac{d}{ds} \left[M_{\gamma}(s) \right] |_{s=0}, \tag{2.9}$$

where $M_{\gamma}(s)$ is the MGF of the combiner output SNR.

Outage Probability: The outage probability is given by [3, (1.6)]

$$P_{\text{out}}(\gamma_{th}) = \frac{1}{2\pi j} \int_{\sigma - j\infty}^{\sigma + j\infty} \frac{M_{\gamma}(-s)}{s} e^{\gamma_{th} s} ds, \tag{2.10}$$

where σ is chosen in the region of convergence of the integral in the complex s-plane.

Average BER: The average BER using MGF approach is given by [3, (1.14)]

$$P_e(\bar{\gamma}) = \frac{1}{2\pi j}\int_{\sigma-j\infty}^{\sigma+j\infty} \frac{M_D(-s)}{s} ds. \tag{2.11}$$

2.3.4 Characteristic Function Based Method

In this approach CF of the receiver variables is used to obtain performance measures. For a coherent receiver with BPSK modulation, the ABER can be obtained using the following formula (Gil-Palaez lemma) [36]

$$P_e(\bar{\gamma}) = \Pr(D_1 < 0) = \frac{1}{2} - \frac{1}{2\pi}\int_{-\infty}^{\infty} \frac{\Im\{\Phi_{D_1}(j\omega)\}}{\omega} d\omega, \tag{2.12}$$

where Φ_{D_1} is the CF of the receiver output decision variable D_1 assuming a '1' was transmitted.

For receivers with noncoherent modulations, the CF based formula for ABER can be given as (using Parseval's theorem) [49]

$$P_e(\bar{\gamma}) = \frac{1}{\pi}\int_{0}^{\infty} \Re\{G^*(s)\Phi_\alpha(s)\} ds, \tag{2.13}$$

where $\Phi_\alpha(s)$ is the CF of the combiner output instantaneous amplitude, $G(s)$ is the Fourier transform of the conditional error probability and $*$ is the complex conjugate operator. This method is appropriate for ABEP performance of EGC receiver. Since, the Equation 2.13 requires only the combiner output CF, this formula can be safely used both for coherent and noncoherent modulation schemes. Besides, it can also be used to analyze combiners with both independent and correlated fading branches.

Chapter 3

Performance of EGC Receiver

Among known diversity combining techniques, EGC can achieve a performance close to the optimum performance of MRC with relatively less implementation complexity [47]. As discussed in Section 1.2.1, multipath diversity signals received at the input branches of the EGC combiner are co-phased and added whereas in MRC the received signals are required to be weighted by their respective complex channel fading gains before being added, prior to detection. Due to two most important features such as 'closeness of performance to MRC' and 'less implementation complexity relative to MRC,' EGC can be preferred over MRC in practical applications.

Performance analysis of EGC receiver is challenging since the combiner output signal amplitude variable is a function of sum of L received random fading signal amplitudes [3]. The received fading signals can also be either statistically independent or correlated. Mathematical analysis would be relatively less complex if the received multipath signals are statistically independent. If the receiving antennas of the combiner are spaced sufficiently apart the received signals can be statistically independent. As reported in literature, in a uniform scattering environment with omnidirectional transmitting and receiving antennas, the minimum separation needed between any two successive antennas to achieve independent faded signals is approximately 0.38λ, where λ is the received carrier signal wavelength [47]. With independent signal assumption, a closed form expression for the PDF

of EGC combiner output RV for $l > 2$ is not available even for Rayleigh fading channels [49]. The challenge in the analysis increases with the assumption that the fading is correlated which further goes up with the consideration of the presence of phase error and CCI signals besides AWGN.

In this chapter, we present ABEP and outage performance of dual EGC ($L = 2$) receiver in the presence of phase error and CCI, for various fading channels. The ABEP analysis has been performed using MGF based approach. Since analysis of the above system is not mathematically tractable beyond $L = 2$, for $L > 2$ we present the analysis by considering the presence of phase error and AWGN only (i.e. no CCI). For this system, we present the outage and ABEP applying PDF based approach.

In an ideal EGC combiner, received L faded copies of the transmitted signal are equiphased and each is weighted by unity gain [3]. Equiphasing operation requires the phases to be estimated and the error introduced in this estimation is known as the phase estimation error. Assuming the estimated phase of the input signal of the l^{th} branch of the combiner is $\widehat{\phi}_{l,s}$, the demodulated signal at the combiner output at the sampling instant T can be given for synchronous case ($\tau_i = 0$) as (derived in Appendix A.1) [19, 22]

$$y = E_g a_s \sum_{l=1}^{L} \alpha_{l,s} e^{j\psi_{l,s}} + \sum_{l=1}^{L} n_{0,l} e^{-j\widehat{\phi}_{l,s}} + E_g \sum_{i=1}^{N} \sum_{l=1}^{L} a_i \alpha_{l,i} e^{j\left(\phi_{l,i} - \widehat{\phi}_{l,s}\right)}, \tag{3.1}$$

where $E_g = \int_0^{\infty} g_T^2(t)dt$, $n_{0,l} = \int_0^{T} n_{l,s}(\tau) g_T(\tau) d\tau$ which can be shown to be Gaussian with zero mean and power spectral density $N_0 E_g$, $\psi_{l,s} = \phi_{l,s} - \widehat{\phi}_{l,s}$ is the phase estimation error and N is the number of cochannel users in the system. Throughout the thesis the phase estimation error is assumed to be Tikhonov distributed. The random phase $(\phi_{l,i} - \widehat{\phi}_{l,s})$ is i.i.d and uniformly distributed in $(0, 2\pi)$. It is assumed that $\alpha_{l,s}$ and $\alpha_{l,i}$ are independent and $\psi_{l,s}$, and $(\phi_{l,i} - \widehat{\phi}_{l,s})$ are approximately uncorrelated.

For an L branch EGC receiver, the instantaneous output SINR with phase error and CCI can be derived from Equation 3.1 which is given in Appendix A.2. Thus, the expression for the SINR can

be given as

$$\gamma_{egc} = \frac{E_g^2 \left[\sum_{l=1}^{L} \alpha_{l,s} \cos \psi_{l,s} \right]^2}{LN_0E_g + E_g^2 \sum_{i=1}^{N} \sum_{l=1}^{L} [\alpha_{l,i}^2]}, \tag{3.2}$$

Since, N cochannel interferes are i.i.d with the identical fading parameters m and identical average power, the instantaneous interfering signal voltage phasors are added together to produce the resultant instantaneous interfering signal with resultant interference power $\sum_{i=1}^{N} \sum_{l=1}^{L} [\alpha_{l,i}^2]$ [23, (8b)].

As per the performance analysis measures discussed in Section 2.3, it requires an expression for the PDF of combiner output SNR. Hence, for the analysis of the system under consideration an expression for the PDF of SINR is required. The SINR expression presented in Equation 3.2 has a term in its numerator carrying summation of L RVs i.e. $\alpha_{l,s} \cos \psi_{l,s}$. To obtain the PDF of SINR we require an expression for the joint PDF of the $L-$variable above RV. A general expression for the PDF of sum of L RVs although can be written in integral form i.e. as a convolution of PDF of individual RVs (applicable for independent RVs only), the complexity goes up handling it further. Hence, in this presentation we limit our analysis of the system to dual EGC i.e, $L = 2$ only. Below we present the analysis for a dual-EGC receiver with phase error, CCI and AWGN.

3.1 ABEP Analysis for Dual-EGC

An expression for the PDF of SINR at the output of the dual EGC receiver can be obtained by putting $L = 2$ in Equation 3.2, as

$$\gamma_{egc} = \frac{E_g^2 \left[\sum_{l=1}^{2} \alpha_{l,s} \cos \psi_{l,s} \right]^2}{2N_0E_g + E_g^2 \sum_{i=1}^{N} \sum_{l=1}^{2} [\alpha_{l,i}^2]}. \tag{3.3}$$

Moments of EGC Output SINR

The n^{th} moment of γ_{egc} can be obtained from Equation 3.3 as

$$E\left[\gamma_{egc}^{n}\right] = \left(\frac{1}{2}\right)^{n} E\left[\frac{\left[\sum_{l=1}^{2}\sqrt{\gamma_{l,s}}\cos\left(\psi_{l,s}\right)\right]^{2}}{\left(1+\frac{1}{2}\sum_{i=1}^{N}\sum_{l=1}^{2}\left[\gamma_{l,i}\right]\right)}\right]^{n}$$
$$= \left(\frac{1}{2}\right)^{n} E\left[\sum_{l=1}^{2}\sqrt{\gamma_{l,s}}\cos\left(\psi_{l,s}\right)\right]^{2n} E\left[\left(\frac{1}{\left(1+\frac{1}{2}\sum_{i=1}^{N}\sum_{l=1}^{2}\gamma_{l,i}\right)}\right)^{n}\right], \quad (3.4)$$

where $\gamma_{l,s}=\frac{\alpha_{l,s}^2 E_g}{N_0}$ is the SNR of the desired user's signal and $\gamma_{l,i}=\frac{\alpha_{l,i}^2 E_g}{N_0}$ is the SNR of the received CCI signal at the l^{th} input branch of EGC. Then, applying binomial identity [10, (1.111)] (reproduced in Equation A.88) to the expression $\left[\sum_{l=1}^{2}\sqrt{\gamma_{l,s}}\cos\left(\psi_{l,s}\right)\right]^{2n}$ in Equation 3.4, the n^{th} moment of γ_{egc} can be expressed as

$$E\left[\gamma_{egc}^{n}\right] = \frac{(2n)!}{2^n}\sum_{\substack{k_1=0\\ k_2=2n-k_1}}^{2n}\frac{E\left[\gamma_{1,s}^{k_1/2}\gamma_{2,s}^{k_2/2}\right]}{k_1!k_2!}\prod_{l=1}^{2}E\left[\cos^{k_l}\left(\psi_{l,s}\right)\right]E\left[\left(\frac{1}{\left(1+\frac{1}{2}\sum_{i=1}^{N}\sum_{l=1}^{2}\left[\gamma_{l,i}\right]\right)}\right)^{n}\right] \quad (3.5)$$

The k_lth order moment of the cosine function in Equation 3.5 can be given as [19, (8)]

$$E[\cos^{k_l}(\psi_{l,s})] = \frac{1}{2^{k_l}}\sum_{j=0}^{k_l}\binom{k_l}{j}\frac{I_{|2j-k_l|}\left(\zeta_{l,s}\right)}{I_0\left(\zeta_{l,s}\right)}, \quad (3.6)$$

where $\zeta_{l,s}=(1/\sigma_{\Psi_{l,s}})^2$. An expression for the nth order moment $E\left[\left(\frac{1}{\left(1+\frac{1}{2}\sum_{i=1}^{N}\sum_{l=1}^{2}\gamma_{l,i}\right)}\right)^{n}\right]$ in the Equation 3.5 for Nakagami-m distributed CCI has been derived in Appendix A.2, which can be given as

$$E\left[\left(\frac{1}{\left(1+\frac{1}{2}\sum_{i=1}^{N}\sum_{l=1}^{2}\gamma_{l,i}\right)}\right)^{n}\right] = \Psi\left(2m_iN, 2m_iN+1-n, \frac{2m_i}{\bar{\gamma}_i}\right), \quad (3.7)$$

where $\bar{\gamma}_i$ is the average SNR of the interfering signal and $\Psi(a,b,z)$ is the "confluent hypergeometric function" [10, (9.21)]. Thus, substituting Equations 3.6, 3.7 and E $\left[\gamma_{1,s}^{k_1/2}\gamma_{2,s}^{k_2/2}\right]$ in Equation 3.5, an

expression for the n^{th} moment of γ_{egc} can be expressed in closed-form. As the term $\mathrm{E}\left[\gamma_{1,s}^{k_1/2}\gamma_{2,s}^{k_2/2}\right]$ is fading distribution dependent expressions can be derived for it for the fading channels under consideration.

3.1.1 ABEP Evaluation Method

From the expression obtained for the dual-EGC SINR in Equation 3.3, derivation of an expression for its PDF is not straightforward. So, the MGF method as discussed in Section 2.3.2 can be used to obtain ABEP for a given modulation scheme. As we know from Equation 2.8, we need an expression for the MGF of SINR γ_{egc}. For a number of fading channels we present below the MGF of γ_{egc} and apply the MGF expression in Equation 2.8 followed by numerical integration to obtain ABEP.

3.1.2 Correlated Hoyt Fading Channels

According to the system model discussed in Chapter 2 and the mathematical expression for EGC receiver output signal given in Equation 2.2, the desired user's channel is assumed to be correlated Hoyt fading with marginal PDF given in Equation (1.3) with fading parameter q. The signals received at the desired user's receiver due to CCI users is assumed to be received through a Nakagami-m fading channel i.e., the fading amplitude $\alpha_{l,i}$ is Nakagami-m distributed with the PDF expression given in Equation 1.2. The fading amplitudes $\alpha_{l,i}$s are assumed to be i.i.d Nakagami-m RV with fading parameter m_i. To simplify the analysis in the work presented here we assume that the CCI users are transmitting synchronously i.e. $\tau_i = 0$.

To obtain ABEP for BPSK modulation using the integral expression derived in Equation 2.8 we require an expression for the moments of of γ_{egc} which is given in Equation 2.7. To use this expression for ABEP evaluation we also require an expression for $\mathrm{E}\left[\gamma_{1,s}^{k_1/2}\gamma_{2,s}^{k_2/2}\right]$, where k_1 and k_2 are integers and $\gamma_{1,s}$ and $\gamma_{2,s}$ are SNRs of the Hoyt faded signals received at the dual-EGC inputs.

For Hoyt distributed RVs $\alpha_{1,s}$ and $\alpha_{2,s}$, an expression for $E\left[\left(\frac{\alpha_{1,s}^2}{E[\alpha_{1,s}^2]}\right)^{n_1}\left(\frac{\alpha_{2,s}^2}{E[\alpha_{2,s}^2]}\right)^{n_2}\right]$ is pre-

sented in [35]. This expression cann be modified using the relation in Equation 3.4, i.e., $\gamma_{l,s} = \frac{E_g(\alpha_{l,s}^2)}{N_0}$ and the expression for $E\left[\gamma_{1,s}^{k_1/2}\gamma_{2,s}^{k_2/2}\right]$ can be obtained as shown in Appendix A.3, as

$$\begin{aligned} E\left[\gamma_{1,s}^{k_1/2}\gamma_{2,s}^{k_2/2}\right] &= \left(\frac{q}{1+q}\right)^{n_1+n_2} \sum_{t_1=0}^{n_1}\sum_{t_2=0}^{n_2} \frac{\Gamma(n_1+1)\Gamma(n_2+1)}{\Gamma(t_1+1)\Gamma(t_2+1)\Gamma(n_1-t_1+1)} \\ &\times \left(\frac{1}{q}\right)^{t_1+t_2} \frac{(2t_1)!(2n_1-2t_1)!}{\Gamma(n_2-t_2+1)} \left(\frac{\rho^2}{2}\right)^{n_1} \\ &\times \sum_{i_1=0}^{t_1}\sum_{j_1=0}^{n_1-t_1}\sum_{i_2=0}^{2t_1-2i_1}\sum_{j_2=\lceil i_2/2\rceil}^{n_1+\lfloor i_2/2\rfloor-t_1-j_1} (-1)^{i_2} \frac{[2(n_1+n_2-t_2-i_1-j_1-j_2)-1]!!}{(2t_1-2i_1-i_2)![2(n_1-t_1-j_1-j_2)+i_2]!} \\ &\times \frac{(2t_2+2j_2-1)!!(1-\rho^2)^{i_1+j_1}\bar{\gamma}_{1,s}^{n_1}\bar{\gamma}_{1,s}^{n_2}}{i_1!i_2!j_1!(2j_2-i_2)!\rho^{2(i_1+j_1)}}, \end{aligned} \tag{3.8}$$

where $n_1 = k_1/2$ and $n_2 = k_2/2$. Substituting Equations 3.6, 3.7 and 3.8 in Equation 3.5, the n^{th} moment of γ_{egc} can be written as

$$\begin{aligned} E\left[\gamma_{egc}^n\right] &= \frac{(2n)!}{8^n} \sum_{\substack{k_1=0 \\ k_2=2n-k_1}}^{2n} \left(\frac{q}{1+q}\right)^{n_1+n_2} \sum_{t_1=0}^{n_1}\sum_{t_2=0}^{n_2} \frac{\Gamma(n_1+1)\Gamma(n_2+1)}{\Gamma(t_1+1)\Gamma(t_2+1)\Gamma(n_1-t_1+1)} \\ &\times \sum_{t_1=0}^{n_1}\sum_{t_2=0}^{n_2} \frac{\Gamma(n_1+1)\Gamma(n_2+1)}{\Gamma(t_1+1)\Gamma(t_2+1)\Gamma(n_1-t_1+1)} \frac{(2t_1)!(2n_1-2t_1)!}{\Gamma(n_2-t_2+1)} \left(\frac{1}{q}\right)^{t_1+t_2} \left(\frac{\rho^2}{2}\right)^{n_1} \\ &\times \sum_{i_1=0}^{t_1}\sum_{j_1=0}^{n_1-t_1}\sum_{i_2=0}^{2t_1-2i_1}\sum_{j_2=\lceil i_2/2\rceil}^{n_1+\lfloor i_2/2\rfloor-t_1-j_1} (-1)^{i_2} \frac{[2(n_1+n_2-t_2-i_1-j_1-j_2)-1]!!}{(2t_1-2i_1-i_2)![2(n_1-t_1-j_1-j_2)+i_2]!} \\ &\times \frac{(2t_2+2j_2-1)!!(1-\rho^2)^{i_1+j_1}\bar{\gamma}_{1,s}^{n_1}\bar{\gamma}_{2,s}^{n_2}}{i_1!i_2!j_1!(2j_2-i_2)!\rho^{2(i_1+j_1)}k_1!k_2!} \prod_{l=1}^{2}\sum_{r=0}^{k_l} \binom{k_l}{r} \frac{I_{|2r-k_l|}\left(\frac{1}{\sigma_{\psi_{l,s}}{}^2}\right)}{I_0\left(\frac{1}{\sigma_{\psi_{l,s}}{}^2}\right)} \\ &\times \Psi\left(2m_iN, 2m_iN+1-n, \frac{2m_i}{\bar{\gamma}_i}\right). \end{aligned} \tag{3.9}$$

Thus, MGF of dual-EGC output SNR can be obtained from Equation 2.7 by substituting Equation 3.9 in it. The infinite series can be evaluated using the Padé approximation method discussed in Section 2.3.2. Then, the ABEP for BPSK modulation can be obtained by the numerical integration of Equation 2.8 using the above obtained MGF in it.

Numerical and Simulation Results

The ABEP performance of the dual-EGC receiver for correlated Hoyt fading channels is numerically evaluated and plotted in Figures 3.1-3.7, for BPSK modulation. The assumptions made in the numerical evaluations are $\sigma_{\psi_{1,s}} = \sigma_{\psi_{2,s}} = \sigma_{\psi}$ and $\bar{\gamma}_{1,s} = \bar{\gamma}_{2,s} = \bar{\gamma}$. Figure 3.1 represents the ABEP vs $\bar{\gamma}$, for $q = 1$, $m_i = 0.5$, $\bar{\gamma}_i = 1$, $\rho = 0$, for varying N. It can be observed that as N increases the ABEP decreases correspondingly, as expected, due to the increase in CCI signal. Table 3.1 tabulates the ABEP values for $\bar{\gamma} = 5$ dB as a function of N and σ_{ψ}. Figure 3.2 shows the ABEP vs $\bar{\gamma}$, for $\rho = 1$, $m_i = 0.5$, $\bar{\gamma}_i = 1$ dB, $N = 6$, $\sigma_{\psi} = 2^{\circ}, 8^{\circ}$ and for different values of q. As q decreases from 1 to 0.1 the ABEP decreases as smaller values of q indicate severe fading. For each value of q the ABEP is plotted for $\sigma_{\psi} = 2^{\circ}$ and 8°. Figure 3.3 shows the ABEP vs $\bar{\gamma}$, for $\rho = 0$, $N = 6$, $q = 1$, $\bar{\gamma}_i = 1$ dB, $\sigma_{\psi} = 2^{\circ}$ and 8°, and for different values of m_i. For $m_i = 0.5$ the ABEP is plotted for $\sigma_{\psi} = 8^{\circ}$. As the value of σ_{ψ} is decreased from 8° to 2° the performance relatively improves. As m_i increases from 0.5 to 1, the performance improves gradually. For each value of m_i, the ABEP is plotted for $\sigma_{\psi} = 2^{\circ}$ and 8°. Figure 3.4 shows the ABEP vs $\bar{\gamma}$, for $\rho = 0$, $m_i = 0.5$, $N = 6$, $q = 1$, $\sigma_{\psi} = 2^{\circ}$ and 8° and for different values of $\bar{\gamma}_i$. For $\bar{\gamma}_i$=1 dB, the ABEP is plotted for $\sigma_{\psi} = 2^{\circ}$ and 8°. It can be observed that as the value of $\bar{\gamma}_i$ is varied from 1 dB to 15 dB, the performance decreases gradually, as expected.

Comparisons:

Figure 3.5 shows the comparison of ABEP results with CCI and without CCI. The ABEP results with CCI represents the ABEP vs $\bar{\gamma}$, for $q = 1$, $m_i = 0.5$, $\bar{\gamma}_i = 1$ dB, $\rho = 0$, $N = 1$, and for $\sigma_{\psi} = 2^{\circ}$ and 8°. The ABEP results without CCI is plotted by the numerical evaluation of [19, (9),(12)] for $\bar{\gamma}_s$, with m=1, $\rho = 0$ and $\sigma_{\psi} = 2^{\circ}$ and 8°. On comparison it can be observed that, in the absence of CCI, an ABEP value of 10^{-2} is reached at an SNR of 5dB whereas in the presence of CCI it requires an SNR penalty of approximately 2.5 dB to reach the same value of ABEP. Figure 3.6 shows the ABEP for a range of σ_{ψ} from 2° to 8°. The SNR penalty for reaching an ABEP value of 10^{-2}, is approximately 0.6 dB for small values of ρ and is approximately 0.3 dB for higher values of ρ. In all figures computer simulation results are also plotted to verify the correctness of the numerical

results. The simulation results being exact becomes at different points from the numerical results with it on an average. Figure 3.7 shows the ABEP vs $\bar{\gamma}$, for $\rho = 0$, $m_i = 0.5$, $N = 6$, $q = 1$, $\bar{\gamma}_i = 1$ dB and $\sigma_\psi = 0.5^\circ, 2^\circ$ and 8°. The ABEP for $\sigma_\psi = 0.5^\circ$ is plotted as a reference.

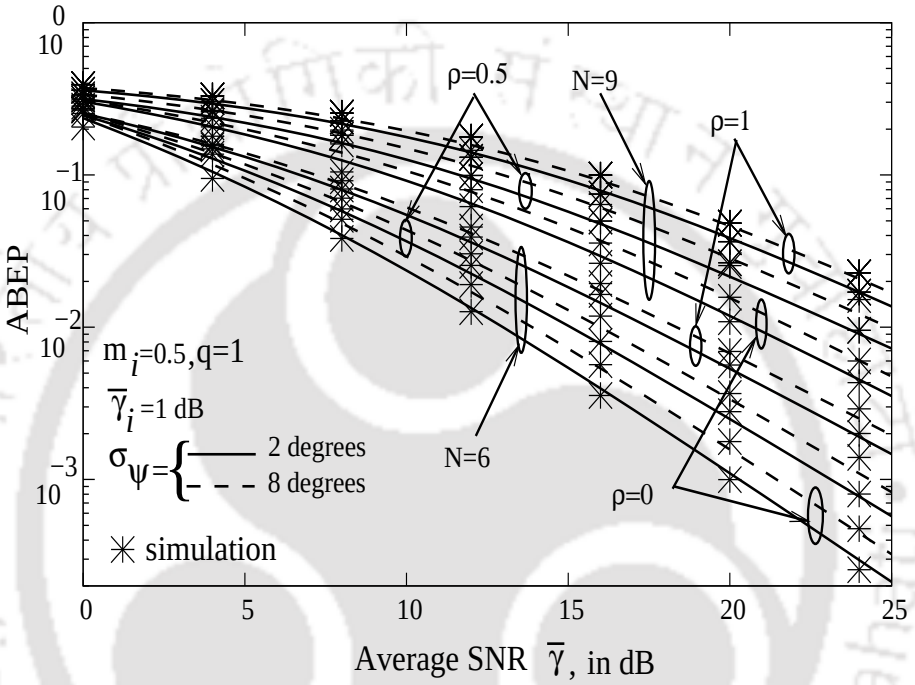

Figure 3.1: ABEP in correlated Hoyt fading channels with varying N and ρ.

Table 3.1: ABEP in correlated Hoyt fading channels with varying N, σ_ψ at $\bar{\gamma} = 5$ dB.

	ABEP	
N	$\sigma_\psi = 2^\circ$	$\sigma_\psi = 8^\circ$
6	0.0837172	0.0949952
8	0.184664	0.207626

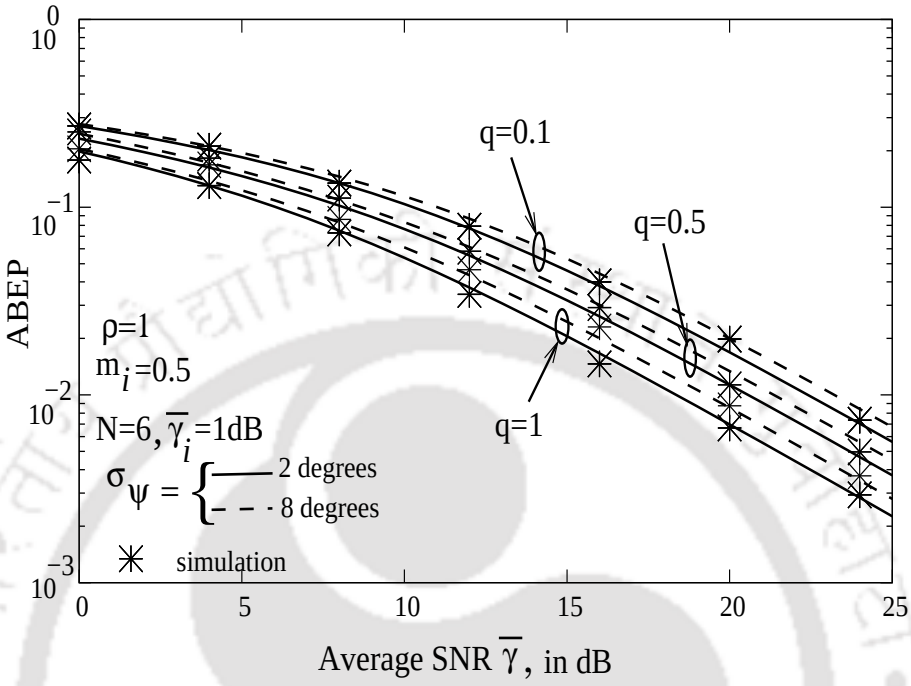

Figure 3.2: Effect of q on ABEP in correlated Hoyt fading channels.

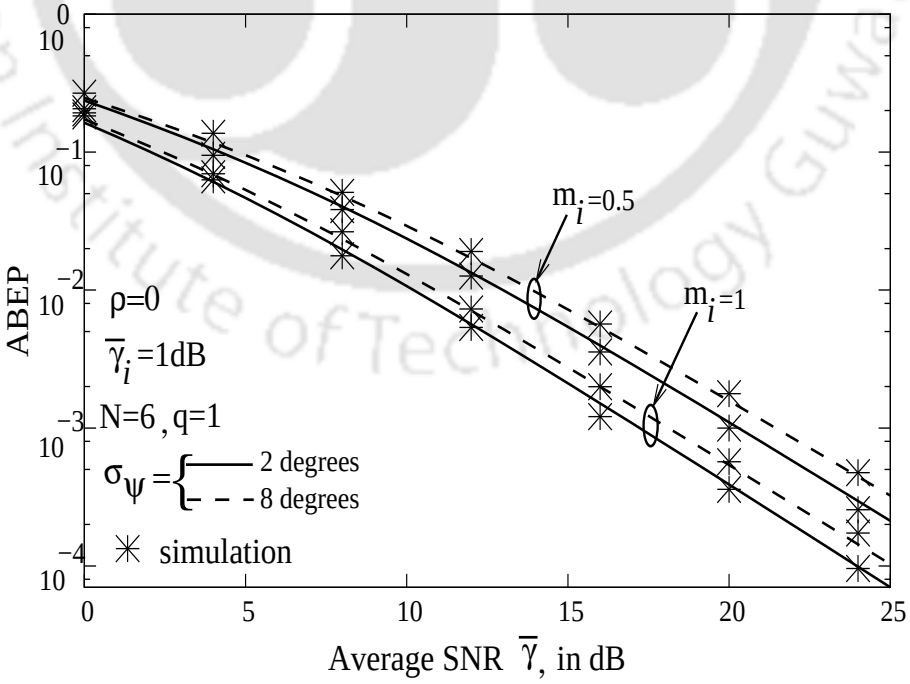

Figure 3.3: Effect of m_i on ABEP in correlated Hoyt fading channels.

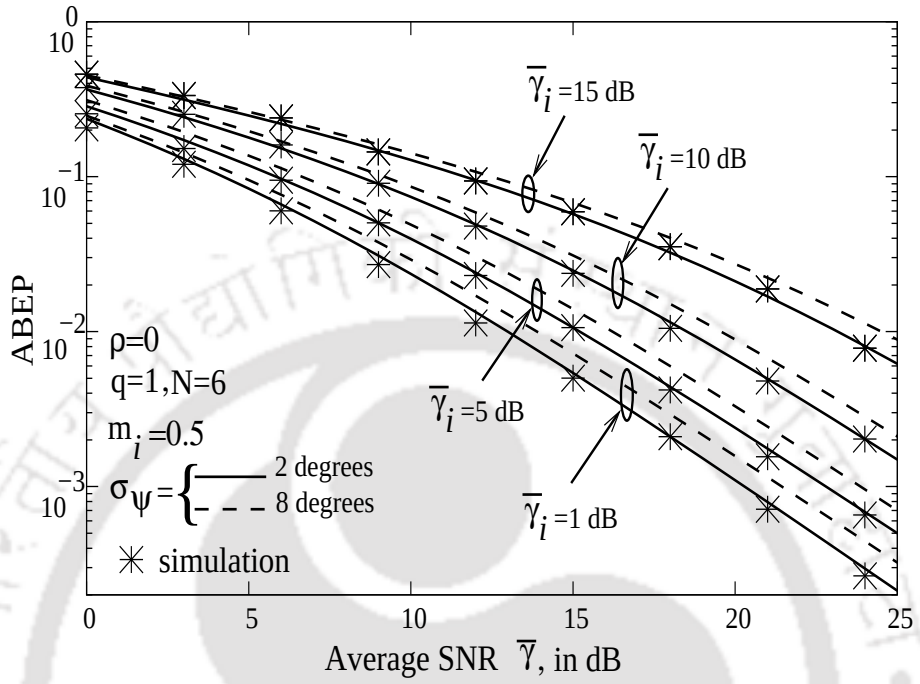

Figure 3.4: ABEP in correlated Hoyt fading channels with varying $\bar{\gamma}_i$.

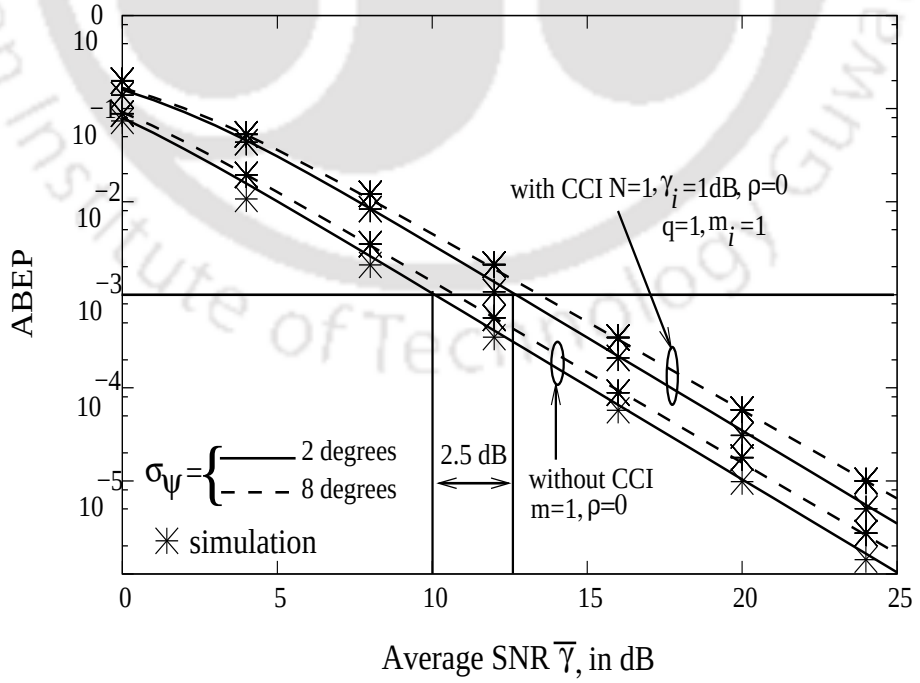

Figure 3.5: Comparison of ABEP of in correlated Hoyt fading channels with and without CCI.

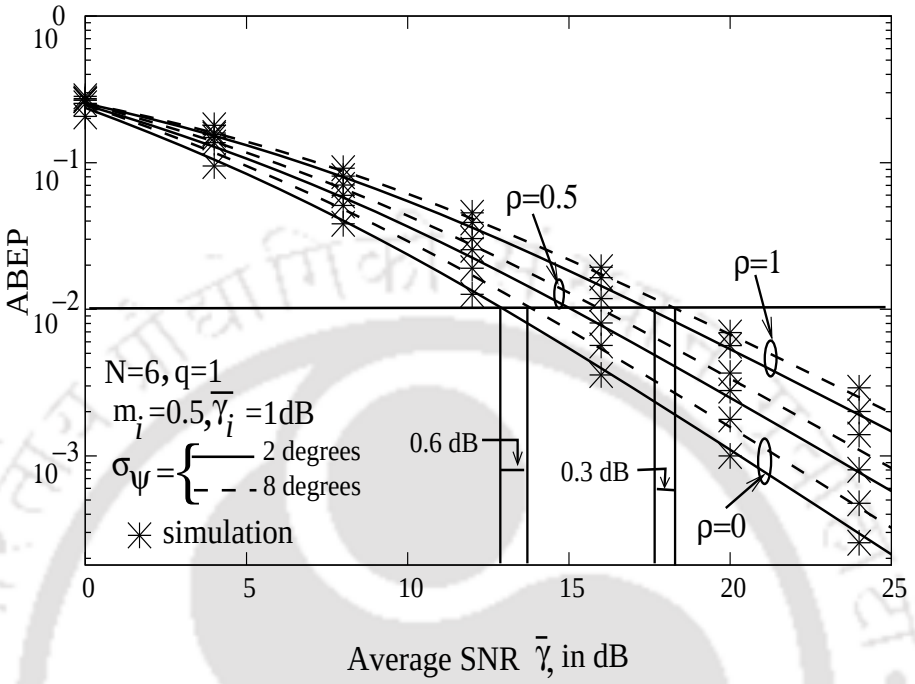

Figure 3.6: ABEP in correlated Hoyt fading channels with varying ρ .

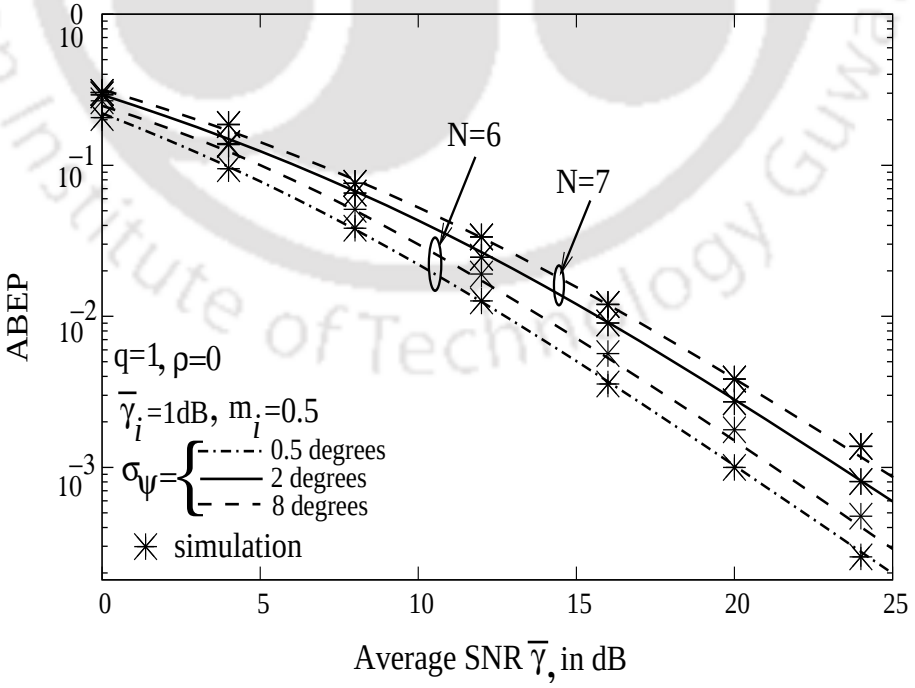

Figure 3.7: ABEP in correlated Hoyt fading channels with $N = 6$ and $N = 7$.

Table 3.2: ABEP in correlated Hoyt fading channels with varying N, ρ, σ_ψ .

SNR (dB)	ρ	$N = 6$	
		$\sigma_\psi = 2^\circ$	$\sigma_\psi = 8^\circ$
5	0	0.0837172	0.0949952
	0.5	0.106586	0.117194
10	0	0.023597	0.0291533
	0.5	0.0367018	0.0434257

3.1.3 Composite and Non-homogeneous Fading Channels

Channel and Receiver Model

According to the system model described by Equation 2.2, in this case the desired user signal is assumed to be transmitted through a slowly varying fading channel which may be either correlated GG distributed, or correlated K_G distributed or i.i.d $\kappa-\mu$ or i.i.d $\eta-\mu$ distributed fading channels. The marginal PDF for these distributions are presented in Equations 1.6, 1.7, 1.8 and 1.9, respectively. The interfering signal is assumed to be Nakagami-m distributed and to simplify the analysis τ_i is assumed to be zero. Accordingly, for the n^{th} moment of EGC in Equation 3.5 we need to obtain the expression for $E\left[\gamma_{1,s}^{\frac{k_1}{2}}\gamma_{2,s}^{\frac{k_2}{2}}\right]$ to obtain the ABEP. Expressions for this expectation depends on the fading distributions. These are obtained below for each type of fading channel mentioned above.

1. For GG distribution the marginal PDF is given in Equation 1.6. An expression for $E\left[\gamma_{1,s}^{\frac{k_1}{2}}\gamma_{2,s}^{\frac{k_2}{2}}\right]$ is derived in Appendix A.4 (Equation A.18) as [8, 50]

$$E\left[\gamma_{1,s}^{\frac{k_1}{2}}\gamma_{2,s}^{\frac{k_2}{2}}\right] = \frac{\bar{\gamma}_{1,s}^{\frac{k_1}{2}}\bar{\gamma}_{2,s}^{\frac{k_2}{2}}\Delta^{\frac{k_1+k_2}{2}}}{[\Gamma(m_g)]^2}\Gamma\left(m_g+\frac{k_1}{\beta_g}\right)\Gamma\left(m_g+\frac{k_2}{\beta_g}\right){}_2F_1\left(-\frac{k_1}{\beta_g},-\frac{k_2}{\beta_g},m_g,\rho\right), \tag{3.10}$$

where $\Gamma(\cdot)$ is the Gamma function, ${}_2F_1(\cdot,\cdot,\cdot,\cdot)$ is the Gauss hypergeometric function, $m_g = m_1 = m_2$, $\Delta = \frac{\Gamma(m_g)}{\Gamma\left(m_g+\frac{2}{\beta_g}\right)}$, $\beta_g = \beta_1 = \beta_2 \geq 0$ is the shaping parameter and ρ is the correlation coefficient [50].

2. For K_G distribution, the marginal PDF is given in Equation 1.7. An expression for $E\left[\gamma_{1,s}^{\frac{k_1}{2}}\gamma_{2,s}^{\frac{k_2}{2}}\right]$ is derived in Appendix A.5 (Equation A.21) as [5, 51]

$$E\left[\gamma_{1,s}^{\frac{k_1}{2}}\gamma_{2,s}^{\frac{k_2}{2}}\right] = \bar{\gamma}_{1,s}^{\frac{k_1}{2}}\bar{\gamma}_{2,s}^{\frac{k_2}{2}}\prod_{l=1}^{2}\frac{\Gamma\left(m_k+\frac{k_l}{2}\right)\Gamma\left(\beta_k+\frac{k_l}{2}\right)}{\Gamma(m_k)\Gamma(\beta_k)m_k^{\frac{k_l}{2}}\beta_k^{\frac{k_l}{2}}} \times {}_2F_1\left(-\frac{k_1}{2},-\frac{k_2}{2},m_k,\rho\right){}_2F_1\left(-\frac{k_1}{2},-\frac{k_2}{2},\beta_k,\rho\right), \tag{3.11}$$

where ρ is the correlation coefficient, m_k and β_k are the Generalized-$K(K_G)$ fading parameters

[5].

3. For $\eta-\mu$ distribution the marginal PDF is given in Equation 1.9. An expression for $E\left[\gamma_{l,s}^{\frac{k_1}{2}}\right]$ presented in [12, 13] can be given as

$$E\left[\gamma_{l,s}^{k_l/2}\right] = \frac{\Gamma(2\mu_l+k_l/2)}{\left(2+\eta_l^{-1}+\eta_l\right)^{\mu_l+k_l/2}}\frac{2^{2\mu_l+k_l/2}\bar{\gamma}_{l,s}^{k_l/2}}{(2\mu_l)^{k_l/2}\Gamma(2\mu_l)} \times {}_2F_1\left(\mu_l+\frac{k_l}{4}+\frac{1}{2},\mu_l+\frac{k_l}{4},\mu_l+\frac{1}{2},\left(\frac{1-\eta_l}{1+\eta_l}\right)^2\right). \tag{3.12}$$

4. For $\kappa-\mu$ distribution the marginal PDF is given in Equation 1.8. An expression for $E\left[\gamma_{l,s}^{\frac{k_1}{2}}\right]$ can be given as [11, 12]

$$E\left[\gamma_{l,s}^{k_l/2}\right] = \frac{\Gamma(\mu_l+k_l/2)\exp(-\kappa_l\mu_l)\bar{\gamma}_{l,s}^{k_l/2}}{[(1+\kappa_l)\mu_l]^{k_l/2}\Gamma(\mu_l)}{}_1F_1\left(\mu_l+\frac{k_l}{2},\mu_l,\kappa_l\mu_l\right). \tag{3.13}$$

where ${}_1F_1(\cdot,\cdot,\cdot)$ is the confluent hypergeometric function [10, (9.210.1)].

Moments of Output SINR

1. Substituting Equations 3.6, 3.7, and 3.10 in Equation 3.5 and simplifying the resulting expression, we obtain $E[\gamma_{egc}^n]$ for GG distribution which is given by

$$E[\gamma_{egc}^n] = \frac{(2n)!}{8^n}\sum_{\substack{k_1=0\\k_2=2n-k_1}}^{2n}\frac{1}{k_1!k_2!}\frac{\left(\bar{\gamma}_{1,s}\right)^{\frac{k_1}{2}}\left(\bar{\gamma}_{2,s}\right)^{\frac{k_2}{2}}\Delta^{\frac{k_1+k_2}{2}}}{[\Gamma(m_g)]^2} \times\Gamma\left(m_g+\frac{k_1}{\beta_g}\right)\Gamma\left(m_g+\frac{k_2}{\beta_g}\right){}_2F_1\left(-\frac{k_1}{\beta_g},-\frac{k_2}{\beta_g},m_g,\rho\right)\prod_{l=1}^{2}\sum_{q=0}^{k_l}\binom{k_l}{q}\frac{I_{|2q-k_l|}\left(\varsigma_{l,s}\right)}{I_0\left(\varsigma_{l,s}\right)} \times\Psi\left(2m_iN,2m_iN+1-n,\frac{2m_i}{\bar{\gamma}_i}\right). \tag{3.14}$$

2. Substituting Equations 3.6, 3.7, and 3.11 in Equation 3.5 and simplifying the resulting ex-

pression, we obtain $E[\gamma_{egc}^n]$ for K_G distribution and it is given by

$$E\left[\gamma_{egc}^n\right] = \frac{(2n)!}{8^n} \sum_{\substack{k_1=0 \\ k_2=2n-k_1}}^{2n} \frac{\left(\bar{\gamma}_{1,s}\right)^{\frac{k_1}{2}} \left(\bar{\gamma}_{2,s}\right)^{\frac{k_2}{2}}}{k_1!k_2!} \left\{ \prod_{l=1}^{2} \frac{\Gamma\left(m_k+\frac{k_l}{2}\right)\Gamma\left(\beta_k+\frac{k_l}{2}\right)}{\Gamma(m_k)\Gamma(\beta_k)m_k^{\frac{k_l}{2}}\beta_k^{\frac{k_l}{2}}} \right\}$$
$$\times {}_2F_1\left(-\frac{k_1}{2},-\frac{k_2}{2},m_k,\rho\right) {}_2F_1\left(-\frac{k_1}{2},-\frac{k_2}{2},\beta_k,\rho\right) \left\{ \prod_{l=1}^{2} \sum_{q=0}^{k_l} \binom{k_l}{q} \frac{I_{|2q-k_l|}\left(\varsigma_{l,s}\right)}{I_0\left(\varsigma_{l,s}\right)} \right\}$$
$$\times \Psi\left(2m_iN, 2m_iN+1-n, \frac{2m_i}{\bar{\gamma}_i}\right). \tag{3.15}$$

3. Substituting Equations 3.6, 3.7 and 3.12, in Equation 3.5 and simplifying the resulting expression, we obtain $E[\gamma_{egc}^n]$ for $\eta-\mu$ distribution and it is given by

$$E\left[\gamma_{egc}^n\right] = \frac{(2n)!}{8^n} \sum_{\substack{k_1=0 \\ k_2=2n-k_1}}^{2n} \prod_{l=1}^{2} \frac{2^{2\mu_l+k_l/2}\Gamma\left(2\mu_l+k_l/2\right)\bar{\gamma}_{l,s}^{k_l/2}}{\Gamma\left(2\mu_l\right)k_l!\left(2+\eta_l^{-1}+\eta_l\right)^{\mu_l+k_l/2}(2\mu_l)^{k_l/2}}$$
$$\times {}_2F_1\left(\mu_l+\frac{k_l}{4}+\frac{1}{2},\mu_l+\frac{k_l}{4},\mu_l+\frac{1}{2},\left(\frac{1-\eta_l}{1+\eta_l}\right)^2\right) \sum_{q=0}^{k_l} \binom{k_l}{q} \frac{I_{|2q-k_l|}\left(\varsigma_{l,s}\right)}{I_0\left(\varsigma_{l,s}\right)}$$
$$\times \Psi\left(2m_iN, 2m_iN+1-n, \frac{2m_i}{\bar{\gamma}_i}\right), \tag{3.16}$$

where $\eta_1=\eta_2=\eta$, $0<\eta<1$ and $\mu_1=\mu_2=\mu$, $\mu>0$ are the $\eta-\mu$ fading parameters [13].

4. Substituting Equations 3.6, 3.7 and 3.13 in Equation 3.5 and simplifying the resulting expression, we obtain $E[\gamma_{egc}^n]$ for $\kappa-\mu$ distribution and it is given by

$$E\left[\gamma_{egc}^n\right] = \frac{(2n)!}{8^n} \sum_{\substack{k_1=0 \\ k_2=2n-k_1}}^{2n} \prod_{l=1}^{2} \frac{\Gamma\left(\mu_l+k_l/2\right)\exp\left(-\kappa_l\mu_l\right)\bar{\gamma}_{l,s}^{k_l/2}}{\Gamma\left(\mu_l\right)k_l!\left[\left(1+\kappa_l\right)\mu_l\right]^{k_l/2}}$$
$$\times {}_1F_1\left(\mu_l+\frac{k_l}{2},\mu_l,\kappa_l\mu_l\right) \sum_{q=0}^{k_l} \binom{k_l}{q} \frac{I_{|2q-k_l|}\left(\varsigma_{l,s}\right)}{I_0\left(\varsigma_{l,s}\right)}$$
$$\times \Psi\left(2m_iN, 2m_iN+1-n, \frac{2m_i}{\bar{\gamma}_i}\right), \tag{3.17}$$

where $\kappa_1=\kappa_2=\kappa$, $0<\kappa<1$ and $\mu_1=\mu_2=\mu$, $\mu>0$ are the $\kappa-\mu$ fading parameters [11].

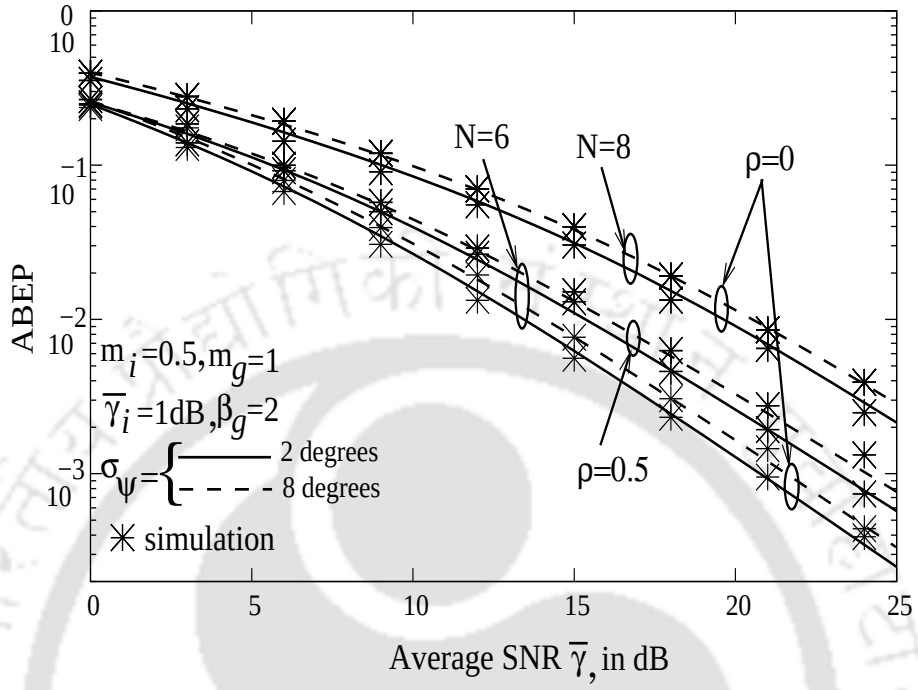

Figure 3.8: ABEP in GG fading channels with $\sigma_\psi = 2^\circ, 8^\circ$, m_g=1, $\beta_g = 2$, varying N and ρ.

Numerical and Simulation Results

The ABEP performance of the EGC receiver for GG fading channels is numerically evaluated using the method in Section 3.1.1 and are plotted in Figures 3.8 - 3.11 for BPSK modulation. The values for different parameters in the figures are chosen arbitrarily for the purpose of demonstration and covers the entire range off parameters in suitable subdivisions. In the numerical evaluation it is assumed that $\sigma_{\psi_{1,s}} = \sigma_{\psi_{2,s}} = \sigma_\psi$ and $\overline{\gamma}_{1,s} = \overline{\gamma}_{2,s} = \overline{\gamma}$. In all the graphs when σ_ψ is varied from 2° to 8°, the ABEP degrades gradually. Figure 3.8 shows the ABEP vs. average SNR (in dB) for m_g = 1, β_g = 2, m_i = 0.5, and different values of N, ρ and σ_ψ. With the increase in N, ρ the ABEP is observed to be degrading. Table 3.3 shows different values of N, ρ and σ_ψ for *GG*. The values of m_g = 1, β_g = 2 is the condition for Rayleigh in GG fading. The results closely approximates the results for Rayleigh in the previous section of correlated Hoyt fading channels. Figure 3.9 shows the ABEP for varying m_g. When m_g is increased from 0.5 to 1 and 2 the ABEP values improves. Figure 3.10 shows the ABEP results for different values of m_i. Figure 3.11 shows the ABEP results for different

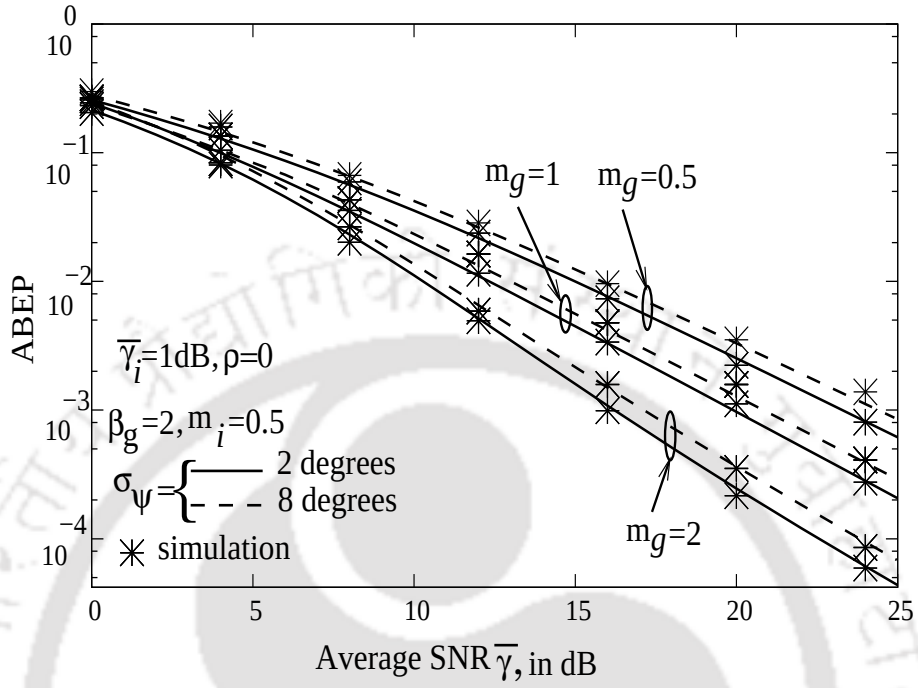

Figure 3.9: ABEP in GG fading channels with $\sigma_\psi = 2^\circ, 8^\circ$, $\beta_g = 2$ and varying m_g.

values of $\overline{\gamma}_i$.

For K_G fading channel, Figure 3.12 shows the ABEP vs average SNR in (dB) for different values of N, ρ, σ_ψ. Table 3.4 shows different values of N, ρ and σ_ψ for K_G. Figure 3.13 shows ABEP results for different values of m_k. Figure 3.14 shows the ABEP of $\eta - \mu$ fading. Figure 3.15 shows the ABEP of $\kappa - \mu$ fading. Simulation results for ABEP are also plotted in the figures. A close match between both numerical and simulation results can be observed. In all figures computer simulation results are also plotted to verify the correctness of the numerical results. The simulation results on an average match with the numerical results.

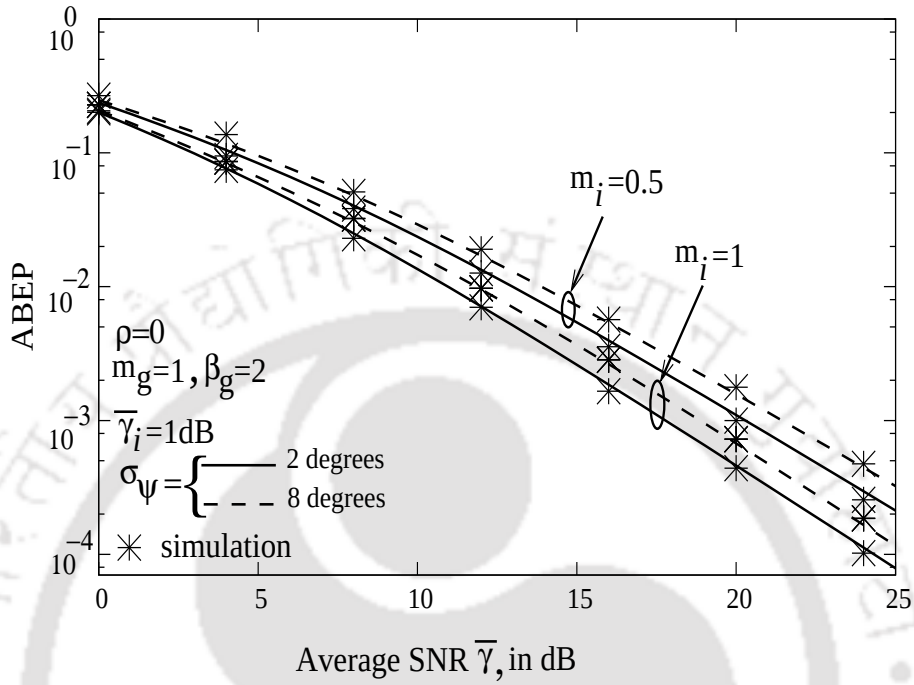

Figure 3.10: ABEP in GG fading channels with $\sigma_\psi = 2^\circ, 8^\circ$, $m_g = 1$, $\beta_g = 2$ and varying m_i.

Table 3.3: ABEP in GG fading channels with varying N, ρ and σ_ψ.

SNR (dB)	ρ	$N = 6$	
		$\sigma_\psi = 2^\circ$	$\sigma_\psi = 8^\circ$
5	0	0.0815126	0.0837172
	0.5	0.112373	0.119031
10	0	0.0207825	0.0233184
	0.5	0.0397035	0.0445481

Table 3.4: ABEP in K_G fading channels with varying N, ρ and σ_ψ .

SNR (dB)	ρ	$N = 6$	
		$\sigma_\psi = 2^\circ$	$\sigma_\psi = 8^\circ$
5	0	0.0456125	0.0508464
	0.5	0.0607775	0.0740016
10	0	0.0117354	0.0133339
	0.5	0.0213264	0.0266639

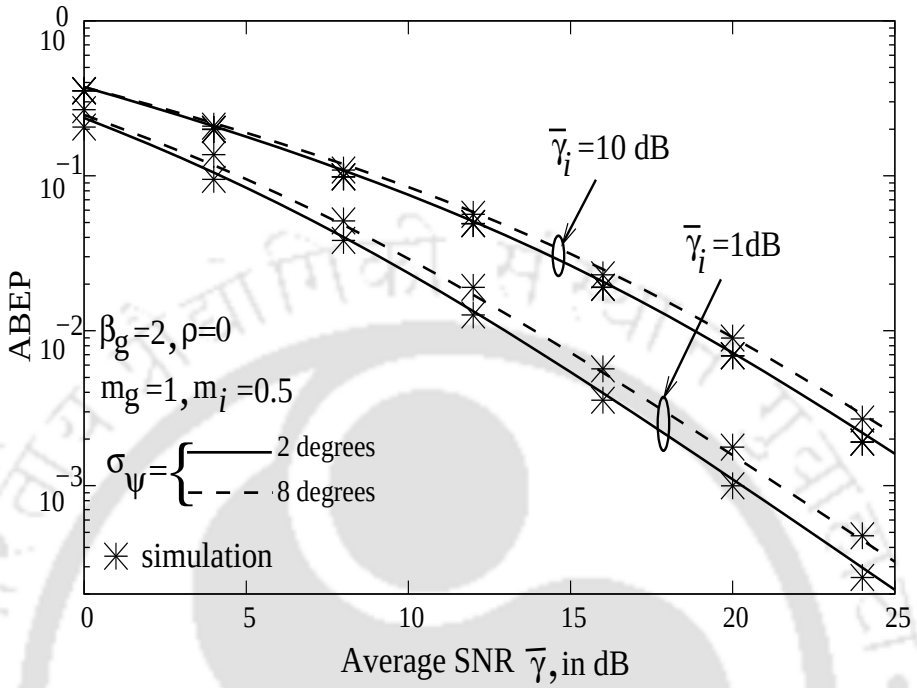

Figure 3.11: ABEP in GG fading channels with $\sigma_\psi = 2^\circ, 8^\circ$, m_g = 1,$\beta_g = 2$ and varying $\bar{\gamma}_i$.

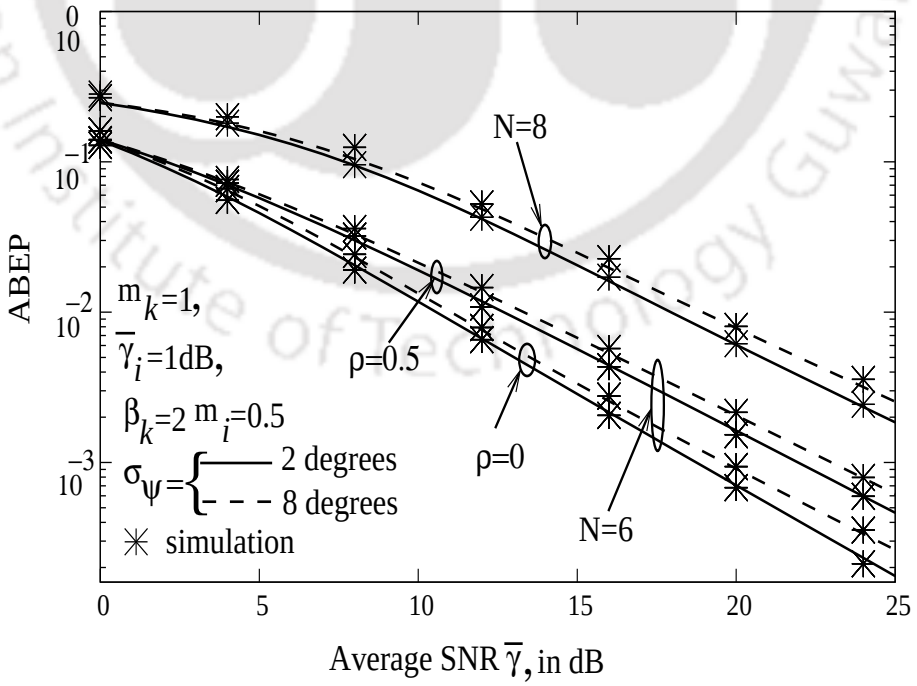

Figure 3.12: ABEP in K_G fading channels with $\sigma_\psi = 2^\circ, 8^\circ$ and varying ρ, N.

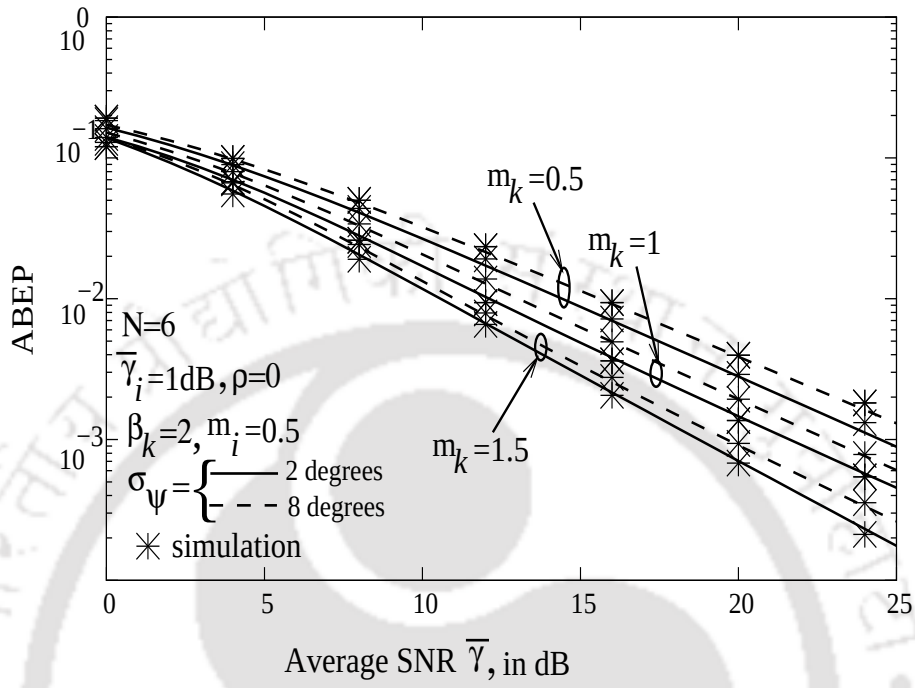

Figure 3.13: ABEP in K_G fading channels with $\sigma_\psi = 2^\circ, 8^\circ$ and varying m_k.

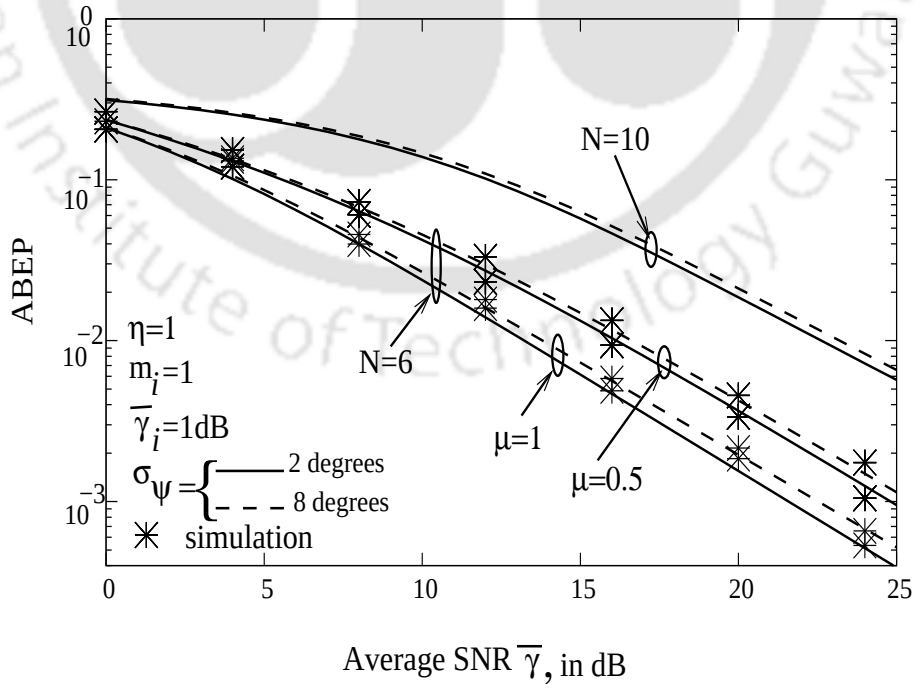

Figure 3.14: ABEP in $\eta - \mu$ fading channels with $\sigma_\psi = 2^\circ, 8^\circ$ and varying N and μ.

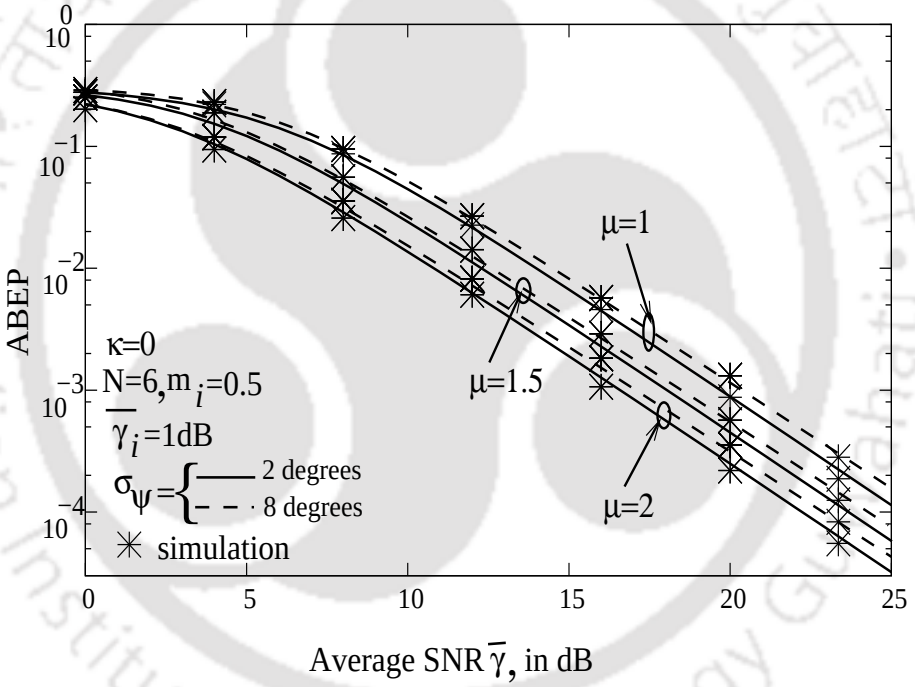

Figure 3.15: ABEP in $\kappa-\mu$ fading channel with $\sigma_\psi = 2^\circ, 8^\circ$, $\kappa = 0$ and varying μ.

3.1.4 Independent Nakagami-*m* Fading Channels

In this case ABEP performance of a dual branch EGC receiver is analyzed assuming the desired user's channel is Nakagami-*m* distributed. The CCI signals are assumed to be asynchronous i.e., $\tau_i \neq 0$. The interfering signals are also assumed to be Nakagami-*m* distributed. Closed form expression for moments of the combiner output SINR is derived. Using the obtained expression, ABEP for BPSK modulation is obtained applying moment generating function and Padé approximation approach.

Channel and Receiver Model

The desired signal is transmitted through a slowly varying Nakagami-*m* fading channel. We assume N CCI users in the system and the channel between a CCI user and the desired user's receiver is a Nakagami-*m* distributed. Assuming the desired user and N CCI users are transmitting asynchronously, the transmitted signals can be given as

$$\begin{aligned} s_s(t) &= \sqrt{P_s T} \sum_{m=-\infty}^{\infty} a_s[m] h_T(t-mT), \\ s_i(t) &= \sqrt{P_i T} \sum_{m=-\infty}^{\infty} a_i[m] h_T(t-mT-\tau_i), i = 1,2,\ldots,N, \end{aligned} \tag{3.18}$$

where a_s and a_i are information bits of the desired and i^{th} CCI user, respectively, P_s and P_i are transmitted powers of the desired user and the i^{th} CCI user, respectively, $\alpha_{l,s}$ is Nakagami-*m* distributed with fading parameter m_l, $\alpha_{l,i}$ is i.i.d Nakagami-*m* RV with fading parameter m_i. The function $h_T(t)$ is the transmitter impulse response, with a square root raised cosine pulse with a roll-off factor β.

Substituting Equation 3.18 in Equation 2.2 the complex baseband received signal can be obtained as

$$r_l(t) = \sqrt{P_s T}\alpha_{l,s} e^{j\phi_{l,s}} \sum_{m=-\infty}^{\infty} a_s[m] h_T(t-mT) + \sum_{i=1}^{N} \sqrt{P_i T}\alpha_{l,i} e^{j\phi_{l,i}} \sum_{m=-\infty}^{\infty} a_i[m] h_T(t-mT-\tau_i) + n_{l,s}(t). \tag{3.19}$$

The demodulated signal at the combiner output at the sampling instant nT can be derived as [22,29]

$$y[n] = \sum_{l=1}^{L} \sqrt{P_s T}\alpha_{l,s} e^{j\psi_{l,s}} a_s[n] + \sum_{l=1}^{L}\sum_{i=1}^{N} \sqrt{P_i T}\alpha_{l,i} e^{j(\phi_{l,i}-\widehat{\phi}_{l,s})} z_i[n] + \sum_{l=1}^{L} v[n] e^{-j\widehat{\phi}_{l,s}}, \tag{3.20}$$

where the interference source is represented by a random time series $z_i[n]$ as

$$z_i[n] = \sum_{m=-\infty}^{\infty} a_i[m] h(nT - mT - \tau_i) \tag{3.21}$$

where h(t) is the Nyquist pulse. Each of the interference source is represented by a random time series $z_i[n]$, with following properties (1). $E\{z_i[n]\}$=0, (2). $E\{|z_i[n]|^2\} = 1 - (\beta/4)$ [33], (3). $E\{z_i[n]z_j^*[n]\} = 0$, for $i \neq j$ [22, 24, 28] and $*$ denotes the complex conjugate operation and the square root raised cosine pulse can be given by [15]

$$h(t) = \frac{\sin\left[\pi\frac{t}{T_s}(1-\beta)\right] + 4\beta\frac{t}{T_s}\cos\left[\pi\frac{t}{T_s}(1+\beta)\right]}{\pi\frac{t}{T_s}\left[1-\left(4\beta\frac{t}{T_s}\right)^2\right]} \tag{3.22}$$

where T_s is the symbol duration and β is the roll of factor.

Moments of Output SINR

The n^{th} moment of the output SINR for asynchronous case, derived in Appendix A.6, can be given as

$$E\left[\gamma_{egc}^n\right] = \frac{(2n)!}{2^n} \sum_{\substack{k_1=0 \\ k_2=2n-k_1}}^{2n} \frac{E\left[\gamma_{1,s}^{k_1/2}\gamma_{2,s}^{k_2/2}\right]}{k_1!k_2!} \prod_{l=1}^{2} E\left[\cos^{k_l}\left(\psi_{l,s}\right)\right] E\left[\left(\left(1 + r\sum_{i=1}^{N}\sum_{l=1}^{2}\left[\gamma_{l,i}\right]\right)\right)^{-n}\right], \tag{3.23}$$

where $r = \frac{1-\frac{\beta}{4}}{2}$. For Nakagami- m distributed RVs $\alpha_{l,i}$, an expression for $E\left[\left(\frac{1}{\left(1+r\sum_{i=1}^{N}\sum_{l=1}^{2}\gamma_{l,i}\right)}\right)^n\right]$ can be given as (Appendix A.6)

$$E\left[\left(\frac{1}{\left(1+r\sum_{i=1}^{N}\sum_{l=1}^{2}\gamma_{l,i}\right)}\right)^n\right] = \Psi\left(2m_iN, 2m_iN+1-n, \frac{m_i}{r\bar{\gamma}_i}\right). \tag{3.24}$$

Substituting Equations 3.6, 3.7 and 3.24 in Equation 3.23 and on simplifying the resulting expression, we obtain

$$\bar{\gamma}_{egc}^{n} = \frac{(2n)}{8^n} \sum_{\substack{k_1=0 \\ k_2=2n-k_1}}^{2n} \prod_{l=1}^{2} \frac{\Gamma\left(m_l+\frac{k_l}{2}\right)\bar{\gamma}_{l,s}^{k_l/2}}{\Gamma(m_l)\, m_l^{\frac{k_l}{2}} k_l!} \sum_{r=0}^{k_l} \binom{k_l}{r} \frac{I_{|2r-k_l|}\left(\frac{1}{{\sigma_{\psi_{l,s}}}^2}\right)}{I_0\left(\frac{1}{{\sigma_{\psi_{l,s}}}^2}\right)} \times \Psi\left(2m_iN, 2m_iN+1-n, \frac{m_i}{r\bar{\gamma}_i}\right) \tag{3.25}$$

where $\bar{\gamma}_{l,s} = \frac{E_g E[\alpha_{l,s}^2]}{N_0}$, is the average SNR of the desired user's signal at the l^{th} input branch.

The evaluation of the ABEP is based on the Gaussian assumption for the interference. Particularly, the interference term $\sum_{l=1}^{L}\sum_{i=1}^{N}\sqrt{P_iT}\alpha_{l,i}e^{j(\phi_{l,i}-\widehat{\phi}_{l,s})}z_i[n]$ in Equation 3.20 is assumed to have a Gaussian distribution as discussed in Section 2.2. ABEP results have been analyzed in based on Gaussian assumption in [28], [25], [44]- [45].

Numerical and Simulation Results

ABEP performance for Nakagami-*m* fading channels is numerically evaluated, following the numerical evaluation method discussed in Section 3.1.1, and the plots are shown in Figures 3.16-3.19 for BPSK modulation. The assumptions taken are: $\sigma_{\psi_{1,s}} = \sigma_{\psi_{2,s}} = \sigma_\psi$, $\bar{\gamma}_{1,s} = \bar{\gamma}_{2,s} = \bar{\gamma}$, $m_1 = m_2 = m$, $\beta = 1$. Figure 3.16 shows ABEP vs. $\bar{\gamma}$ (in dB) for $m = 1$, $m_i = 0.5$, $\bar{\gamma}_i = 1$ dB, $N = 6$, 7 and 8, and σ_ψ = 2° and 8°. ABEP degrades with increase in N and σ_ψ. For example, for $\sigma_\psi = 2°$ when N increases from 6 to 7 and 8 ABEP at $\bar{\gamma} = 10$ dB degrades from 0.0166352, to 0.0304774 and 0.0991738, respectively. Similar observations can be seen for $\sigma_\psi = 8°$ with varying N. Table 3.5 tabulates ABEP values for $\bar{\gamma} = 5$ dB as a function of N and σ_ψ. Figure 3.17 shows ABEP vs. $\bar{\gamma}$ for $\bar{\gamma}_i = 1$ dB, $N = 6$, $\sigma_\psi = 2°$ and 8° and varying m and m_i. As m decreases ABEP degrades as smaller values of m indicate increase in fading. ABEP degrades with decrease in m and with increase in σ_ψ. For example, for $\sigma_\psi = 2°$, when m decreases from 1 to 0.5 the ABEP at $\bar{\gamma} = 10$ dB degrades from 0.0166352 to 0.0281243 respectively. Similar observations can be seen for σ_ψ = 8° with varying m. Figure 3.17 also shows ABEP vs. $\bar{\gamma}$ for $N = 6$, $\bar{\gamma}_i$ = 1 dB, σ_ψ = 2° and 8°, and varying m_i. ABEP

degrades with decrease in m_i and with increase in σ_ψ. For σ_ψ = 2°, when m_i decreases from 2 to 1, ABEP at $\bar{\gamma}$ = 10 dB degrades from 0.00549599 to 0.0166352. Figure 3.18 shows ABEP vs. $\bar{\gamma}$ for m=1, N =6, m_i = 0.5, $\sigma_\psi = 2^\circ$ and 8° and for different values of $\bar{\gamma}_i$. ABEP degrades with increase in $\bar{\gamma}_i$ and with increase in σ_ψ. For $\sigma_\psi = 2^\circ$, when $\bar{\gamma}_i$ increases from 1 to 8, 12 dB the ABEP at $\bar{\gamma} = 10$ dB degrades from 0.0166352 to 0.0566119 and 0.0991037, respectively.

Figure 3.19 illustrates comparison between the synchronous and asynchronous cases, of CCI. It can be observed that the asynchronous case gives a better performance than the synchronous case. It is because of the fact that synchronous case gives an over-estimation of the CCI power compared to asynchronous case as discussed in Section 2.1. Similar results are also reported in [29,33,41,52,53]. In all figures computer simulation results are also plotted to verify the correctness of the numerical results. The simulation results closely matches with the numerical results.

Table 3.5: ABEP in Nakagami-*m* fading channels varying N, σ_ψ for $\bar{\gamma} = 10$ dB.

	ABEP	
N	σ_ψ = 2°	σ_ψ = 8°
6	0.0166352	0.0199104
7	0.0304774	0.0326223
8	0.0991738	0.111275

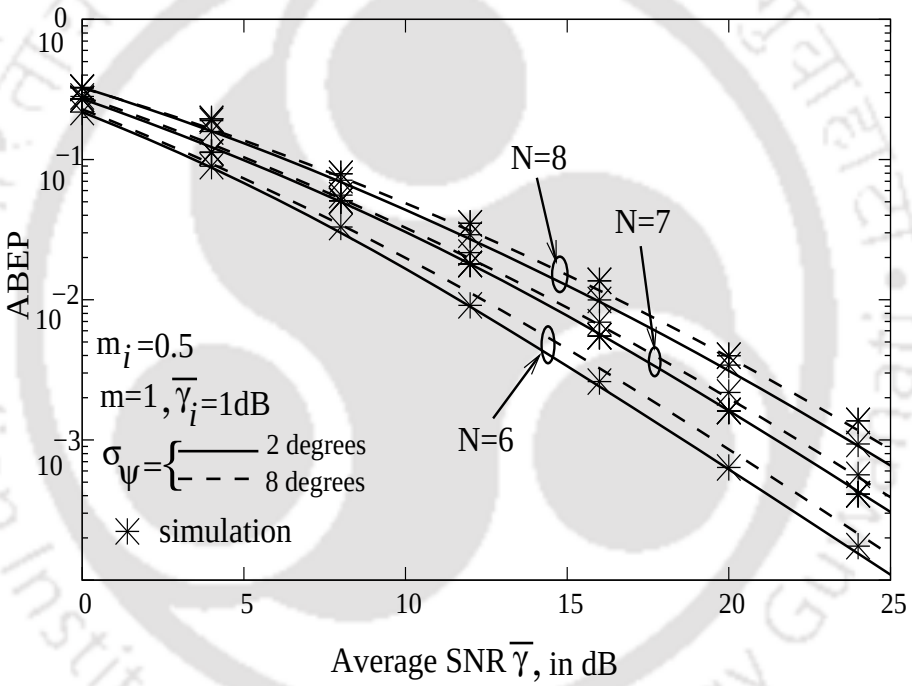

Figure 3.16: ABEP in independent Nakagami-*m* fading channels with $\sigma_\psi = 2^\circ, 8^\circ$, $m = 1$, m_i=1 and $\bar{\gamma}_i = 1$ dB with varying N.

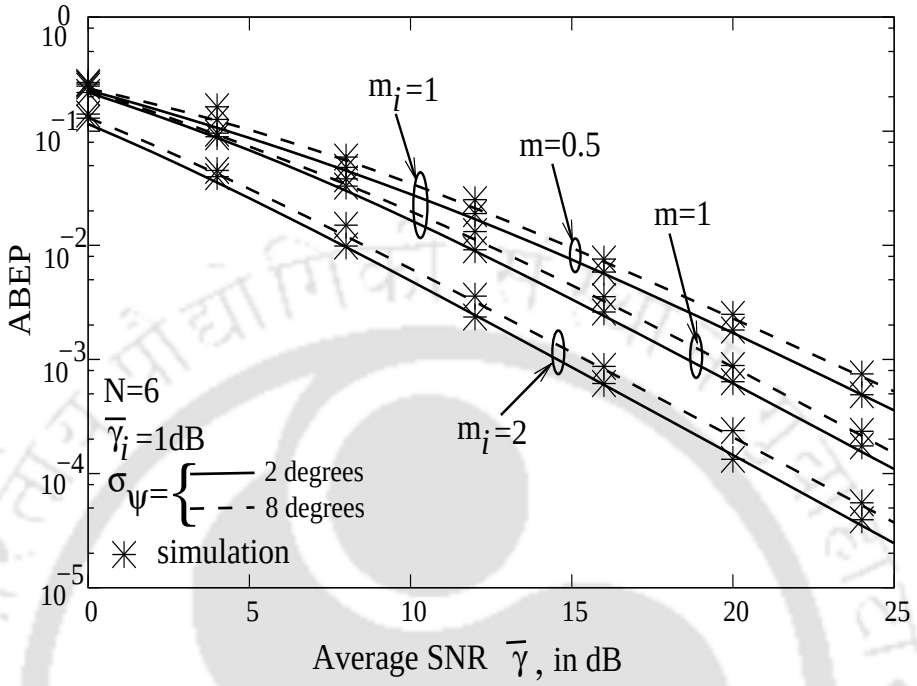

Figure 3.17: ABEP in independent Nakagami-*m* fading channels with $\sigma_\psi = 2°, 8°$, $N = 6$ and $\bar{\gamma}_i$ =1 dB with varying m and m_i.

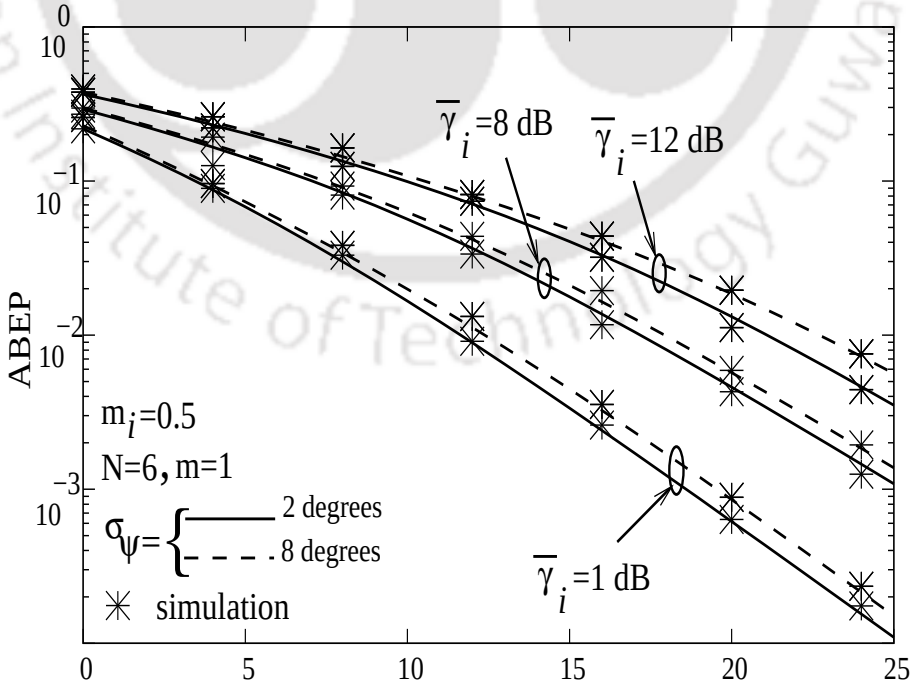

Figure 3.18: ABEP in independent Nakagami-*m* fading channels with varying $\bar{\gamma}_i$.

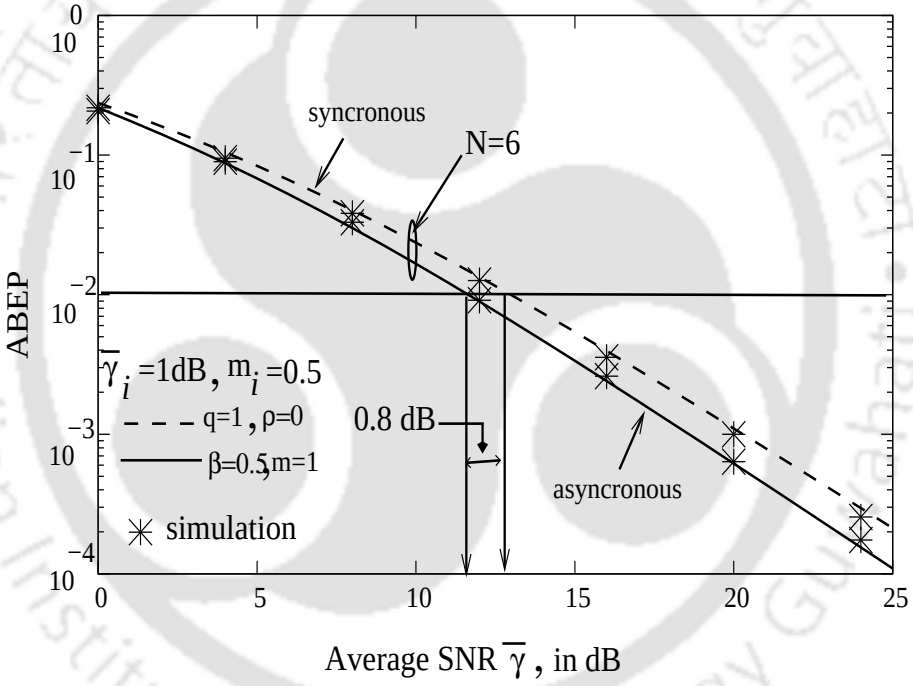

Figure 3.19: Comparison dual-EGC in Nakagami-*m* fading channels for synchronous and asynchronous cases.

3.2 Performance of Dual-EGC in Nakagami-*m* Fading - PDF Based Approach

In this section performance of dual-EGC is analyzed in independent Nakagami-*m* fading channels using the PDF based approach discussed in Section 2.3. A closed-form expressions for the PDF of the EGC output SNR and outage probability are derived. Further, ABEP for BPSK modulation can be obtained using the derived PDF.

Consider the received signal with CCI interfering signals as given in Equation 2.2. The matched filter output of the EGC receiver sampled at symbol instant is derived in Appendix A.1 (Equation A.3) as

$$y = E_g a_s \sum_{l=1}^{L} \alpha_{l,s} e^{j\psi_{l,s}} + \sum_{l=1}^{L} n_{0,l} e^{-j\hat{\phi}_{l,s}} + E_g \sum_{i=1}^{N} \sum_{l=1}^{L} a_i \alpha_{l,i} e^{j\left(\phi_{l,i} - \hat{\phi}_{l,s}\right)}, \tag{3.26}$$

where RVs $\alpha_{l,s}$ and $\alpha_{l,i}$ are independent and identically distributed with Nakagami-*m* distribution.

The SINR at the dual-EGC combiner output can be given as

$$\gamma_{egc} = \frac{\left[\sum_{l=1}^{2} \sqrt{\bar{\gamma}_{l,s}} \cos\psi_{l,s}\right]^2}{1 + \sum_{i=1}^{N} [\sum_{l=1}^{2} \sqrt{\bar{\gamma}_{l,i}} \cos\psi_{l,i}]^2} = \frac{x}{1+z}, \tag{3.27}$$

where $x = \left[\sum_{l=1}^{2} \sqrt{\bar{\gamma}_{l,s}} \cos\psi_{l,s}\right]^2$ and $z = \sum_{i=1}^{N} \left[\sum_{l=1}^{2} \sqrt{\bar{\gamma}_{l,i}} \cos\psi_{l,i}\right]^2$.

3.2.1 Probability Density Function of Output SINR

The PDF of $\gamma_{egc} = \frac{x}{1+z}$ can be derived using the following formula [25, (8)]

$$f_{\gamma_{egc}}(\gamma_{egc}) = \int_0^\infty (1+z) f_x((1+z)\gamma_{egc}) f_z(z) dz, \tag{3.28}$$

where $f_x(x)$ and $f_z(z)$ are the PDFs of x and z, respectively. The PDF of $x = \left[\sum_{l=1}^{L} \sqrt{\bar{\gamma}_{l,s}} \cos\psi_{l,s}\right]^2$ is derived in Equation A.44. Substituting $L = 2$ in it, an expression for the PDF of $x = \left[\sum_{l=1}^{2} \sqrt{\bar{\gamma}_{l,s}} \cos\psi_{l,s}\right]^2$

can be given as

$$f_x(x) = \left(\frac{m}{\bar{\gamma}}\right)^{m-\frac{1}{2}} \frac{\zeta^{m+\frac{1}{2}}\left[\Gamma\left(m-\frac{1}{2}\right)\right]^2}{2^{m-\frac{1}{2}}[\Gamma(m)]^2\Gamma(2m-1)}\left(\sqrt{x}\right)^{2(m-1)-1} e^{-\sqrt{\frac{2m\zeta x}{\bar{\gamma}}}}. \tag{3.29}$$

where ζ is the loop SNR due to desired signal, m and $\bar{\gamma}$ are the desired user Nakagami-*m* fading parameter and average SNR, respectively.

Similarly, the PDF of z is can be derived as

$$f_z(z) = \left(\frac{m_i}{N\bar{\gamma}_i}\right)^{m_i-\frac{1}{2}} \frac{\zeta_i^{m_i+\frac{1}{2}}\left[\Gamma\left(m_i-\frac{1}{2}\right)\right]^2}{2^{m_i-\frac{1}{2}}[\Gamma(m_i)]^2\Gamma(2m_i-1)}\left(\sqrt{z}\right)^{2(m_i-1)-1} e^{-\sqrt{\frac{2m_i\zeta_i z}{N\bar{\gamma}_i}}}. \tag{3.30}$$

where ζ_i is the loop SNR due to interfering signals, m_i and $\bar{\gamma}_i$ are the interfering user signal Nakagami-*m* parameter and average SNR respectively.

After a series of mathematical steps as shown in Appendix (A.9.1), the PDF of γ_{egc} can be derived as

$$\begin{aligned} f_{\gamma_{egc}}(\gamma_{egc}) &= \left(\frac{m_i}{N\bar{\gamma}_i}\right)^{m_i-\frac{1}{2}} \frac{\zeta_i^{m_i+\frac{1}{2}}\left[\Gamma\left(m_i-\frac{1}{2}\right)\right]^2}{2^{m_i-\frac{1}{2}}[\Gamma(m_i)]^2\Gamma(2m_i-1)} \\ &\times \left(\frac{m}{\bar{\gamma}}\right)^{m-\frac{1}{2}} \frac{\zeta^{m+\frac{1}{2}}\left[\Gamma\left(m-\frac{1}{2}\right)\right]^2}{2^{m-\frac{1}{2}}[\Gamma(m)]^2\Gamma(2m-1)}\left(\sqrt{\gamma_{egc}}\right)^{2(m-1)-1} e^{-\sqrt{\frac{2m\zeta}{\bar{\gamma}}}\left(\sqrt{\gamma_{egc}}\right)} \\ &\times \sum_{k=0}^{2m-1}\binom{2m-1}{k}\Gamma[2(m_i+k)-1]\left(\sqrt{\frac{2m\zeta\gamma_{egc}}{\bar{\gamma}}}+\sqrt{\frac{2m_i\zeta_i}{N\bar{\gamma}_i}}\right)^{-(2(m_i+k)-1)} \end{aligned} \tag{3.31}$$

3.2.2 Outage Probability

The outage probability of γ_{egc} can be derived as [25, (8)]

$$P_{out}(\gamma_{th}) = \int_0^{\gamma_{th}}\int_0^{\infty}(1+z)f_x[(1+z)\gamma_{egc}]f_z(z)dz.d\gamma_{egc} \tag{3.32}$$

After a series of mathematical steps shown in Appendix A.9.2, an expression for P_{out} can be given as

$$P_{out} = 1-\left(\frac{m_i}{N\bar{\gamma}_i}\right)^{m_i-\frac{1}{2}} \frac{\zeta_i^{m_i+\frac{1}{2}}\left[\Gamma\left(m_i-\frac{1}{2}\right)\right]^2}{2^{m_i-\frac{3}{2}}[\Gamma(m_i)]^2\Gamma(2m_i-1)}\sum_{k=0}^{2m-1}\sum_{l=0}^{k}\binom{k}{l}\frac{\left(\sqrt{\frac{2m\zeta}{\bar{\gamma}}}\gamma_{th}\right)^k}{k!}e^{-\sqrt{\frac{2m\zeta}{\bar{\gamma}}}\gamma_{th}}$$

$$\times\Gamma\left[2\left(m_i+l\right)-1\right]\left(\sqrt{\frac{2m_i\zeta_i}{N\bar{\gamma}_i}}+\sqrt{\frac{2m\zeta}{\bar{\gamma}}}\gamma_{th}\right)^{-(2(m_i+l)-1)} \tag{3.33}$$

3.2.3 Average Bit Error Probability

The average bit error probability of γ_{egc}, for BPSK modulation can be numerically evaluated as

$$\overline{P}_e=\int_0^\infty P_e\left(\gamma_{egc}\right)f_{\gamma_{egc}}(\gamma_{egc})d\gamma_{egc}=\int_0^\infty Q(\sqrt{2\gamma_{egc}})f_{\gamma_{egc}}\left(\gamma_{egc}\right)d\gamma_{egc}. \tag{3.34}$$

The above Equation 3.34 can be evaluated by putting Equation 3.31 in it. In this work, the integral is numerically evaluated to obtain the probability of error.

3.2.4 Numerical and Simulation Results

Outage and ABEP performance of dual-EGC receiver numerically evaluated and shown in Figures 3.20-3.26, for BPSK modulation assuming $\zeta_i=\zeta$ and $\sigma_\psi\approx 1/\sqrt{\zeta}$. Figure 3.20 represents the outage probability vs. γ_{th} (in dB), for $m=1$, $m_i=1$, $\bar{\gamma}_i=1$ and varying N. For increasing values of N the outage probability is plotted. As the values of N increases, the outage performance decreases correspondingly. Figure 3.21 represents the outage probability vs. γ_{th} (in dB), $\bar{\gamma}_i$ = 1 dB, σ_ψ = 2°, 12°, $N=1$ and for different values of m, m_i. The performance improves with increase in the values of m and m_i. Figure 3.22 represents the outage probability vs. $\bar{\gamma}$ for $\bar{\gamma}_i=1$ dB, σ_ψ = 2°, 12°, and for different values of N. When N is increased from 1 to 2 the performance degrades. Figure 3.23 represents the outage probability vs γ_{th} (in dB) for N =1, σ_ψ = 2°, 6°, m = 1, m_i = 1, $\bar{\gamma}_i$ = 1 dB, 5 dB, 10 dB. For higher values interfering SNR the performance degrades.

ABEP has been evaluated by numerical integration of Equation 3.34. Figure 3.24 illustrates the ABEP vs. average SNR for $m=1$, m_i = 1, $\bar{\gamma}_i$ = 1 dB, σ_ψ = 2°, 8° and for different values $N\geq 6$. Figure 3.25 represents the ABEP vs average SNR for m_i = 1, $\bar{\gamma}_i$ = 1 dB, $N=6$, σ_ψ = 2°, 8° and for different values m. Figure 3.26 represents the ABEP vs average SNR for m = 1, m_i = 1, $N=6$, σ_ψ = 2°, 8° and for different values of $\bar{\gamma}_i$. For increasing values of SNR the performance degrades

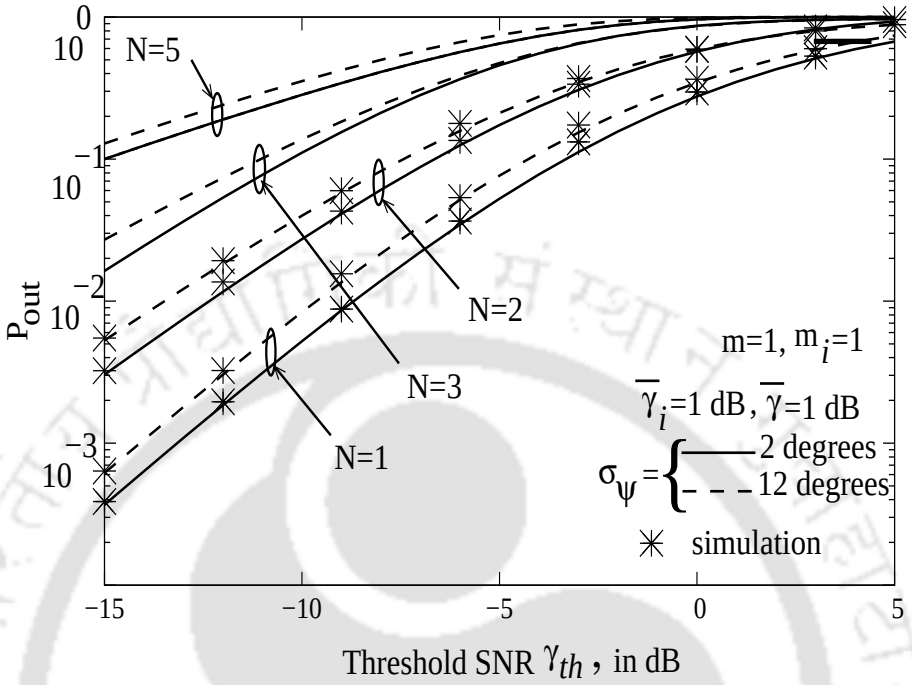

Figure 3.20: Outage probability in Nakagami-*m* fading channels with $\sigma_\psi = 2^\circ, 12^\circ$ and varying N.

comparatively. In all figures computer simulation results are also plotted to verify the correctness of the numerical results. The simulation results on an average match with the numerical results. The ABEP results when compared with the ABEP results obtained in the MGF and Padé approximation method closely matches with the ABEP results obtained in the PDF method.

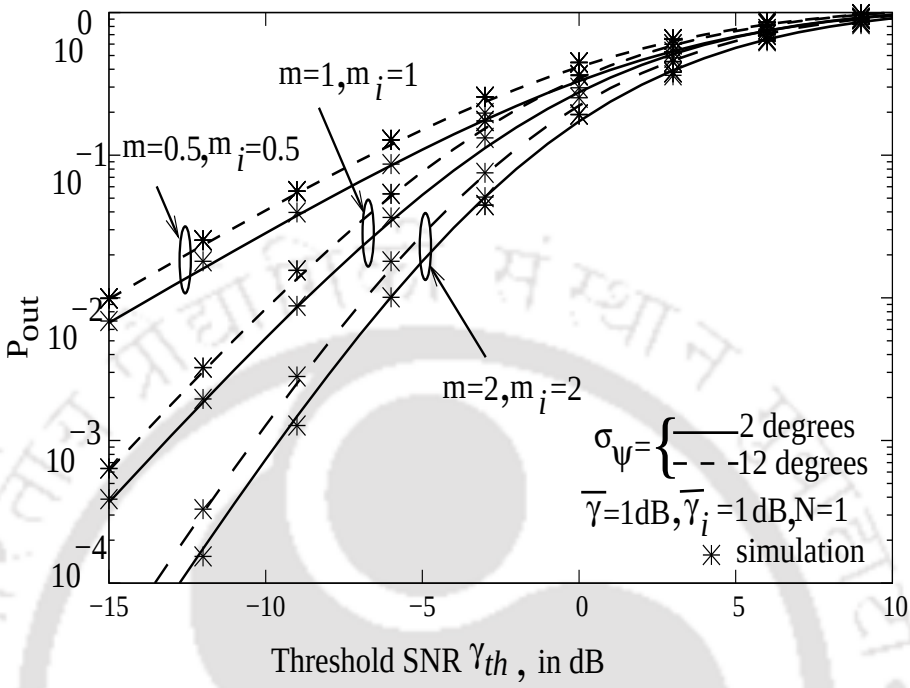

Figure 3.21: Outage probability in Nakagami-*m* fading channels with $\sigma_\psi = 2^\circ, 12^\circ$ varying m, m_i.

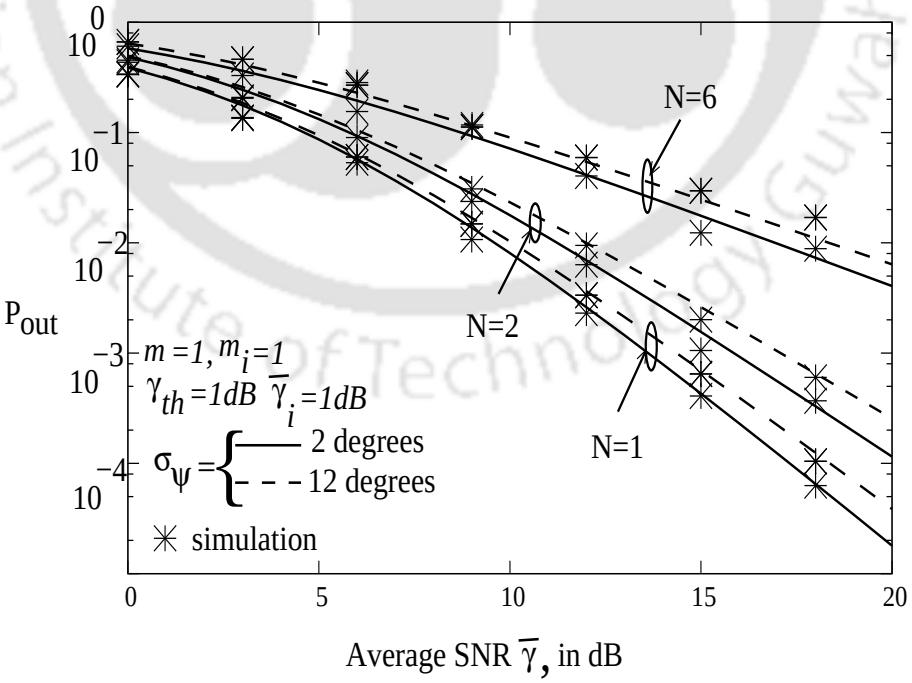

Figure 3.22: Outage probability in Nakagami-*m* fading channels with $\sigma_\psi = 2^\circ, 12^\circ$ $\gamma_{th} = 1$ dB and varying N.

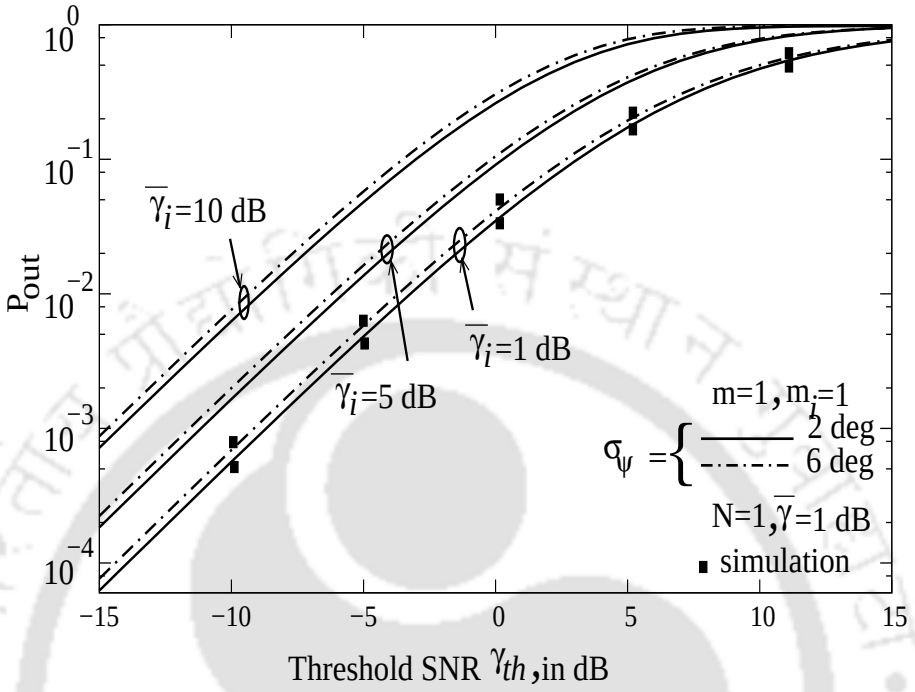

Figure 3.23: Outage probability in Nakagami-*m* fading channels with $\sigma_\psi = 2^\circ, 12^\circ$ and varying γ_i.

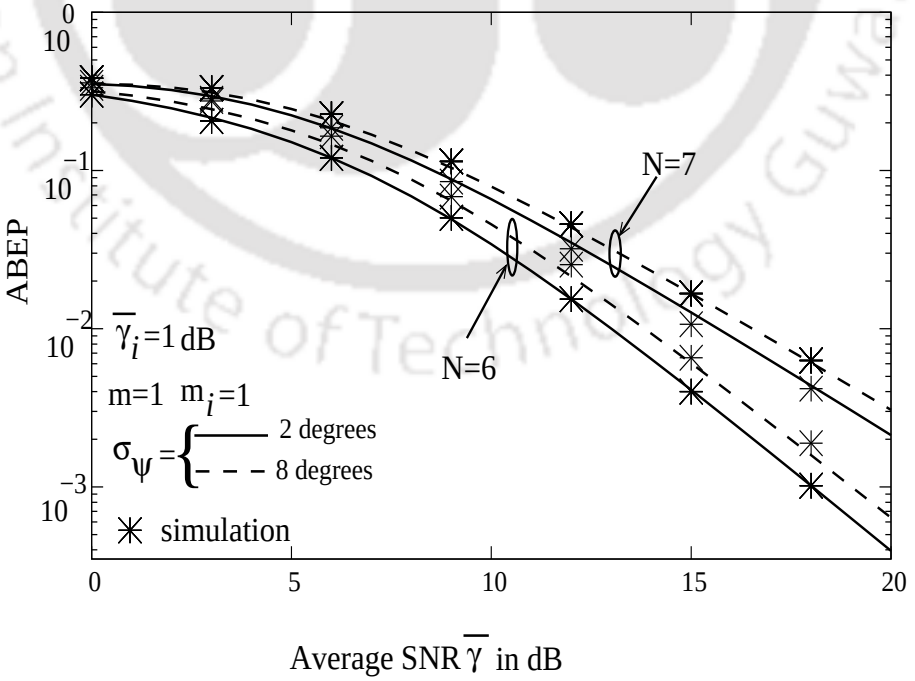

Figure 3.24: ABEP in Nakagami-*m* fading channels with $\sigma_\psi = 2^\circ, 12^\circ$ and varying N.

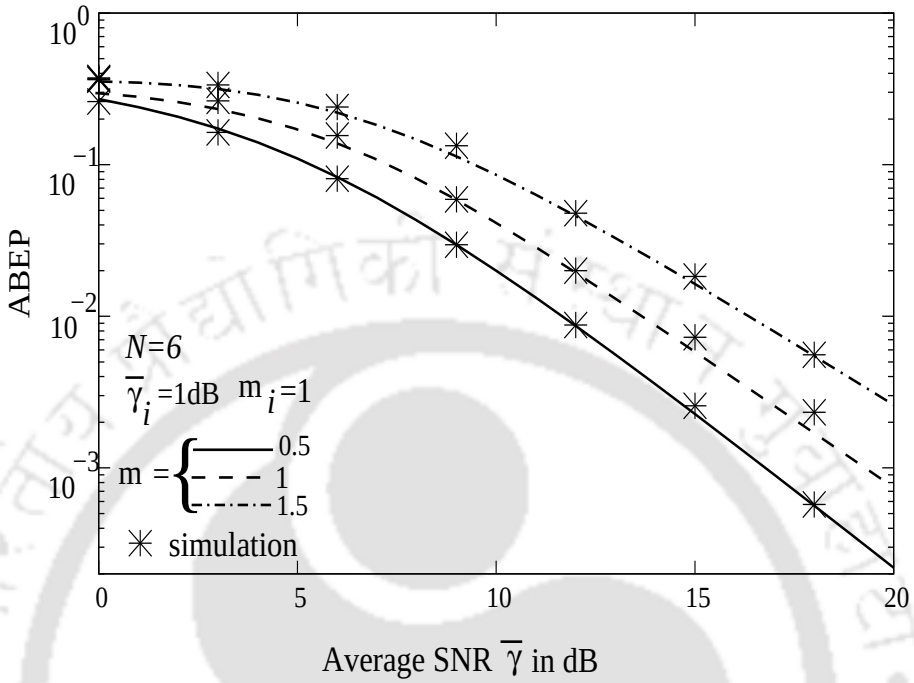

Figure 3.25: ABEP in Nakagami-*m* fading channels with $\sigma_\psi = 2^\circ, 12^\circ$ and varying *m*.

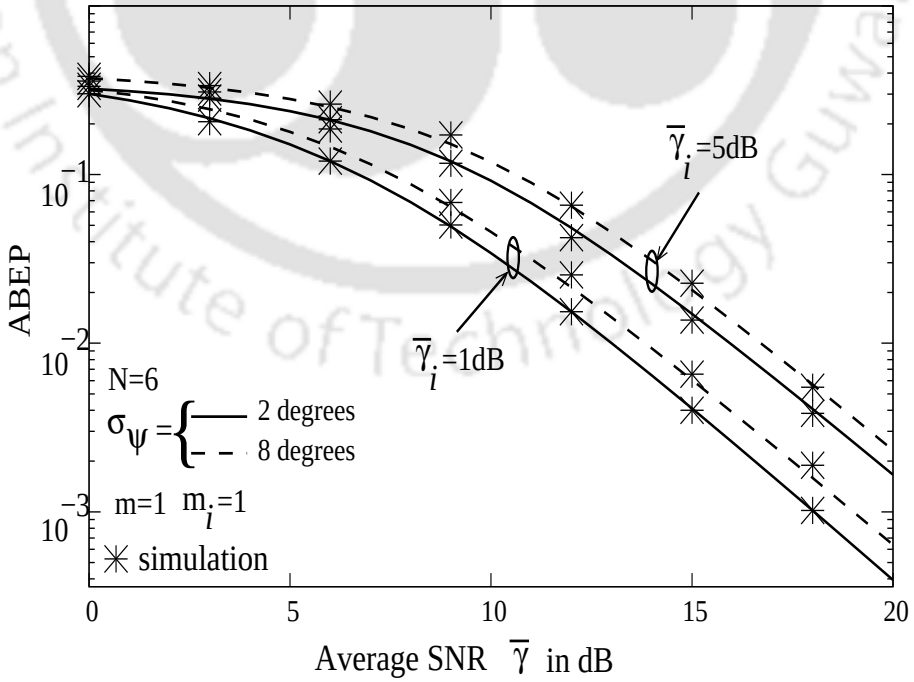

Figure 3.26: ABEP in Nakagami-*m* fading channels with $\sigma_\psi = 2^\circ, 12^\circ$ and varying γ_i.

3.3 Outage of L-EGC over Composite Fading Channels

In this section outage performance of L-EGC receiver is presented for composite fading channels i.e., GG and K_G fading channels, without AWGN. The marginal PDF of GG and K_G distributions are given in Equation 1.6 and Equation 1.7, respectively. Using a combination of PDF based approach and characteristic function outage performance has been evaluated. The final expression requires a numerical integration for evaluation.

Consider a desired user whose signal is transmitted through a slowly varying i.i.d composite *GG* or K_G fading channels. Assuming that there are N CCI users in the system and the fading channel between a CCI user and the desired user's receiver is Nakagami-m faded. For simplicity the thermal noise is omitted and only CCI is considered. Assuming a desired user and all N CCI users are transmitting simultaneously, in an interference limited environment, the baseband received signal at the l^{th} element of an L element receiving antenna array can be written as [24, 29]

$$r_l(t) = \alpha_{l,s} e^{j\phi_{l,s}} s_s(t) + \sum_{i=1}^{N} \alpha_{l,i} e^{j\phi_{l,i}} s_i(t), \tag{3.35}$$

where $\alpha_{l,s}$ is either *GG* or K_G distributed random variable and $\alpha_{l,i}$ is Nakagami-m distributed RV with PDFs given as in Equations 1.6, 1.7 and 1.2, respectively.

The demodulated signal at the combiner output at the sampling instant $t = T$ can be derived from Equation 3.35 as shown in Appendix A.1 can be given as

$$y = a_s \sum_{l=1}^{L} \alpha_{l,s} e^{j\psi_{l,s}} + \sum_{i=1}^{N} \sum_{l=1}^{L} a_i \alpha_{l,i} e^{j\left(\phi_{l,i} - \widehat{\phi}_{l,s}\right)}, \tag{3.36}$$

3.3.1 Output Signal-to-Interference Ratio

For an arbitrary number of branch EGC receiver, the output Signal-to-Interference Ratio (SIR) at the combiner output with phase error and CCI for BPSK can be written from Equation 3.36 as [19, 23]

$$SIR = \frac{\left[\sum_{l=1}^{L} \alpha_{l,s} \cos(\psi_{l,s})\right]^2}{\sum_{i=1}^{N} \sum_{l=1}^{L} \alpha_{l,i}^2} \tag{3.37}$$

Since, N cochannel interferes are i.i.d with the identical fading parameter, m and average power, the instantaneous interfering signal voltage phasors are added together to produce the resultant instantaneous interfering signal with resultant interference power $\sum_{i=1}^{N}\sum_{l=1}^{L}[\alpha_{l,i}^2]$ [23, (8b)].

Substituting, $X=\sum_{l=1}^{L}\alpha_{l,s}\cos(\psi_{l,s})$ and $U=\sum_{i=1}^{N}\sum_{l=1}^{L}\alpha_{l,i}^2$ in Equation 3.37, the combiner output SIR can be expressed as

$$SIR=\frac{X^2}{U} \tag{3.38}$$

3.3.2 Outage Probability of Output SIR

Thus, the outage probability at the combiner output can be given as [24]

$$\begin{aligned} P_{out}(\gamma_{th}) &= P_r(SIR<\gamma_{th})=E_U\left[P_r\left(X<\sqrt{\gamma_{th}U}\,|U\right)\right] \\ &= \frac{1}{2}-\sum_{\substack{n=1\\ n=odd}}^{\infty}\frac{2\Im\{E_U\{e^{-jn\omega_0\sqrt{\gamma_{th}U}}\}\Phi_X(n\omega_0)\}}{n\pi}, \end{aligned} \tag{3.39}$$

where γ_{th} is the threshold SIR, $\omega_0=2\pi/T$, T is the parameter which controls the accuracy [24], $\Phi_X(n\omega_0)$ is the characteristic function of X and $\Im\{z\}$ denotes the imaginary part of z, $E_U\{\cdot\}$ is the expectation of the argument over the PDF of the RV U.

An expression for the PDF of U for Nakagami-m fading distribution can be given as [23].

$$f_U(u)=\left(\frac{m_i}{\Omega_i}\right)^{\eta}\frac{u^{\eta-1}}{\Gamma(\eta)}\exp\left(-\frac{m_i}{\Omega_i}u\right), \tag{3.40}$$

where m_i is the Nakagami-m fading parameter and $\eta=m_iLN$. Hence, $E_U\{\cdot\}$ can be derived as

$$\begin{aligned} E_U\{e^{-jn\omega_0\sqrt{\gamma_{th}U}}\} &= \int_0^{\infty}e^{-jn\omega_0\sqrt{\gamma_{th}U}}f_U(u)du. \\ &= \left(\frac{m_i}{\Omega_i}\right)^{\eta}\frac{1}{\Gamma(\eta)}\int_0^{\infty}e^{-jn\omega_0\sqrt{\gamma_{th}U}}u^{\eta-1}\exp\left(-\frac{m_i}{\Omega_i}u\right)du. \end{aligned} \tag{3.41}$$

Integrating Equation 3.41 as shown in Appendix A.7 (Equation A.30) we get

$$E_U\{e^{-jn\omega_0\sqrt{\gamma_{th}U}}\} = {}_1F_1\left(\eta,\frac{1}{2},-\frac{n^2{\omega_0}^2\gamma_{th}\Omega_i}{4m_i}\right)-jn\omega_0\sqrt{\gamma_{th}}\frac{\Gamma\left(\eta+\frac{1}{2}\right)}{\Gamma(\eta)}\sqrt{\frac{\Omega_i}{m_i}}$$

$$\times {}_1F_1\left(\frac{1}{2}+\eta,\frac{3}{2},-\frac{n^2{\omega_0}^2\gamma_{th}\Omega_i}{4m_i}\right), \tag{3.42}$$

The characteristic function $\Phi_X(n\omega_0)$ in Equation 3.39 can be obtained as below. Since, $\alpha_{l,s}$ and $\psi_{l,s}$ are independent RVs, $\Phi_{\alpha_{l,s}\cos\psi_{l,s}}(n\omega_0)$ can be given as

$$\begin{aligned}\Phi_{\alpha_{l,s}\cos\psi_{l,s}}(n\omega_0) &= E\left[e^{jn\omega_0\alpha_{l,s}\cos\psi_{l,s}}\right] = \int_0^{\infty}\int_0^{2\pi} e^{jn\omega_0\alpha_{l,s}\cos\psi_{l,s}} p_{\psi_{l,s}}\left(\psi_{l,s}\right) p_{\alpha_{l,s}}\left(\alpha_{l,s}\right) d\psi_{l,s} d\alpha_{l,s} \\ &= \frac{1}{2\pi I_0\left(\xi_{l,s}\right)} \int_0^{\infty}\int_0^{2\pi} e^{\left(\xi_{l,s}+jn\omega_0\alpha_{l,s}\right)\cos\psi_{l,s}} p_{\alpha_{l,s}}\left(\alpha_{l,s}\right) d\psi_{l,s} d\alpha_{l,s}. \end{aligned} \tag{3.43}$$

Using the definition of Bessel function [39, (3.3)] in Equation 3.43, $\Phi_X(n\omega_0)$ can be expressed as

$$\Phi_X(n\omega_0) = \left(\int_0^{\infty} \frac{I_0(\zeta_{l,s}+jn\omega_0\alpha_{l,s})}{I_0(\zeta_{l,s})} p_{\alpha_{l,s}}(\alpha_{l,s}) d\alpha_{l,s}\right)^L. \tag{3.44}$$

Thus, evaluation of the outage probability for GG and K_G fading using Equation 3.39 requires the evaluation of Equation 3.42 and Equation 3.44. Evaluation of Equation 3.44 is to be done by numerical integration technique. The range of integration for $\alpha_{l,s}$ can be taken safely over $(0, 10\Omega_{l,s})$ [21]. It can be mentioned here that for Nakagami-m fading channels a closed-form expression for the CHF in (3.44) is available for uniform phase error in [33].

3.3.3 Numerical and Simulation Results

The outage probability expression given by Equation 3.39 is numerically evaluated for GG and K_G fading distributions and plotted in Figures 3.27-3.35, for BPSK modulation. The Padé approximation coefficients used in the numerical evaluation of MGF for these fading distributions are given in AppendixA.12. The values for different parameters in the figures are chosen arbitrarily for the purpose of demonstration and covers the entire range off parameters in suitable subdivisions. In the numerical evaluation it is assumed that $\sigma_{\psi_{1,s}} = \sigma_{\psi_{2,s}} = \ldots = \sigma_{\psi_{L,s}} = \sigma_{\psi}$.

Figure 3.27 shows the P_{out} vs. γ_{th} for GG fading channels for $N = 1$, $m_g = 1$ and $\beta_g = 2$ and different values of σ_{ψ} and L. P_{out} improves with increase in L and degrades with increase in σ_{ψ}. For

example, for $\sigma_\psi = 2^\circ$, when L increases from 1 to 3, P_{out} at $\gamma_{th} = -5$ dB improves from 0.0756576 to 0.0180152. Improvements for other values of σ_ψ can also be observed from the figure. Figure 3.28 shows the P_{out} vs. γ_{th} for $L = 1$, $\sigma_\psi = 2^\circ, 8^\circ$, $m_g = 1$, $\beta_g = 2$ and for different values of N. It can be observed that P_{out} degrades with increase in N and σ_ψ. For $\sigma_\psi = 2^\circ$, when N increases from 1 to 3, P_{out} at $\gamma_{th} = -5$ dB degrades from 0.0756576 to 0.271901. Similar performance is observed for other values of σ_ψ. Figure 3.29 demonstrates P_{out} vs. γ_{th} for $N = 1$, $L = 2$, $\sigma_\psi = 2^\circ$ and 8° and for different values of m_g and β_g. P_{out} improves with increase in m_g and β_g and degrades with increase in σ_ψ. Figure 3.30 shows the P_{out} vs. γ_{th} for $N = 1$, $\beta_g = 2$, $\sigma_\psi = 2^\circ, 6^\circ$. P_{out} improves for increase in m_g and L but degrades with increase in $\sigma_\psi = 2^\circ$ and 8°. When m_g increases from 1 to 2 P_{out} at $\gamma_{th} = -5$ dB improves from 0.00673661 to 0.0026261. Similar performance is observed for other values of L. Figure 3.31 shows the P_{out} vs γ_{th} in dB for $N = 1$, $m_g = 1$, $\beta_g = 1.5$, L=2, $\sigma_\psi = 2^\circ, 8^\circ$ and for different values of m_i. As the value of m_i increases from 0.5, 1 and 2 the performance improves.

Figure 3.32 shows the P_{out} vs γ_{th} for K_G fading channels for $N = 1$, $m_k = 1$, $\beta_k = 1$ and different values of σ_ψ and L. For increase in L from 1 to 3, P_{out} at $\gamma_{th} = -5$ dB improves from 0.027582 to 0.00877773. Similar performance can be observed for other values of σ_ψ. Figure 3.33 shows the P_{out} vs γ_{th} in dB for $L = 2$, $\sigma_\psi = 2^\circ, 8^\circ$, $m_k = 1$, $\beta_k = 1$ and for different values of N. Figure 3.34 shows the P_{out} vs γ_{th} for $N = 1$, $L = 2$, $\sigma_\psi = 2^\circ$ and 6° and for different values of m_k and β_k. For ($m_k = 1$, $\beta_k = 1$) and $\sigma_\psi = 2^\circ, 8^\circ$, P_{out} is plotted. When σ_ψ decreases from $\sigma_\psi = 8^\circ$ to 2° P_{out} decreases. For example, when ($m_k = 1$, $\beta_k = 1$) is increased from (0.5, 0.5) to (1, 1), the outage performance improves gradually. Figure 3.35 shows the outage probability for $N = 1$, $L = 2$, $\sigma_\psi = 2^\circ$ and 8°, m_k and $\beta_k = 1$ and for different values of m_i. When m_i increases from 0.5 to 0.8, P_{out} improves. In all figures computer simulation results are also plotted to verify the correctness of the numerical results. The simulation results on an average match with the numerical results.

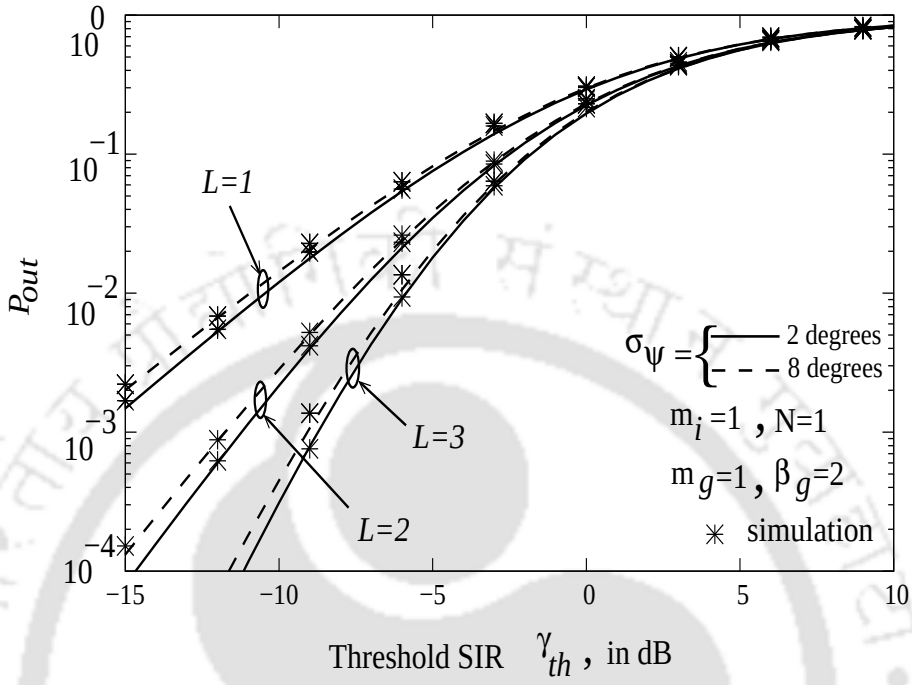

Figure 3.27: Outage probability in GG fading with $\sigma_\psi = 2^\circ, 8^\circ$, $N = 1$, $m_g = 1$ and $\beta_g = 2$.

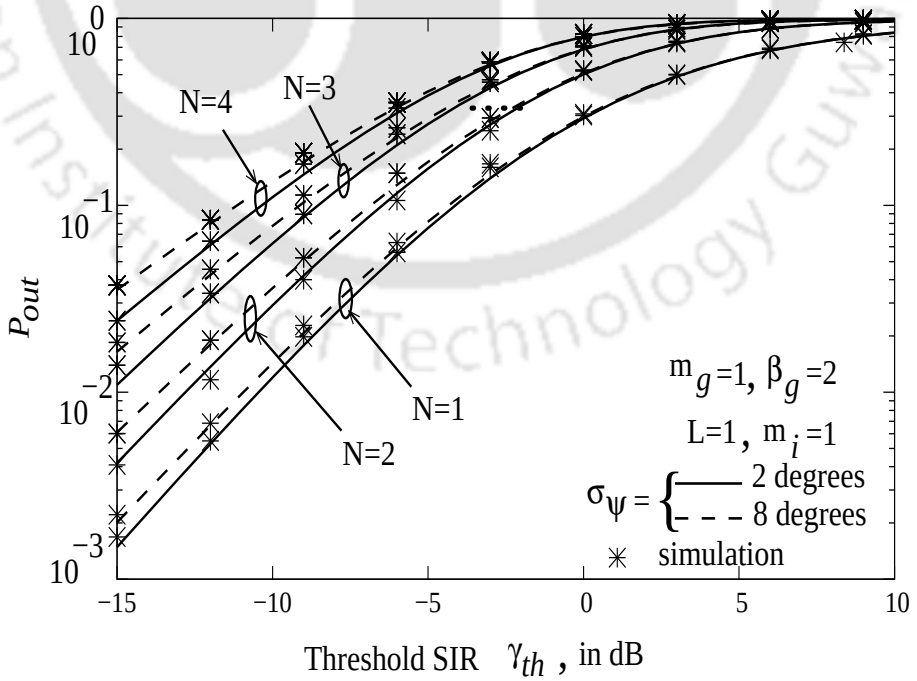

Figure 3.28: Outage probability in GG fading with $\sigma_\psi = 2^\circ, 8^\circ$, $L = 1$, $m_g = 1$ and $\beta_g = 2$.

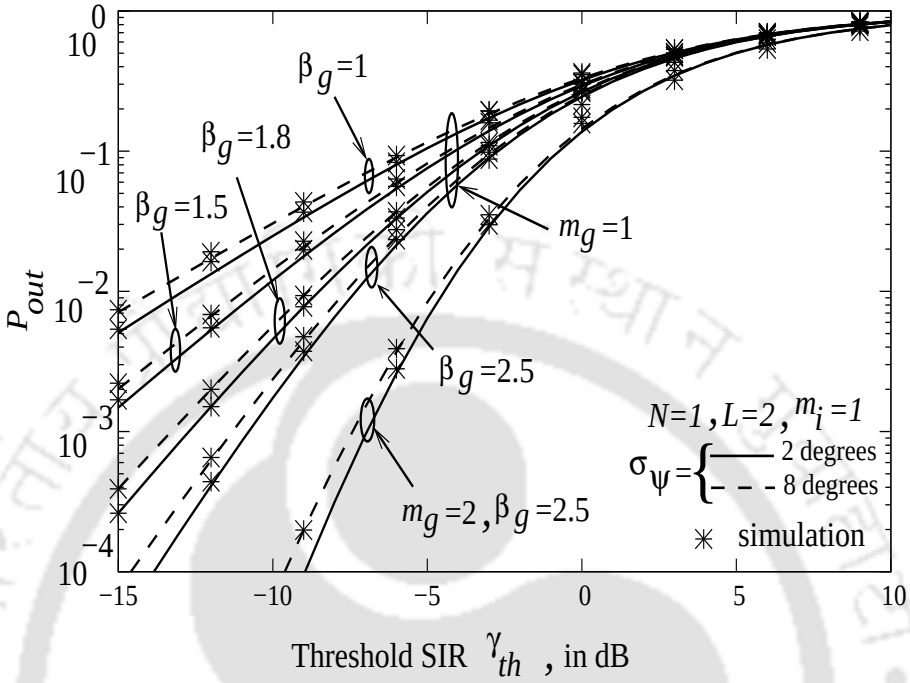

Figure 3.29: Outage probability in GG fading with $\sigma_\psi = 2^\circ, 8^\circ$, $L = 2$ and $N = 1$.

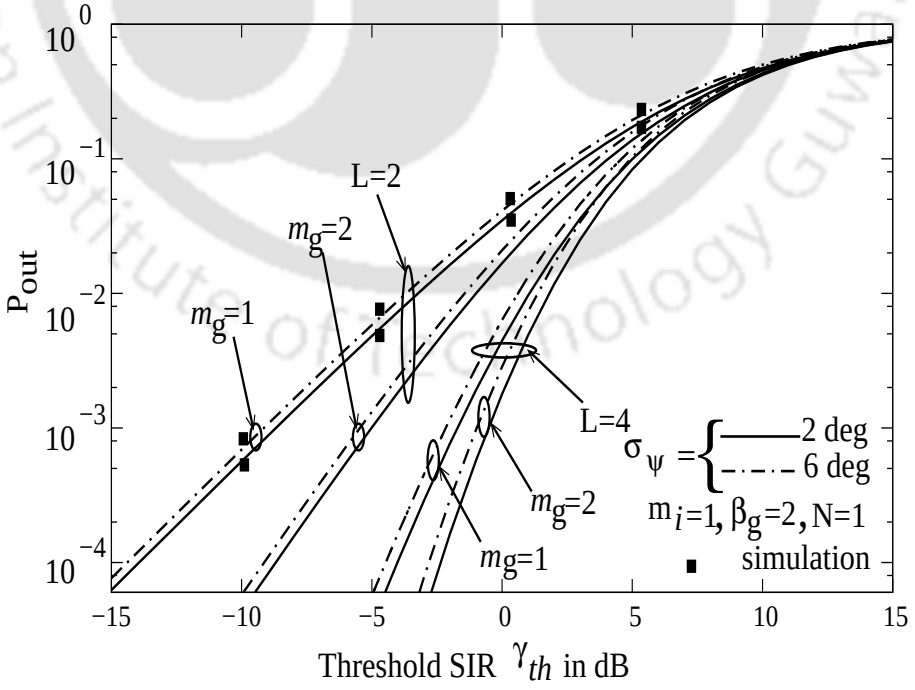

Figure 3.30: Outage probability in GG fading with $\sigma_\psi = 2^\circ, 8^\circ$, $L = 2, 4$ and $N = 1$.

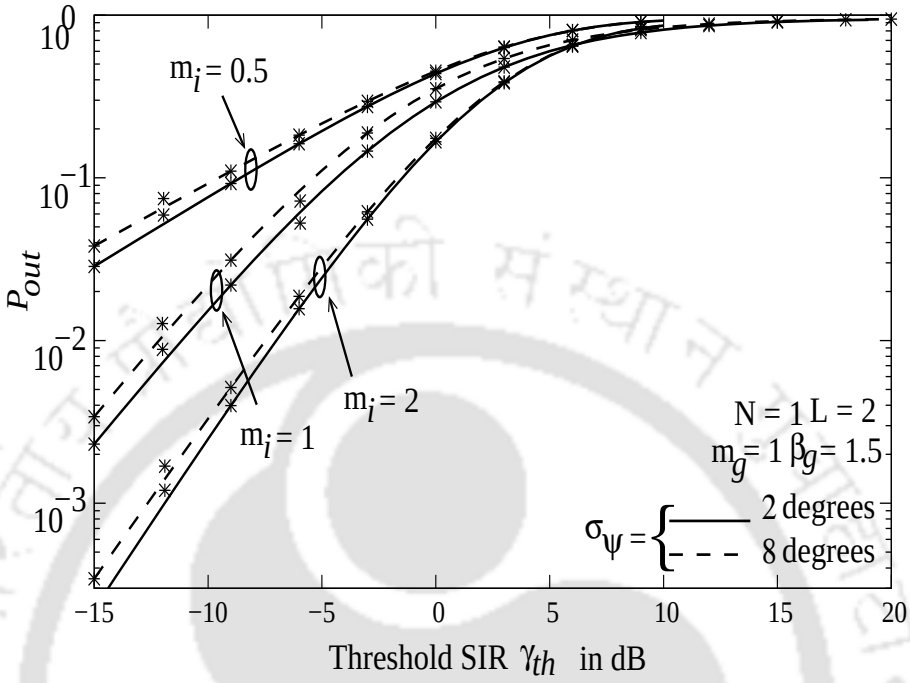

Figure 3.31: Outage probability in GG fading channels with $\sigma_\psi = 2^\circ, 8^\circ$, $L = 2$, $N = 1$, $m_g = 1$ and $\beta_g = 2$.

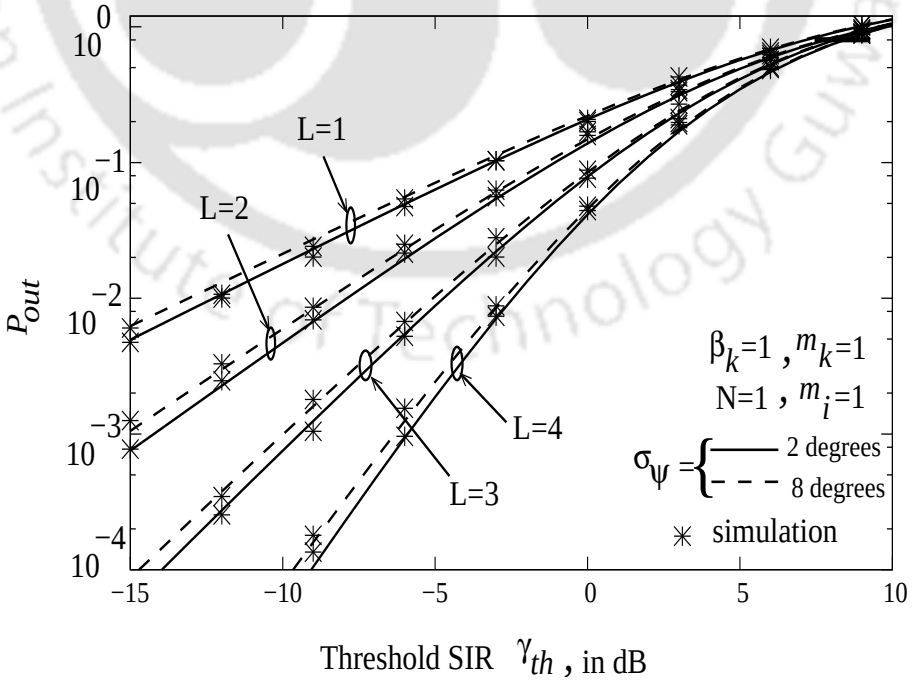

Figure 3.32: Outage probability in K_G fading channels with $\sigma_\psi = 2^\circ, 8^\circ$, N=1, m_k= 1 and β_k =1.

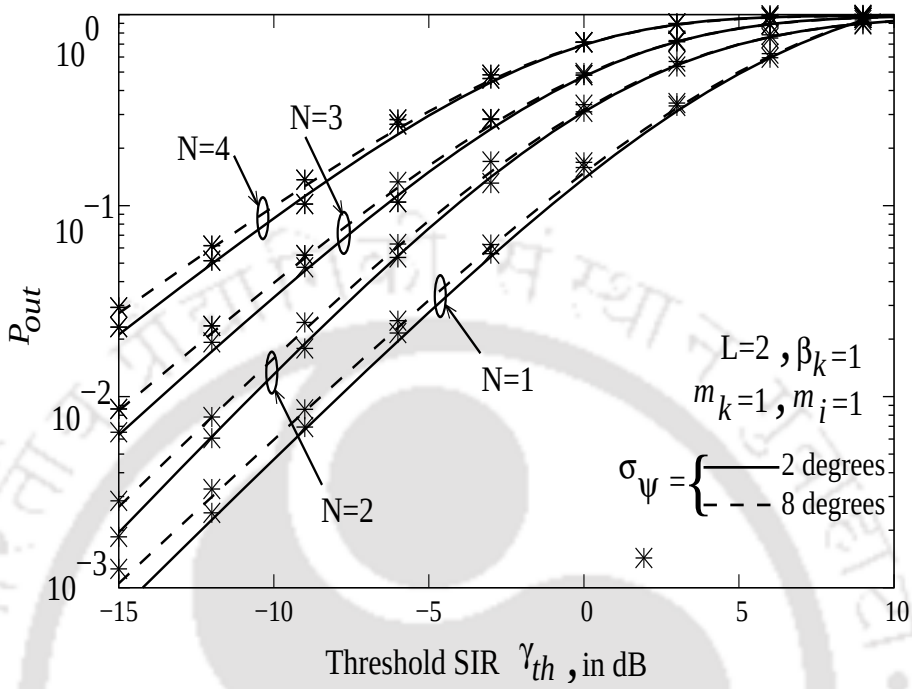

Figure 3.33: Outage probability in K_G fading channels with $\sigma_\psi = 2^\circ, 8^\circ$, L=2, m_k= 1 and β_k =1.

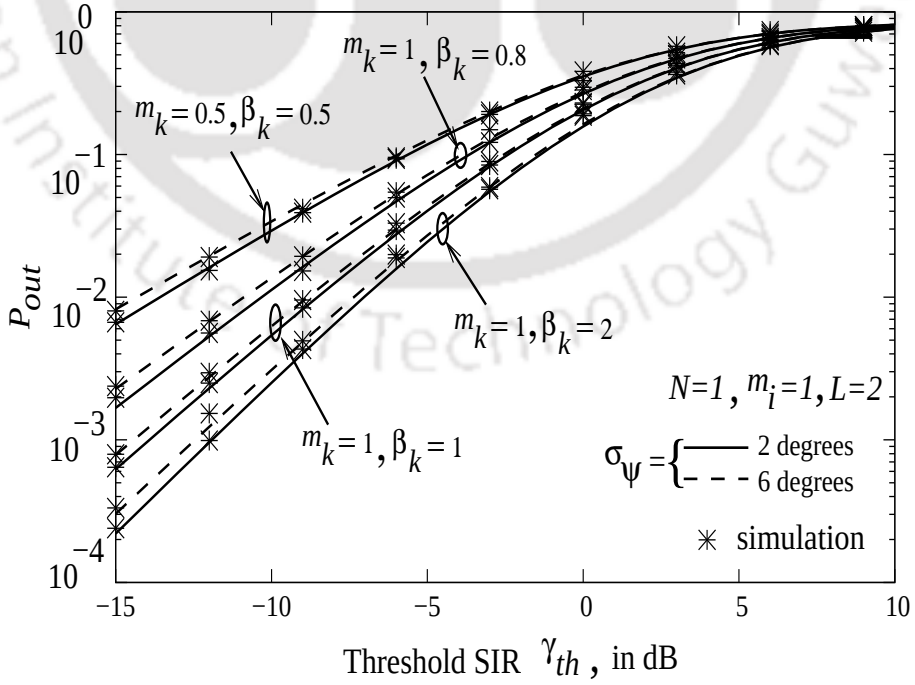

Figure 3.34: Outage probability in K_G fading channels with $\sigma_\psi = 2^\circ, 8^\circ$, $L = 2$ and $N = 1$.

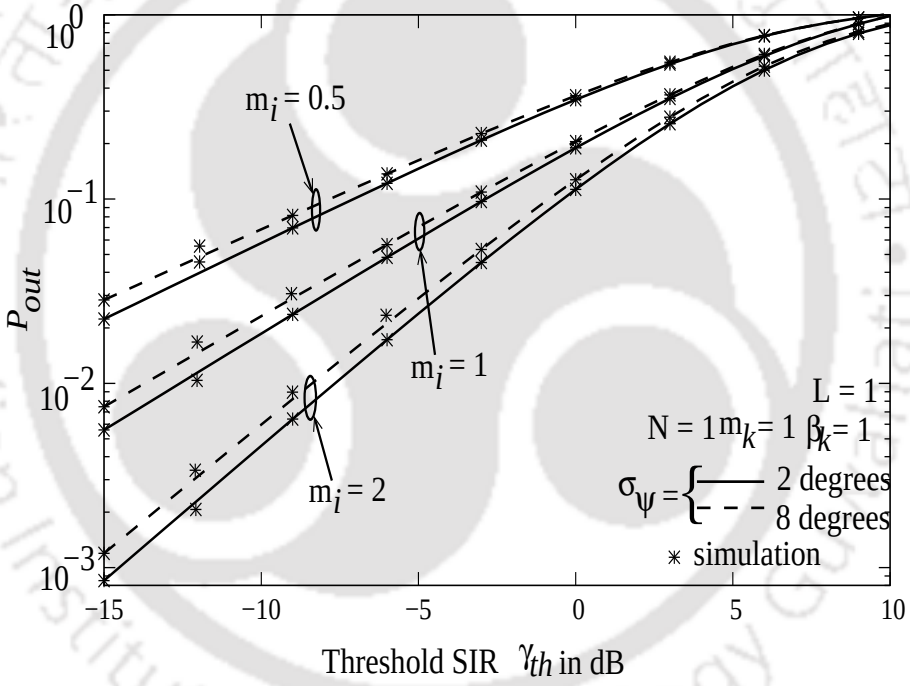

Figure 3.35: Outage probability in K_G fading channels with $\sigma_\psi = 2^\circ, 8^\circ$, $L = 1$ and $N = 1$.

3.4 Performance of $L-$EGC in Nakagami-m Fading with Phase Error and AWGN Only - PDF Based Approach

In this section we analyze the performance of L-EGC receiver in Nakagami-m fading channels assuming the presence of phase error and AWGN i.e., without CCI. The PDF based approach is used to obtain an expression for the PDF of EGC output SNR. Using the derived PDF, expressions for receiver 'outage probability' and 'ABEP for BPSK modulation' are presented.

The complex baseband received signal at the l^{th} element of an L element receiving antenna array over a symbol duration T can be given as [19, (1)]

$$r_l(t) = \alpha_l e^{j\phi_l} s_s(t) + n_l(t), l = 0, 1, 2, \ldots, L, \tag{3.45}$$

where α_l is Nakagami-m RV with fading parameter m, n_l is the AWGN sample with zero mean and power spectral density $N_0/2$. The RV ϕ_l is the carrier phase.

3.4.1 Output SNR

In an ideal EGC combiner, received L faded copies of the transmitted signal are equiphased and each is weighted with unity gain [3]. Assuming the estimated phase of the input signal of the l^{th} branch of the combiner is $\widehat{\phi}_l$, the demodulated signal at the combiner output at the sampling instant T can be written as Appendix A.1

$$y = E_g a_s \sum_{l=1}^{L} \alpha_l e^{j\psi_l} + \sum_{l=1}^{L} n_{0,l} \tag{3.46}$$

where $E_g = \int_0^\infty g_T^2(t)dt$, $n_{0,l} = \int_0^T n_l(\tau)s_s(\tau)d\tau$ which can be shown to be Gaussian with zero mean and power spectral density $N_0 E_g/2$. For an L branch EGC receiver, the instantaneous output SNR with only phase error can be derived from Equation 3.46 as

$$\gamma_{egc} = \left(\sum_{l=1}^{L} \sqrt{\gamma_l} \cos(\psi_l) \right)^2. \tag{3.47}$$

3.4.2 Probability Density Function of Output SNR, γ_{egc}

An expression for the PDF of γ_{egc} has been derived as shown in Appendix A.8 in Equation A.44. Thus, the PDF $f_{\gamma_{egc}}(\gamma_{egc})$ can be given as

$$f_{\gamma_{egc}}(\gamma_{egc}) = \left(\frac{m}{\bar{\gamma}}\right)^{L\left(\frac{m}{2}-\frac{1}{4}\right)} \frac{\zeta^{L\left(\frac{m}{2}+\frac{1}{4}\right)}\left[\Gamma\left(m-\frac{1}{2}\right)\right]^{L}}{2^{L\left(\frac{m}{2}-\frac{3}{4}\right)+1}[\Gamma(m)]^{L}\Gamma\left[L\left(m-\frac{1}{2}\right)\right]} \sqrt{\gamma_{egc}}^{L\left(m-\frac{1}{2}\right)-2} e^{-\sqrt{\frac{2m\zeta}{\bar{\gamma}}}\left(\sqrt{\gamma_{egc}}\right)}. \quad (3.48)$$

3.4.3 Outage Probability of Output SNR

The outage probability of EGC receiver with phase estimation error can be derived as

$$P_{out} = \int_{0}^{\gamma_{th}} f_{\gamma_{egc}}(\gamma_{egc}) d\gamma_{egc}, \quad (3.49)$$

Substituting the obtained PDF of γ_{egc} from Equation 3.48 in Equation 3.49, the outage probability can be derived as shown in Appendix A.8.1 (Equation A.47) as

$$P_{out} = 1 - e^{-\sqrt{\frac{2m\zeta_l}{\bar{\gamma}}}\gamma_{th}} \sum_{k=0}^{mL-1} \frac{\left(\sqrt{\frac{2m\zeta_l}{\bar{\gamma}}}\gamma_{th}\right)^{k}}{k!}, \quad (3.50)$$

where γ_{th} is the threshold SNR.

3.4.4 Average Bit Error Probability of Output SNR

The ABEP for BPSK can be derived using the formula [3],

$$\bar{P}_e = \int_{0}^{\infty} Q\left(\sqrt{2\gamma_{egc}}\right) f_{\gamma_{egc}}(\gamma_{egc}) d\gamma_{egc} \quad (3.51)$$

The ABEP expression can be derived as shown in Appendix A.8.2, as

$$\bar{P}_e = \frac{1}{2} - \frac{1}{\sqrt{\pi}} \sum_{n=0}^{\infty} \frac{(-1)^n}{n!\,(2n+1)} \Gamma\left(L\left(m-1/2\right)+(2n+1)\right) \left(\sqrt{\frac{2m\zeta_l}{\bar{\gamma}}}\right)^{-(2n+1)}.$$

3.4.5 Numerical and Simulation Results

The outage probability and ABEP performance of the EGC receiver numerically evaluated and shown in Figures 3.36, 3.37, and 3.38 for BPSK modulation. Figures 3.36 represents the P_{out} vs γ_{th} (in dB) for $\bar{\gamma} = 1dB$ and for different values of L and m. For $L = 2$ the outage performance is plotted for σ_ψ = 2° and 12°. When the value of σ_ψ is increased from 2° to 12° the performance degrades. Similar results are obtained for m = 0.5. When L is increased from 2 to 4 the performance improves. Figure 3.37 represents the P_{out} vs average SNR for σ_ψ = 2° and 12°, γ_{th} = 1dB for $L = 2$ and γ_{th} = 0.5dB for L = 4. and for varying values of L and m. For decrease in the value of m from 1 to 0.5 the performance degrades but for increase in L from 2 to 4 gives a better performance.

Figure 3.38 illustrates the ABEP for σ_ψ = 2° and 12° and for different values of L and m. For higher values of L and m the performance is better. But when the value of L are decreased from 4 to 2, m decreased from 1 to 0.5 the performance decreases. In all figures computer simulation results are also plotted to verify the correctness of the numerical results. The simulation results on an average match with the numerical results.

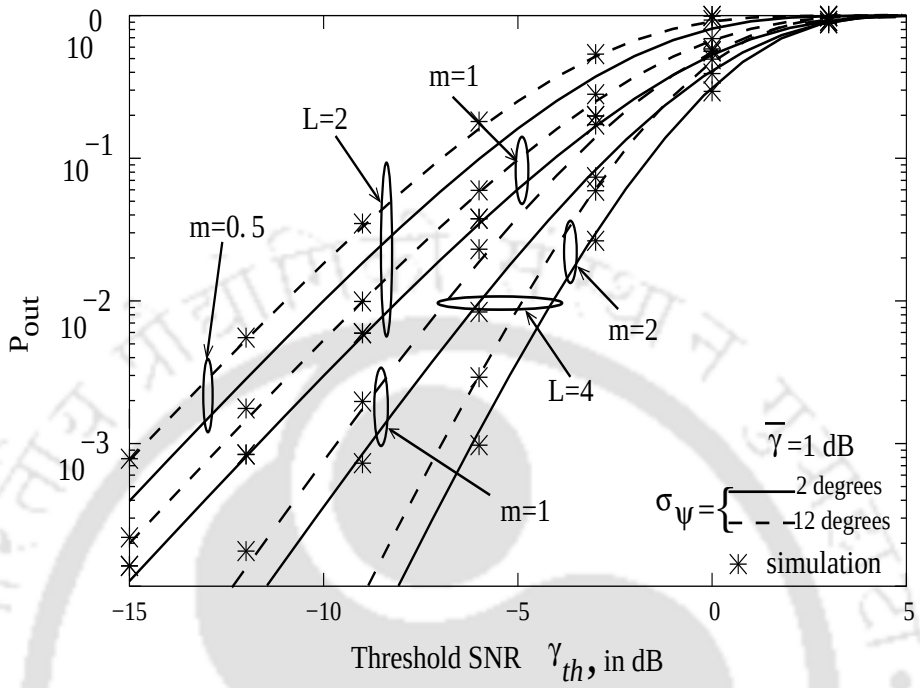

Figure 3.36: Outage probability in Nakagami-*m* fading channels with $\sigma_\psi = 2^\circ, 12^\circ$.

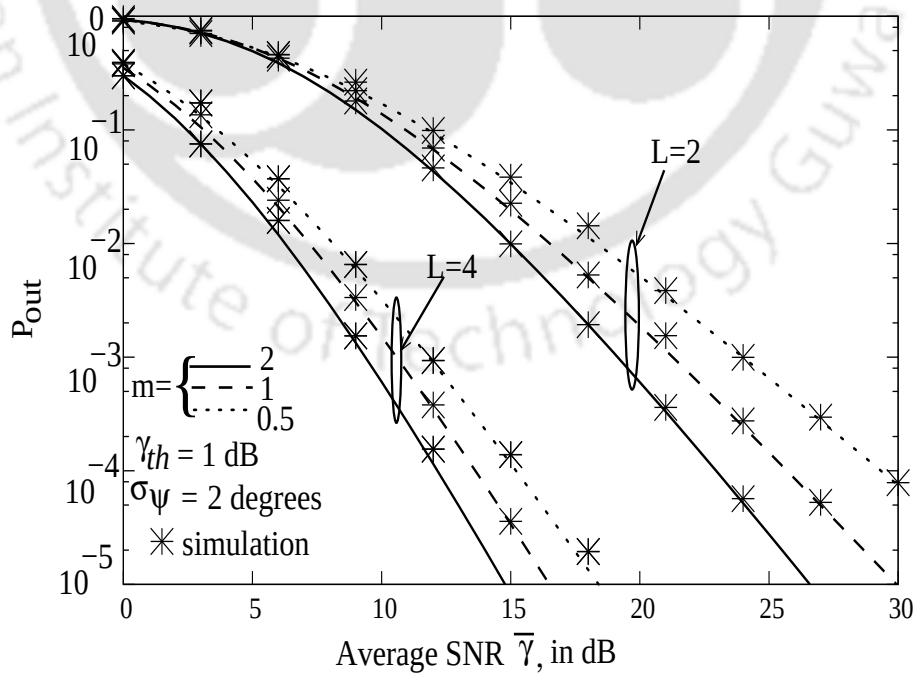

Figure 3.37: Outage probability in Nakagami-*m* fading channels with $\sigma_\psi = 2^\circ, 12^\circ$.

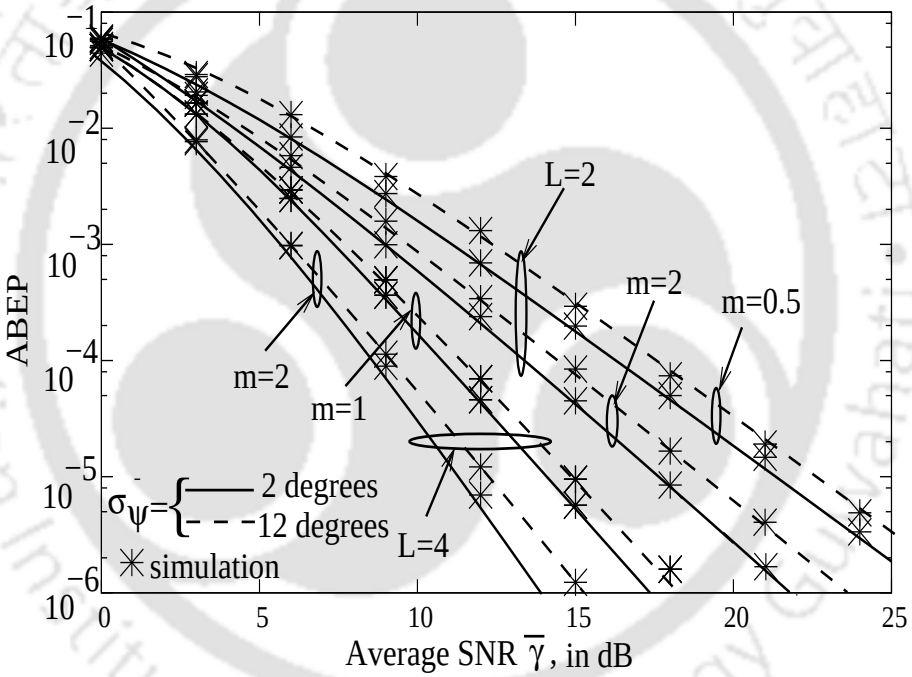

Figure 3.38: ABEP in Nakagami-*m* fading channels with $\sigma_\psi = 2^\circ, 12^\circ$.

3.5 Summary

The summary of works presented in this chapter are enumerated below:

1. ABEP performance of dual-EGC receiver is obtained using 'MGF based approach with Padè approximation' for the following fading channels:
   (a) Correlated Hoyt fading channels.
   (b) Correlated Composite and i.i.d Non-homogeneous fading channels.
   (c) Nakagami-*m* fading channels.
2. Outage and ABEP performance of dual-EGC over Nakagami-*m* fading channels has been presented using PDF based approach.
3. Following works are presented for *L*-EGC receiver.
   (a) Outage probability over Composite fading i.e., GG fading channels is presented.
   (b) Outage and ABEP performance with phase error and AWGN over Nakagami-*m* fading channels are presented using the PDF method
4. Numerical and simulation results for all the above analytical works have been presented. Results have been verified against available results which are special cases for the work presented here.

Chapter 4

MRC Receiver in Nakagami-*m* Channels

Performance of MRC receiver is known to be optimum under ideal assumptions [2, 3]. In practical situations such as in the presence of carrier phase estimation error and/or CCI, the performance is likely to degrade. In this chapter, we derive expressions for the outage and ABEP of MRC receiver in Nakagami-*m* fading channels and study the performance.

According to the system model discussed in Section 2.2 the desired user's channel and the interfering user's channel are considered to be Nakagami-*m* fading. Thus, in Equation 2.2, $\alpha_{l,s}$ is assumed to be Nakagami-*m* distributed RV with fading parameter m and $\alpha_{l,i}$ is assumed to be i.i.d Nakagami-*m* RV with fading parameter m_i. The marginal PDF of a Nakagami-*m* RV is given in Equation 1.2.

Modeling Channel Estimation Error

The channel estimator estimates the coefficients of the channel which ideally should be $\alpha_{l,s}e^{j\phi_{l,s}}$. Assuming the estimated coefficients as $\hat{\alpha}_{l,s}e^{j\hat{\phi}_{l,s}}$, the actual channel coefficients can be modeled as [25]

$$\alpha_{l,s}e^{j\phi_{l,s}} = \sqrt{1-\varepsilon^2}\hat{\alpha}_{l,s}e^{-j\hat{\phi}_{l,s}} + \varepsilon v, \tag{4.1}$$

where v is the channels estimation error which is assumed to be a zero mean and unit variance complex Gaussian distributed RV independent of $\alpha_{l,s}e^{j\phi_{l,s}}$, $\varepsilon \in [0,1]$ is the measure of accuracy of the channel estimation i.e., channel estimation is accurate for $\varepsilon = 0$.

Output SINR of MRC

In a MRC combiner, received L faded copies of the transmitted signal are weighted with estimated channel coefficients and then added together [3]. The output from the MRC combiner is fed to a detector suitable for detecting the modulated signal. An expression for the demodulated signal at the combiner output at the sampling instant T is derived in Appendix A.10. It can be given as

$$y = a_s E_g \sum_{l=1}^{L} \alpha_{l,s} e^{j\phi_{l,s}} \hat{\alpha}^*_{l,s} e^{-j\hat{\phi}_{l,s}} + \sum_{l=1}^{L} n_{0,l} \hat{\alpha}^*_{l,s} e^{-j\hat{\phi}_{l,s}} + E_g \sum_{i=1}^{N} \sum_{l=1}^{L} a_i \alpha_{l,i} e^{j\phi_{l,i}} \hat{\alpha}^*_{l,s} e^{-j\hat{\phi}_{l,s}} \tag{4.2}$$

Substituting Equation 4.1 in Equation 4.2, the signal at the combiner output can be expressed as

$$y = a_s E_g \sum_{l=1}^{L} \left(\sqrt{1-\varepsilon^2}\hat{\alpha}_{l,s} e^{j\hat{\phi}_{l,s}} + \varepsilon v \right) \hat{\alpha}^*_{l,s} e^{-j\hat{\phi}_{l,s}} + \sum_{l=1}^{L} \sum_{i=1}^{N} a_i E_i \alpha_{l,i} e^{j\phi_{l,i}} \hat{\alpha}^*_{l,s} e^{-j\hat{\phi}_{l,s}} + \sum_{l=1}^{L} n_{0,l} \hat{\alpha}^*_{l,s} e^{-j\hat{\phi}_{l,s}}. \tag{4.3}$$

For an L branch MRC receiver, the instantaneous output SINR with phase error and CCI can be derived from Equation 4.3 as shown in Appendix A.10. It can be given as

$$\gamma_{mrc} = \frac{\eta \sum_{l=1}^{L} \gamma_{l,s}}{1 + \beta \sum_{i=1}^{N} \gamma_i} = \frac{x}{1+z}, \tag{4.4}$$

where $\eta = \frac{1-\varepsilon^2}{1+\varepsilon^2}$, $\beta = \frac{1}{1+\varepsilon^2}$, $x = \eta \sum_{l=1}^{L} \gamma_{l,s}$ and $z = \beta \sum_{i=1}^{N} \gamma_i$.

4.1 PDF of MRC Output SINR

The PDF of γ_{mrc} in Equation 4.4 can be derived using the following formula [25, (8)]

$$f_{\gamma_{mrc}}(\gamma_{mrc}) = \int_0^\infty (1+z) f_x[(1+z)\gamma_{mrc}] f_z(z) dz, \tag{4.5}$$

where $f_x(x)$ and $f_z(z)$ are the PDFs of x and z, respectively. The PDF of $x = \eta \sum_{l=1}^{L} \gamma_{l,s}$ is derived in Appendix A.10.1. It can be given as

$$f_x(x) = \left(\frac{m}{\bar{\gamma}}\right)^{mL} \left(\frac{1}{\eta}\right)^{mL} \frac{x^{mL-1}}{\Gamma(mL)} e^{-\frac{m}{\bar{\gamma}}\frac{x}{\eta}}, \tag{4.6}$$

where m is the fading parameter and $\bar{\gamma}$ is the average SNR of desired user signal which is Nakagami-m distributed. Similarly, the PDF of z can be given as

$$f_z(z) = \left(\frac{m_i}{\bar{\gamma}_i}\right)^{m_i N} \left(\frac{1}{\beta}\right)^{m_i N} \frac{z^{m_i N-1}}{\Gamma(m_i N)} e^{-\frac{m_i}{\bar{\gamma}_i}\frac{z}{\beta}}, \tag{4.7}$$

where m_i is the fading parameter and $\bar{\gamma}_i$ is the average SNR of interfering user signal. Using Equations 4.6 and 4.7, the PDF of $\gamma_{mrc} = \frac{x}{z+1}$ is derived in Appendix A.10.2 which can be given as

$$\begin{aligned} & f_{\gamma_{mrc}}(\gamma_{mrc}) = \\ = & \left(\frac{m}{\eta\bar{\gamma}}\right)^{mL} \left(\frac{m_i}{\beta\bar{\gamma}_i}\right)^{mN} \int_0^{\infty} \frac{[(1+z)\gamma_{mrc}]^{mL-1}}{\Gamma(mL)\Gamma(m_i N)} (1+z) z^{m_i N-1} e^{-\left(\frac{m}{\bar{\gamma}}\frac{(1+z)\gamma_{mrc}}{\eta}\right)} e^{-\left(\frac{m_i}{\bar{\gamma}_i}\frac{z}{\beta}\right)} dz. \\ = & \left(\frac{m}{\eta\bar{\gamma}}\right)^{mL} \left(\frac{m_i}{\beta\bar{\gamma}_i}\right)^{m_i N} \gamma_{mrc}^{mL-1} e^{-\frac{m\gamma_{mrc}}{\bar{\gamma}\eta}} \sum_{k=0}^{mL} \frac{mL}{(mL-k)!} \binom{k+m_i N-1}{m_i N} \left(\frac{m\gamma_{mrc}}{\eta\bar{\gamma}} + \frac{m_i}{\beta\bar{\gamma}_i}\right)^{-(k+m_i N)}. \end{aligned} \tag{4.8}$$

4.2 Outage Probability of MRC Output SINR

Outage probability (P_{out}) of a system is defined in Equation 2.4. For γ_{mrc}, it can be given as [3, (1.4)]

$$P_{out} = \int_0^{\gamma_{th}} f_{\gamma_{mrc}}(\gamma_{mrc}) d\gamma_{mrc}, \tag{4.9}$$

where $f_{\gamma_{mrc}}(\gamma_{mrc})$ is the PDF of the output SINR γ_{mrc}. The outage probability can be derived using the formula [25, (8)]

$$P_{out}(\gamma_{th}) = \int_0^{\gamma_{th}} \int_0^{\infty} (1+z) f_x[(1+z)\gamma_{mrc}] f_z(z) dz d\gamma_{mrc}. \tag{4.10}$$

Substituting Equation 4.6 and Equation 4.7 in Equation 4.10, the outage probability can be given as

$$\begin{aligned} P_{out}(\gamma_{th}) &= \int_0^{\gamma_{th}} \int_0^{\infty} (1+z) \left(\frac{1}{\beta}\right)^{m_i N} \left(\frac{m_i}{\bar{\gamma}_i}\right)^{m_i N} \frac{z^{m_i N-1}}{\Gamma(m_i N)} e^{-\frac{m_i}{\bar{\gamma}_i}\frac{z}{\beta}} \left(\frac{1}{\eta}\right)^{mL} \\ &\quad \times \left(\frac{m}{\bar{\gamma}}\right)^{mL} \frac{[(1+z)\gamma_{mrc}]^{mL-1}}{\Gamma(mL)} e^{-\frac{(1+z)\gamma_{mrc} m}{\eta\bar{\gamma}}} dz\, d\gamma_{mrc}. \end{aligned} \tag{4.11}$$

The integration in Equation 4.11 can be evaluated as shown in Appendix A.10.2 and the final expression for outage probability can be given as

$$P_{out} = 1 - e^{-\frac{m\gamma_{th}}{\bar{\gamma}\eta}} \sum_{k=0}^{mL-1} \sum_{l=0}^{k} \left(\frac{m_i}{\beta\bar{\gamma}_i}\right)^{m_i N} \left(\frac{m\gamma_{th}}{\bar{\gamma}\eta}\right)^{k} \frac{1}{(k-l)!} \binom{l+m_i N-1}{l} \left(\frac{\gamma_{th} m}{\eta\bar{\gamma}} + \frac{m_i}{\bar{\gamma}_i \beta}\right)^{-(l+m_i N)} \tag{4.12}$$

4.3 Average Symbol Error Probability

An expression for ASEP of MRC receiver can be derived using the general formula [3]

$$\overline{P}_e = \int_0^{\infty} P_e(\gamma_{mrc}) f_{\gamma_{mrc}}(\gamma_{mrc}) d\gamma_{mrc}, \tag{4.13}$$

where $P_e(\gamma_{mrc})$ is the conditional probability of error for the modulation scheme used and $f_{\gamma_{mrc}}$ is the conditional PDF of combiner output SINR. In practice, $P_e(\gamma) = Q(a\sqrt{2g\gamma_{mrc}})$, a and g are modulation specifying parameters eg. $a = 1, g = 1$ for BPSK, $a = 1, g = 0.5$ for binary frequency shift keying (BFSK), $a = \frac{2(M-1)}{M}, g = \frac{3}{M^2-1}$ for M-ary pulse amplitude modulation, and $a = 2, g = \sin^2\frac{\pi}{M}$ for M-ary phase shift keying. For the SINR derived in Equation 4.4, the ASEP can be derived as [25]

$$\overline{P}_e = \int_0^{\infty} aQ(\sqrt{2g\gamma_{mrc}}) \int_0^{\infty} (1+z) p_x[(1+z)\gamma_{mrc}] p_z(z) dz\, d\gamma_{mrc}. \tag{4.14}$$

Substituting $Q(\sqrt{2g\gamma_{mrc}}) = \frac{1}{\pi}\int_0^{\frac{\pi}{2}} \exp\left(-\frac{g\gamma_{mrc}}{\sin^2\theta}\right) d\theta$ [3], a closed form expression for the ASEP can be derived as shown in Appendix A.10.3, as

$$\overline{P}_e = \frac{a}{2}\left[1 - \sqrt{\frac{g\eta\bar{\gamma}}{m}} \sum_{k=0}^{mL-1} \sum_{l=0}^{k} \binom{2k}{k} \binom{k}{l} \left(\frac{1}{4}\right)^{k} \left(\frac{1}{\beta}\right)^{m_i N} \frac{\Gamma(l+m_i N)}{\Gamma(m_i N)} \left(1 + \frac{g\eta\bar{\gamma}}{m}\right)^{m_i N+l-k-\frac{1}{2}} \left(\frac{m_i}{\bar{\gamma}_i}\right)^{m_i N}\right.$$

$$\times \Phi\left(l+m_iN, l+m_iN-k+\frac{1}{2}, \frac{m_i}{\bar{\gamma}_i\beta}\left(1+\frac{\eta\bar{\gamma}g}{m}\right)\right)\Bigg], \tag{4.15}$$

where $\Gamma(\cdot)$ is the gamma function [10, (8.310.1)] and $\Phi(a,b,c)$ is the hypergeometric function of first kind [10, (9.210.1)].

An expression for ASEP for BPSK modulation $(a=1, g=1)$ can be obtained from Equation 4.15 as

$$\begin{aligned}\overline{P}_e &= \frac{1}{2}\Bigg[1-\sqrt{\frac{\eta\bar{\gamma}}{m}}\sum_{k=0}^{mL-1}\sum_{l=0}^{k}\binom{2k}{k}\binom{k}{l}\left(\frac{1}{4}\right)^k\left(\frac{1}{\beta}\right)^{m_iN}\frac{\Gamma(l+m_iN)}{\Gamma(m_iN)}\left(1+\frac{\eta\bar{\gamma}}{m}\right)^{m_iN+l-k-\frac{1}{2}}\left(\frac{m_i}{\bar{\gamma}_i}\right)^{m_iN} \\ &\quad \times \Phi\left(l+m_iN, l+m_iN-k+\frac{1}{2}, \frac{m_i}{\bar{\gamma}_i\beta}\left(1+\frac{\eta\bar{\gamma}}{m}\right)\right)\Bigg]\end{aligned} \tag{4.16}$$

4.4 Numerical and Simulation Results

The numerical results of the outage probability and ASEP are shown in Figures 4.2-4.12. The outage probability and the ASEP expressions are numerically evaluated using MATHEMATICA. Figure 4.2 shows the outage probability for different values of L. For L = 4, N = 1, m_i = 1, m = 1, $\bar{\gamma}=1$, $\bar{\gamma}_i=1$, P_{out} is plotted for different values of ε. As the value of ε decreases from 0.99 to 0.80, the outage performance improves gradually. When the value of L is increased from 4 to 8 the outage performance improved well. Figure 4.3 shows the outage probability for L = 4, ε = 0.80, m_i = 1, m = 1, $\bar{\gamma}=1$, $\bar{\gamma}_i=1$ and for different values of N. As the value of N increases, the outage performance decreases for each increase in N. Figure 4.4 shows the outage probability for L = 4, ε = 0.99, N = 1, $\bar{\gamma}_i$=1, $\bar{\gamma}$ = 1 and for different values of m and m_i. When m_i decreases from 1 to 0.5 the performance degrades as a low value of m_i indicates severe fading. Similar performance can be observed for variation in m. Figure 4.5 shows the outage performance, for $L=4$, $N=1$, $m_i=1$, $m=1$, $\bar{\gamma}=1$, ε = 0.95 and $\bar{\gamma}_i$ is varied. As the value of $\bar{\gamma}_i$ is varied from 1 to 4 the performance degrades, as expected. Figure 4.7 shows the outage performance, P_{out} vs average SNR for $L=4$, $N=1$, $m_i=1$, $m=1$, and $\bar{\gamma}_i=1$ and L is varied. As the value of L is varied from 4 to 8 the performance improves. For each value of L the outage performance is plotted for different values of ε. Figure 4.8 shows the

ASEP for different values of L. For L = 4, N = 1, m_i = 1, m = 1, $\bar{\gamma}_i = 1$, the ASEP is plotted for different values of ε. As the value of ε is decreased from 0.99 to 0.80 the performance improves. Similar results are obtained for L = 8. Figure 4.9 shows the ASEP for L = 4, m_i = 1, m = 1, $\bar{\gamma}_i = 1$, ε = 0.80 and for different values of N. As the value of N is increased from 1, 2, 3, and 5 the ASEP performance degrades as expected. Figure 4.10 shows the ASEP for L = 4, N=1, $\bar{\gamma}_i = 1$, ε = 0.80 and for different values of m_i and m. For decrease in value of m from 2 to 1 the performance degrades comparatively. Similar results are obtained for variation in m_i. Figure 4.11 shows the ASEP for L = 4, N = 1, m_i = 1, m = 1, ε = 1 and for different values of $\bar{\gamma}_i = 1$. As the value of $\bar{\gamma}_i = 1$ is increased from 1, 2, 5, and 6 the ASEP performance degrades as expected. Figure 4.12 shows the ASEP performance for 4-PSK, 8-PSK, modulations, N = 1, L = 8, m_i = 1, m = 1, $\bar{\gamma}_i = 1$ and ε is varied for each type of modulation. The performance has improved for 4-PSK, when compared to 8-PSK. For each modulation the ASEP is plotted for different values of ε. As the value of ε is increased from 0.99 to 0.85 the ASEP performance improves gradually. In all figures computer simulation results are also plotted to verify the correctness of the numerical results. The simulation results on an average match with the numerical results.

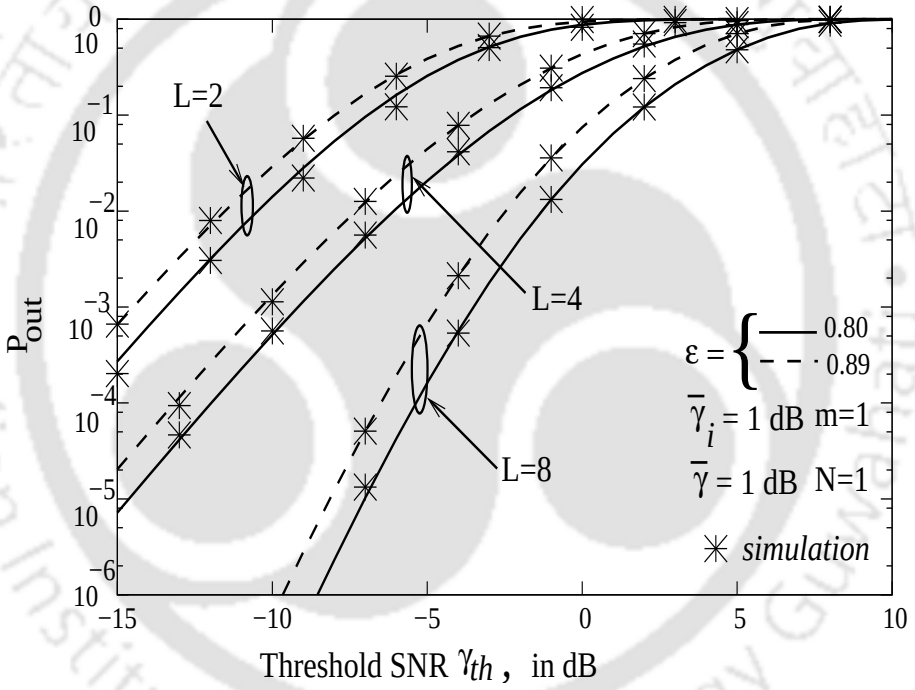

Figure 4.1: Outage probability of L-MRC receiver in Nakagami-m fading channels for $N = 1$, $m = 1$, $m_i = 1$ and $\bar{\gamma} = 1dB$.

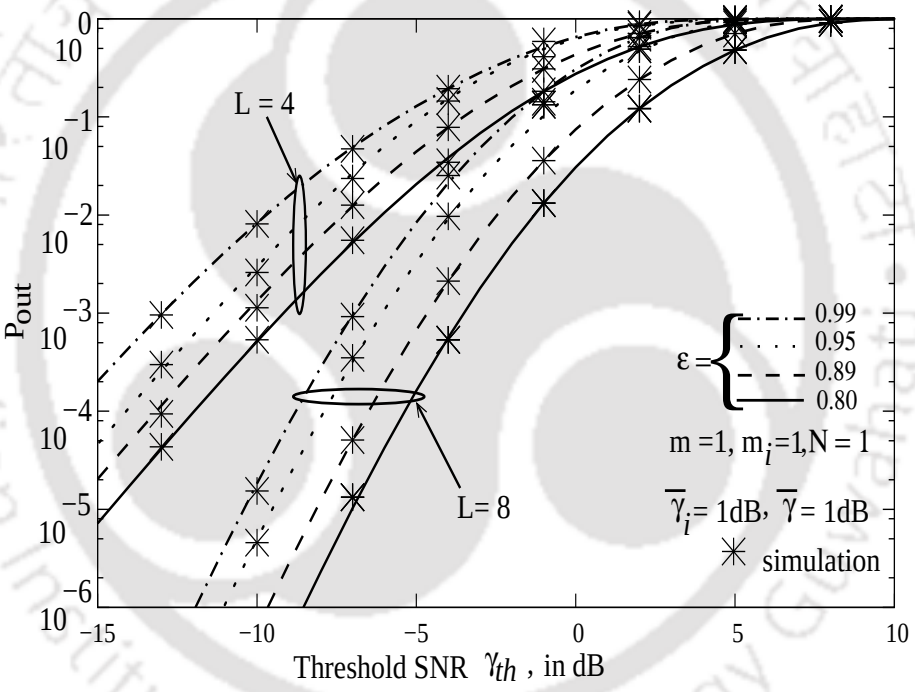

Figure 4.2: Outage probability of L-MRC receiver in Nakagami-m fading channels for $N = 1$, $m = 1$, $m_i = 1$ and $\bar{\gamma} = 1dB$.

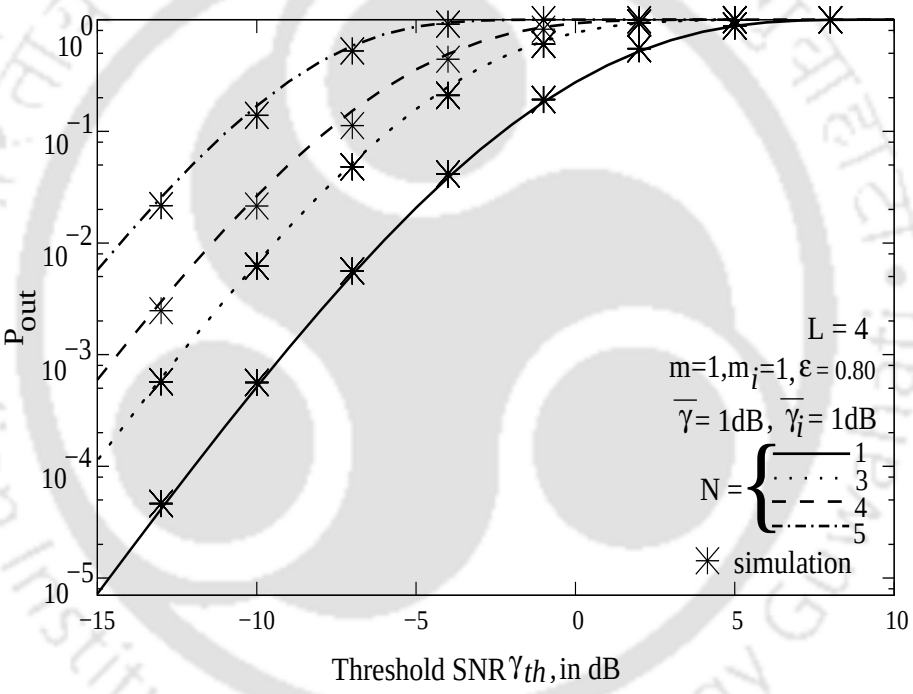

Figure 4.3: Outage probability of L-MRC receiver in Nakagami-m fading channels with $L = 4$, $m = 1$, $m_i = 1$, $\bar{\gamma} = 1dB$ and $\bar{\gamma}_i = 1dB$.

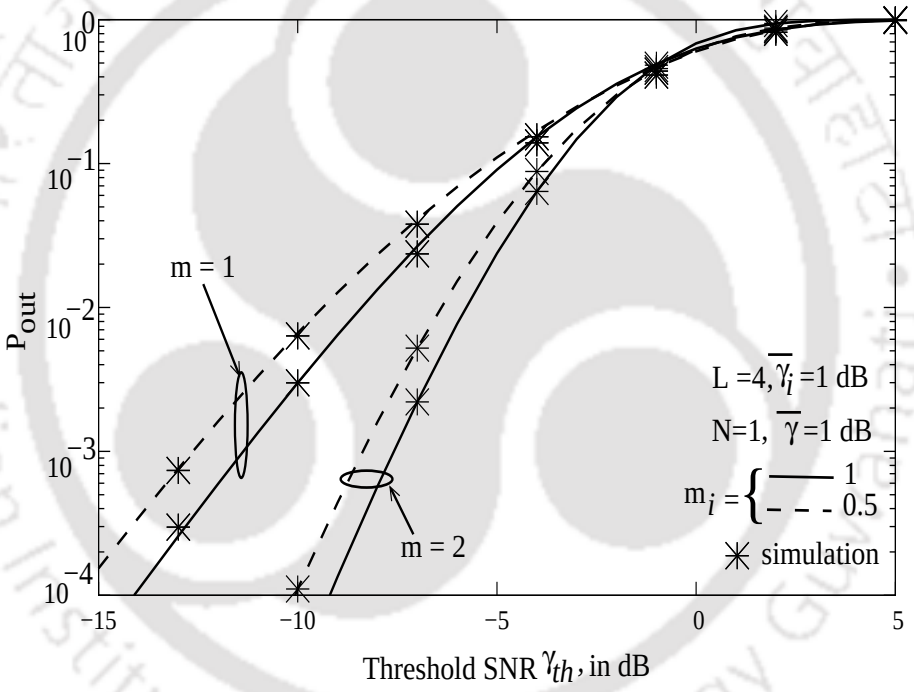

Figure 4.4: Outage probability of L-MRC receiver in Nakagami-m fading channels for L = 4, N=1, $\bar{\gamma} = 1$ and $\bar{\gamma}_i = 1dB$.

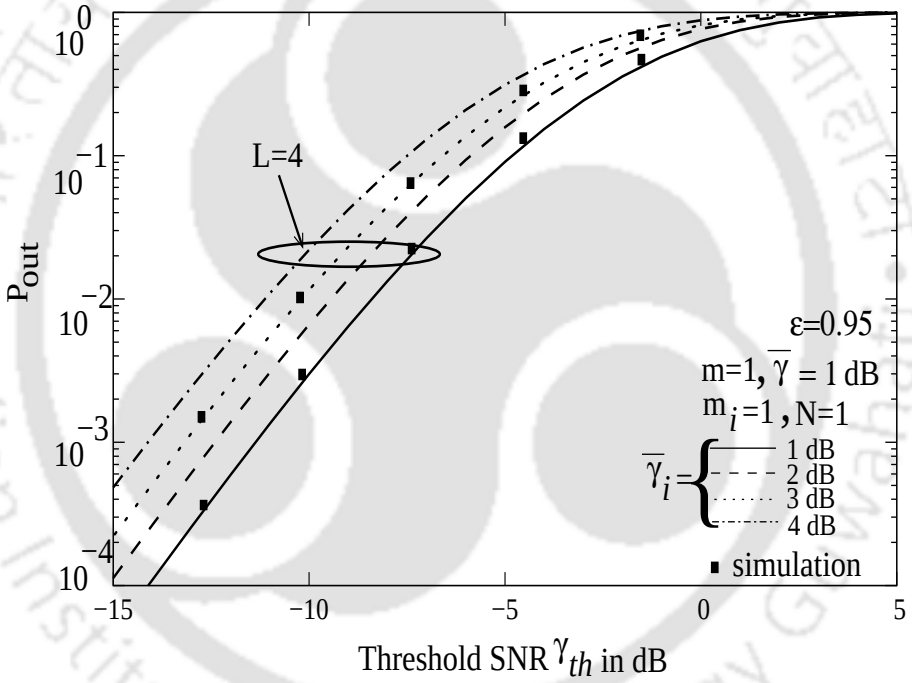

Figure 4.5: Outage probability of L-MRC receiver in Nakagami-m fading channels with $L = 4$, N=1, $m = 1$, $m_i = 1$ and $\bar{\gamma} = 1dB$.

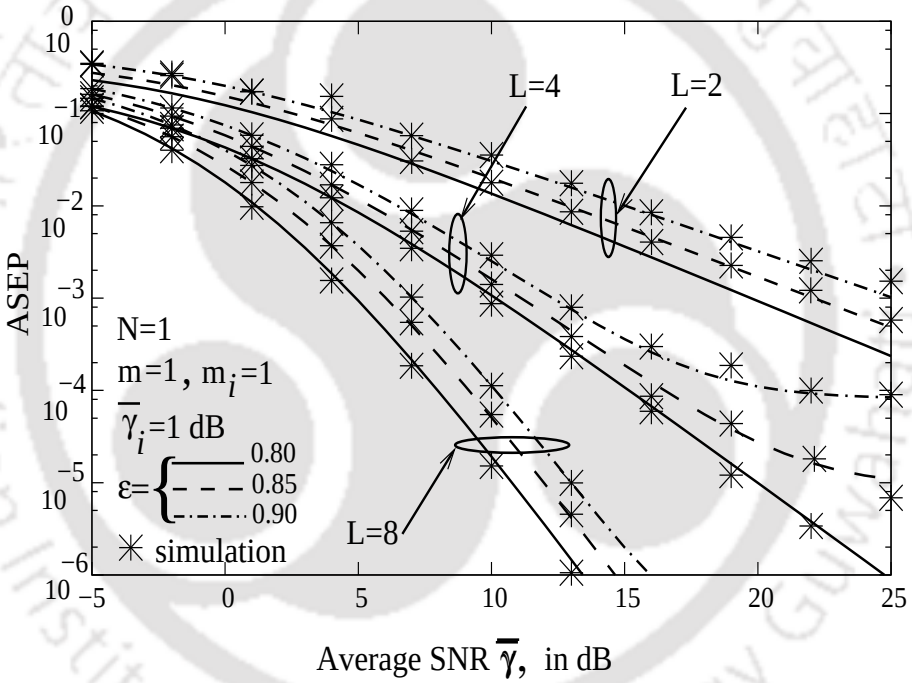

Figure 4.6: ASEP of *L*-MRC receiver in Nakagami-*m* fading channels with *N*=1, $m = 1$, $m_i = 1$ and $\bar{\gamma}_i = 1dB$.

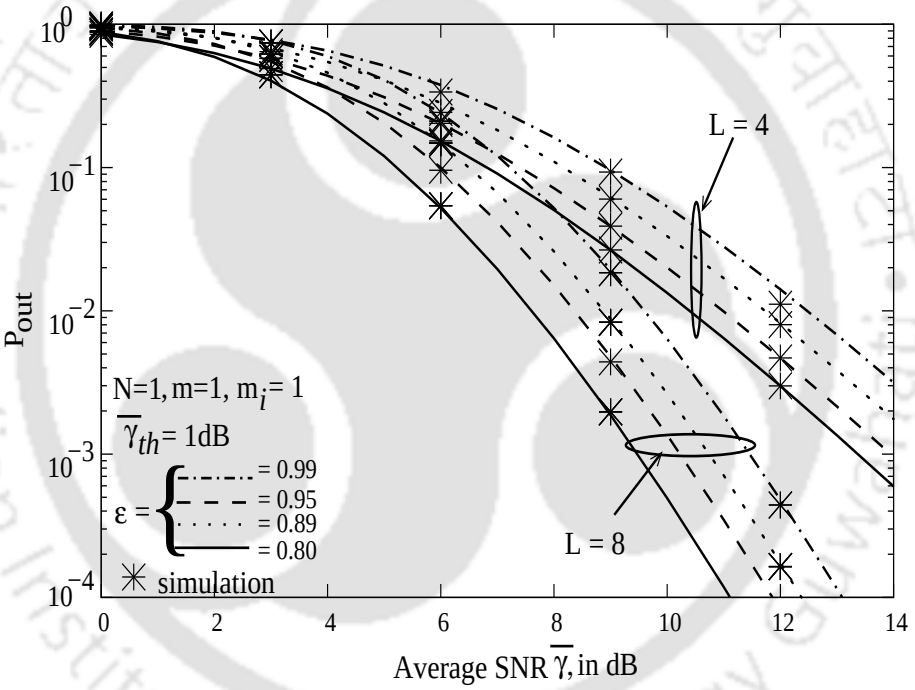

Figure 4.7: Outage probability of *L*-MRC receiver in Nakagami-*m* fading channels with *N*=1, $m = 1$, $m_i = 1$ and $\overline{\gamma}_i = 1dB$.

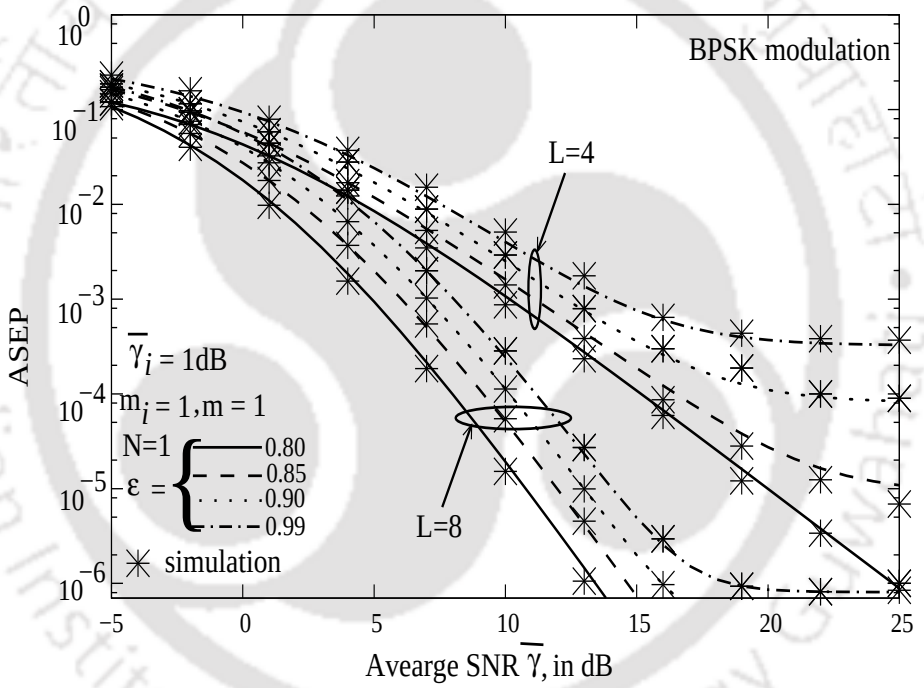

Figure 4.8: ASEP of *L*-MRC receiver in Nakagami-*m* fading channels with *N*=1, $m = 1$, $m_i = 1$ and $\bar{\gamma}_i = 1dB$.

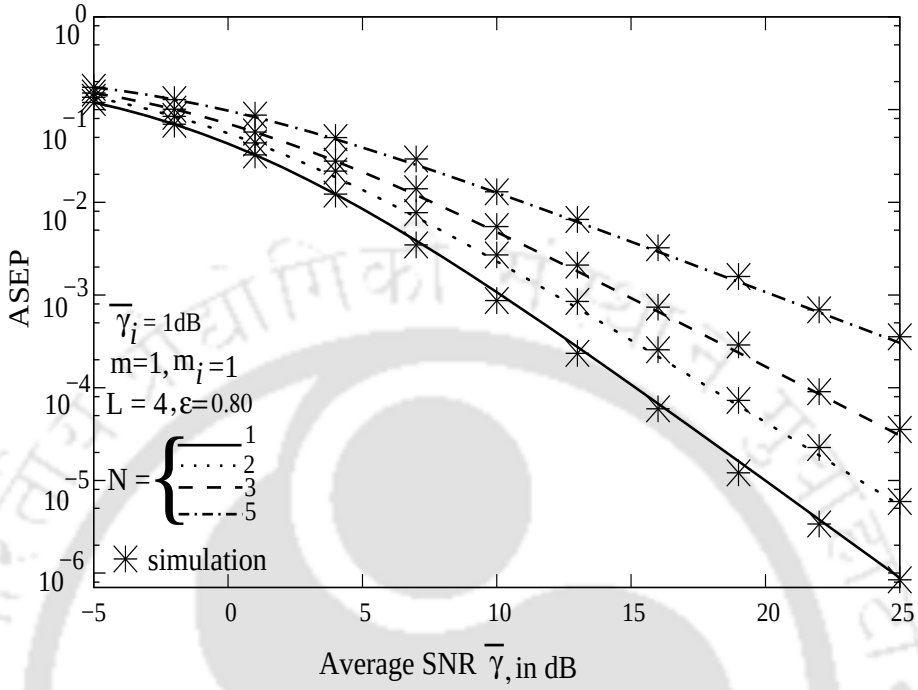

Figure 4.9: ASEP of L-MRC receiver in Nakagami-m fading channels with L=4, m = 1, $m_i = 1$ and $\overline{\gamma}_i = 1dB$.

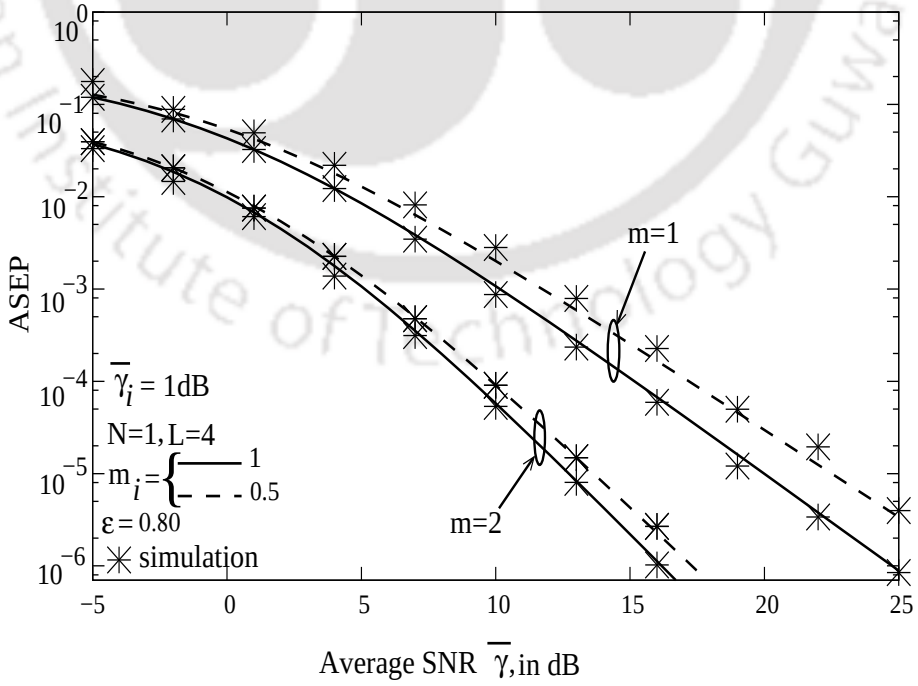

Figure 4.10: ASEP of L-MRC receiver in Nakagami-m fading channels with N=1, L=4, $\overline{\gamma}_i = 1dB$.

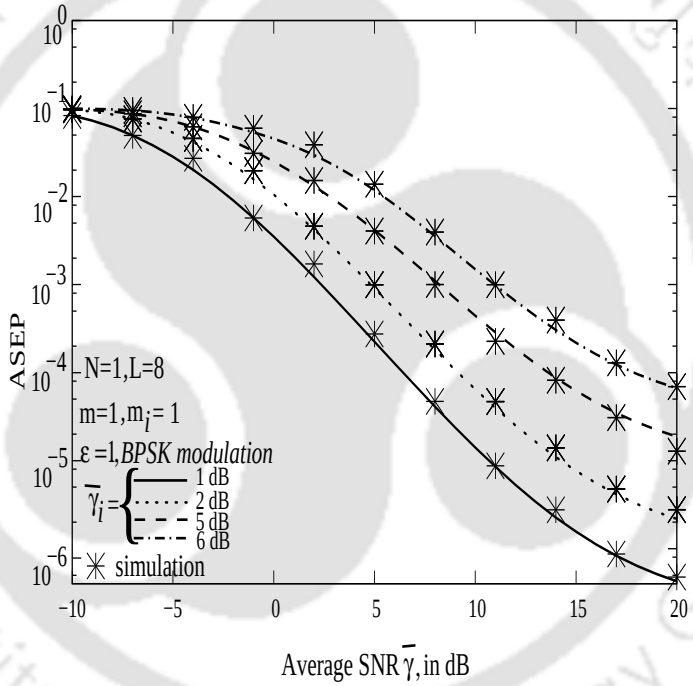

Figure 4.11: ASEP of *L*-MRC receiver in Nakagami-*m* fading channels with *N*=1, *L*=8, $m = 1$ and $m_i = 1$.

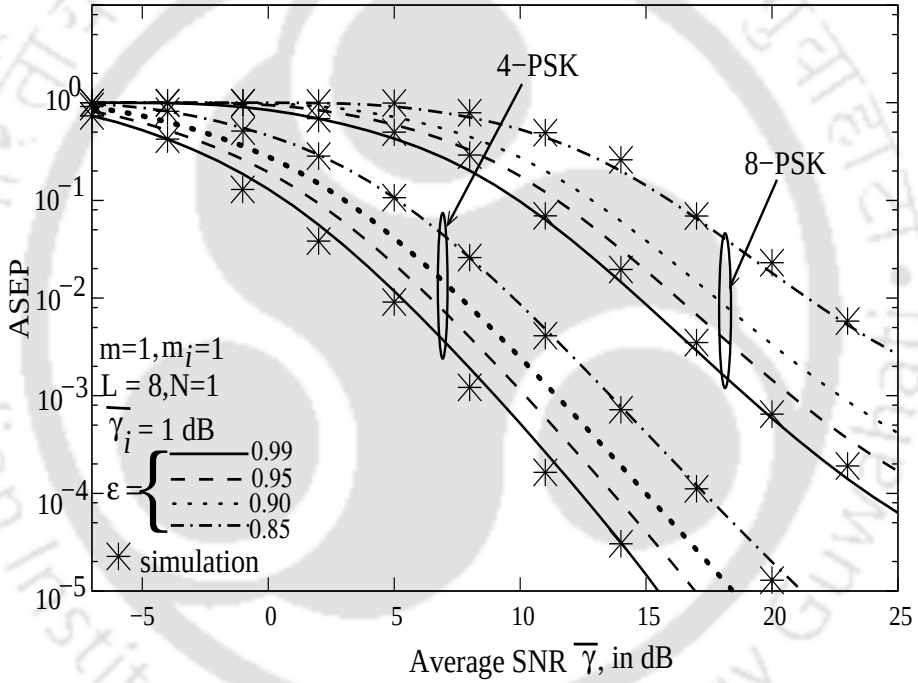

Figure 4.12: ASEP of L-MRC receiver in Nakagami-m fading channels with N=1, m = 1, $m_i = 1$, $\bar{\gamma}_i = 1$ and L=8.

4.5 Summary

In this chapter, performance analysis of L-MRC receiver with channel estimation error and CCI over Nakagami-m fading channels is presented. The summary of the work included is enumerated below.

1. Closed form expression for the PDF of MRC output SINR is derived.
2. Closed form expression for the outage probability of MRC receiver is derived.
3. Closed form expression for the ASEP for digital modulation schemes is derived.
4. Numerical and simulation results for outage and ASEP derived above are presented.

Chapter 5

Conclusions and Future Work

Performance analysis of diversity combining receivers over various fading channels is presented taking phase estimation error, CCI and AWGN into account. The performance measures considered are combiner output SNR, outage probability and ABEP of the system. In particular, for a dual-EGC receiver ABEP performance is obtained for correlated Hoyt, Nakagami-*m*, composite and non-homogeneous fading channels using MGF based approach. A PDF based approach is used to obtain the outage and ABEP performance of dual-EGC in Nakagami-*m* fading channels. For a *L*-EGC, outage probability is obtained over composite fading channels neglecting AWGN. Again using PDF based approach, outage and ABEP of *L*-EGC receiver is obtained for Nakagami-*m* fading channels for phase error and AWGN only.

For *L*-MRC receiver, outage and ASEP performance are obtained for Nakagami-*m* fading channels in the presence of channel estimation error and CCI. Closed-form expressions for MRC output SINR PDF, outage probability and ASEP are presented.

The obtained expressions are verified with published results in literature which are special cases of the system under consideration. Numerical results are plotted as a function of system parameters for the purpose of illustration and the effect of system parameters on the performance is studied. Simulation results are plotted with the numerical results and found to be closely matching.

5.1 Future Work

Some of the potential research works in the area related to the work presented in this thesis can be as listed below:

1. ABEP of L-EGC receiver over fading channels with phase error and CCI for other modulation techniques.
2. Performance analysis of EGC Receivers with phase error and adjacent channel interference.
3. Performance analysis of EGC receivers with arbitrary fading parameters and unequal branch SNRs.

Appendix A

Derivation of Expressions

A.1 Demodulated Signal at the EGC Output

The received signal at the l^{th} receiving antenna of the EGC combiner is given in Equation 2.2 as

$$r_l(t) = \alpha_{l,s} e^{j\phi_{l,s}} s_s(t) + n_{l,s}(t) + \sum_{i=1}^{N} \alpha_{l,i} e^{j\phi_{l,i}} s_i(t), 0 \leq t \leq T_s, l = 0,1,2,\ldots,L,$$

The receiver estimates the phase of the desired signal and uses a matched filter with impulse response $g_T(T-t)$. Let the estimated phase of the carrier of the desired signal received at the l^{th} antenna to be $e^{-j\widehat{\phi}_{l,s}}$. Thus, the matched filter output can be given as

$$\begin{aligned} y_l(t) &= a_s \alpha_{l,s} e^{j(\phi_{l,s}-\widehat{\phi}_{l,s})} \int_0^t g_T(\tau) g_T(T-(t-\tau)) d\tau + e^{-j\widehat{\phi}_{l,s}} \int_0^t n_{l,s}(\tau) g_T(T-(t-\tau)) d\tau \\ &\quad + \sum_{i=1}^{N} a_i \alpha_{l,i} e^{j(\phi_{l,i}-\widehat{\phi}_{l,s})} \int_0^t g_T(\tau) g_T(T-(t-\tau)) d\tau. \end{aligned} \tag{A.1}$$

From Equation A.1, the sampled output of the matched filter at $t = T$ can be obtained as

$$\begin{aligned} y_l &= a_s \alpha_{l,s} e^{j\psi_{l,s}} \int_0^T g_T^2(\tau) d\tau + e^{-j\widehat{\phi}_{l,s}} \int_0^T n_{l,s}(\tau) g_T(\tau) d\tau + \sum_{i=1}^{N} a_i \alpha_{l,i} e^{j(\phi_{l,i}-\widehat{\phi}_{l,s})} \int_0^T g_T^2(\tau) d\tau \\ &= a_s E_g \alpha_{l,s} e^{j\psi_{l,s}} + n_{0,l} e^{-j\hat{\phi}_{l,s}} + E_g \sum_{i=1}^{N} a_i \alpha_{l,i} e^{j(\phi_{l,i}-\hat{\phi}_{l,s})}, \end{aligned} \tag{A.2}$$

where $E_g = \int_0^\infty g_T^2(t)dt$, $n_{0,l} = \int_0^T n_{l,s}(\tau)g_T(\tau)d\tau$ which can be shown to be Gaussian with zero mean and power spectral density N_0E_g and $\psi_{l,s} = \phi_{l,s} - \widehat{\phi}_{l,s}$. Hence, the combined signal sample at the L branch EGC receiver output can be written as

$$y = E_g a_s \sum_{l=1}^{L} \alpha_{l,s} e^{j\psi_{l,s}} + \sum_{l=1}^{L} n_{0,l} e^{-j\widehat{\phi}_{l,s}} + E_g \sum_{i=1}^{N} \sum_{l=1}^{L} a_i \alpha_{l,i} e^{j\left(\phi_{l,i} - \widehat{\phi}_{l,s}\right)}. \tag{A.3}$$

A.2 Output SINR of EGC Receiver

The expression for the EGC receiver output signal in Equation A.3 has three terms. The first term is due to the desired signal, the second term is due to the AWGN noise and the third term is due to the interfering signal of the CCI users. The SINR is defined as the ratio of the signal power to the total power due to the AWGN and the CCI signals. Power of each term is obtained below:

1. Signal power at the combiner output from the first term in Equation A.3 is [3, 16]

$$P_s = E_g^2 \left[\sum_{l=1}^{L} \alpha_{l,s} \cos \psi_{l,s} \right]^2. \tag{A.4}$$

2. Total noise power at the combiner output can be derived as follows:

   Noise power of the noise component $n_{0,l}e^{-j\widehat{\phi}_{l,s}}$ of the second term in Equation A.3 can be given as $E[(n_{0,l}e^{-j\widehat{\phi}_{l,s}})^2]$ [54]. It is derived below:

$$\begin{aligned}
E[(n_{0,l}e^{-j\widehat{\phi}_{l,s}})^2] &= E\left[\left(\int_0^T n_{l,s}(\tau)g_T(\tau)d\tau e^{-j\widehat{\phi}_{l,s}} \right)^2 \right] \\
&= E\left[\left(\int_0^T n_{l,s}(t_1)g_T(t_1)dt_i e^{-j\widehat{\phi}_{l,s}} \right) \left(\int_0^T n_{l,s}(t_2)g_T(t_2)dt_2 e^{-j\widehat{\phi}_{l,s}} \right)^* \right] \\
&= E\left[\int_0^T \int_0^T n_{l,s}(t_1)n_{l,s}^*(t_2)g_T(t_1)dt_1 g_T(t_2)dt_2 \right] \\
&= \int_0^T \int_0^T E\left[n_{l,s}(t_1)n_{l,s}^*(t_2) \right] g_T(t_1)g_T(t_2)dt_1dt_2
\end{aligned}$$

$$= N_0 \int_0^T \int_0^T \delta(t_1 - t_2) g_T(t_1) g_T(t_2) dt_1 dt_2 = N_0 \int_0^T g_T^2(t_1)\, dt_1 = N_0 E_g.$$

Thus, total noise power is LN_0E_g.

3. From the third term in Equation A.3, the total interference power can be given as $E_g^2 \sum_{i=1}^{N} \sum_{l=1}^{L} [\alpha_{l,i}^2]$ [23].

Hence, SINR at the combiner output for dual-EGC receiver ($L = 2$)can be written as

$$\gamma_{egc} = \frac{1}{2} \frac{\frac{E_g}{N_0} \left[\sum_{l=1}^{2} \alpha_{l,s} \cos\left(\psi_{l,s}\right) \right]^2}{1 + \frac{E_g}{2N_0} \sum_{i=1}^{N} \sum_{l=1}^{2} \left[\alpha_{l.i}^2\right]} = \frac{1}{2} \frac{\frac{E_g}{N_0} \left[\sum_{l=1}^{2} \alpha_{l,s} \cos\left(\psi_{l,s}\right) \right]^2}{1 + \frac{E_g}{2N_0} \sum_{i=1}^{N} \sum_{l=1}^{2} \left[\alpha_{l.i}^2\right]} = \frac{1}{2} \frac{\left[\sum_{l=1}^{2} \sqrt{\gamma_{l,s}} \cos\left(\psi_{l,s}\right) \right]^2}{1 + \frac{1}{2} \sum_{i=1}^{N} \sum_{l=1}^{2} \left[\gamma_{l.i}\right]}. \quad \text{(A.5)}$$

Thus, the nth moment of γ_{egc} can be given as

$$\begin{aligned} E\left[\gamma_{egc}^n\right] &= \left(\frac{1}{2}\right)^n E\left[\frac{\left[\sum_{l=1}^{2} \sqrt{\gamma_{l,s}} \cos\left(\psi_{l,s}\right) \right]^2}{\left(1 + \frac{1}{2} \sum_{i=1}^{N} \sum_{l=1}^{2} \left[\gamma_{l.i}\right]\right)} \right]^n \\ &= \left(\frac{1}{2}\right)^n E\left[\sum_{l=1}^{2} \sqrt{\gamma_{l,s}} \cos\left(\psi_{l,s}\right) \right]^{2n} E\left[\left(\frac{1}{\left(1 + \frac{1}{2} \sum_{i=1}^{N} \sum_{l=1}^{2} \gamma_{l,i}\right)} \right)^n \right]. \quad \text{(A.6)} \end{aligned}$$

Applying binomial theorem [10, (1.111)], $E\left[\sum_{l=1}^{2} \sqrt{\gamma_{l,s}} \cos\left(\psi_{l,s}\right) \right]^{2n}$ in Equation A.6 can be expressed as

$$E\left[\sum_{l=1}^{2} \sqrt{\gamma_{l,s}} \cos\left(\psi_{l,s}\right) \right]^{2n} = (2n)! \sum_{\substack{k_1=0 \\ k_2=2n-k_1}}^{2n} \frac{E\left[\gamma_{1,s}^{k_1/2} \gamma_{2,s}^{k_2/2}\right]}{k_1! k_2!} \prod_{l=1}^{2} E\left[\cos^{k_l}\left(\psi_{l,s}\right)\right]. \quad \text{(A.7)}$$

The second expectation term in Equation A.6 can be written as

$$E\left[\left(\frac{1}{\left(1 + \frac{1}{2} \sum_{i=1}^{N} \sum_{l=1}^{2} \gamma_{l,i}\right)} \right)^n \right] = E\left[\left(\frac{1}{(1+z)} \right)^n \right] = \int_0^\infty \left(\frac{1}{(1+z)} \right)^n p_z(z) dz, \quad \text{(A.8)}$$

where $z = \frac{1}{2}\sum_{i=1}^{N}\sum_{l=1}^{2}\gamma_{l,i}$. The PDF of z can be given as (Appendix A.10.1)

$$p_z(z) = \left(\frac{2m_i}{\bar{\gamma}_i}\right)^{2m_iN} \frac{z^{2m_iN-1}}{\Gamma(2m_iN)} \exp\left(-\frac{2m_i}{\bar{\gamma}_i}z\right) \tag{A.9}$$

Assuming $\bar{\gamma}_{l,i}$s are iid, i.e., $\bar{\gamma}_{l,i} = \bar{\gamma}_i$ [3, (2.23)]] and substituting Equation A.9 in Equation A.8, we get

$$\begin{aligned} E\left[\left(\frac{1}{\left(1+\frac{1}{2}\sum_{i=1}^{N}\sum_{l=1}^{2}\gamma_i\right)}\right)^n\right] &= \left(\frac{2m_i}{\bar{\gamma}_i}\right)^{2mN} \frac{1}{\Gamma(2m_iN)} \int_0^\infty \left(\frac{1}{(1+z)}\right)^n z^{2m_iN-1} \exp\left(-\frac{2m_i}{\bar{\gamma}_i}z\right) dz \\ &= \Psi\left(2m_iN, 2m_iN+1-n, \frac{2m_i}{\bar{\gamma}_i}\right), \end{aligned} \tag{A.10}$$

where the integration in Equation A.10 can be solved by applying [10, (3.383/5)] and $\Psi(a;b;z)$ is the "confluent hypergeometric function" [10, (9.21)]. Thus, substituting Equations A.10 and A.7 in Equation A.6 we get the n^{th} moment of γ_{egc} as,

$$E\left[\gamma_{egc}^n\right] = \frac{(2n)!}{2^n} \sum_{\substack{k_1=0 \\ k_2=2n-k_1}}^{2n} \frac{E\left[\gamma_{1,s}^{k_1/2}\gamma_{2,s}^{k_2/2}\right]}{k_1!k_2!} \prod_{l=1}^{2} E\left[\cos^{k_l}\left(\psi_{l,s}\right)\right] \Psi\left(2m_iN, 2m_iN+1-n, \frac{2m_i}{\bar{\gamma}_i}\right). \tag{A.11}$$

A.3 Joint Moments of Correlated Hoyt Fading Channels

Let $\alpha_{1,s}$ and $\alpha_{2,s}$ be two correlated Hoyt distributed RV with correlation coefficient ρ. These RVs can be represented using independent zero mean Gaussian RVs X and Y with variances σ_X^2 and σ_Y^2, respectively, as [35]

$$\alpha_{i,s}^2 = X_i^2 + Y_i^2, i = 1,2. \tag{A.12}$$

In this representation the Hoyt RV $\alpha_{i,s}$ has the marginal PDF given in Equation 1.3, where the fading parameter $q = \sigma_y/\sigma_x$. Let us define $\eta_1 = \eta_2 = \frac{\sigma_y^2}{\sigma_x^2}$, $\mu_1^2 = \frac{E[X_1X_2]}{\sigma_{X_1}\sigma_{X_2}}$ and $\mu_2^2 = \frac{E[X_1Y_2]}{\sigma_{X_1}\sigma_{Y_2}}$ and $\rho^2 = \mu_1^2 + \mu_2^2$.

An expression for $\mathrm{E}\left[\left(\frac{\alpha_{1,s}^2}{\mathrm{E}[\alpha_{1,s}^2]}\right)^{n_1}\left(\frac{\alpha_{2,s}^2}{\mathrm{E}[\alpha_{2,s}^2]}\right)^{n_2}\right]$, is given as [35]

$$
\begin{aligned}
&E\left[\left(\frac{\alpha_{1,s}^2}{E\left[\alpha_{1,s}^2\right]}\right)^{n_1}\left(\frac{\alpha_{2,s}^2}{E\left[\alpha_{2,s}^2\right]}\right)^{n_2}\right] = \\
&= \frac{1}{(1+\eta_1)^{n_1}(1+\eta_2)^{n_2}}\sum_{t_1=0}^{n_1}\sum_{t_2=0}^{n_2}\frac{\Gamma(n_1+1)\Gamma(n_2+1)\eta_1^{t_1}\eta_2^{t_2}(2t_1)!(2n_1-2t_1)!\mu_1^{2n_1-2t_1}\mu_2^{2t_1}}{\Gamma(t_1+1)\Gamma(t_2+1)\Gamma(n_1-t_1+1)(n_2-t_2+1)} \\
&\times\sum_{i_1=0}^{t_1}\sum_{j_1=0}^{n_1-t_1}\sum_{i_2=0}^{2t_1-2i_1}\sum_{j_2=\lceil i_2/2\rceil}^{n_1+\lfloor i_2/2\rfloor-t_1-j_1}\frac{(-1)^{i_2}}{2^{i_1+j_1}}\frac{[2(n_1+n_2-t_2-i_1-j_1-j_2)-1]!!}{(2t_1-2i_1-i_2)![2(n_1-t_1-j_1-j_2)+i_2]!} \\
&\times\frac{(2t_2+2j_2-1)!!}{i_1!i_2!j_1!(2j_2-i_2)!}\left(\frac{\mu_1}{\mu_2}\right)^{2i_2-2j_2}\frac{(1-\rho^2)^{i_1+j_1}}{\mu_1^{2j_1}\mu_2^{2i_1}},
\end{aligned}
\tag{A.13}
$$

where n_1, n_2, t_1, and t_2 are non-negative integers satisfying $t_i \le n_i$, $i=1,2$, $\lfloor v\rfloor$ is the greatest integer less than or equal to v, $\lceil v\rceil$ is the smallest integer greater than or equal to v. The above expression can be simplified by assuming $\sigma_x^2=\sigma_y^2$, $q=\sigma_y^2$ and $\mu_1^2=\mu_2^2$. The simplified expression as a function of $\gamma_{1,s}$ and $\gamma_{2,s}$ can be given as

$$
\begin{aligned}
E\left[\gamma_{1,s}^{n_1}\gamma_{2,s}^{n_1}\right] &= \left(\frac{q}{1+q}\right)^{n_1+n_2}\sum_{t_1=0}^{n_1}\sum_{t_2=0}^{n_2}\frac{\Gamma(n_1+1)\Gamma(n_2+1)}{\Gamma(t_1+1)\Gamma(t_2+1)\Gamma(n_1-t_1+1)} \\
&\times\left(\frac{1}{q}\right)^{t_1+t_2}\frac{(2t_1)!(2n_1-2t_1)!}{\Gamma(n_2-t_2+1)}\left(\frac{\rho^2}{2}\right)^{n_1} \\
&\times\sum_{i_1=0}^{t_1}\sum_{j_1=0}^{n_1-t_1}\sum_{i_2=0}^{2t_1-2i_1}\sum_{j_2=\lceil i_2/2\rceil}^{n_1+\lfloor i_2/2\rfloor-t_1-j_1}\frac{(-1)^{i_2}[2(n_1+n_2-t_2-i_1-j_1-j_2)-1]!!}{(2t_1-2i_1-i_2)![2(n_1-t_1-j_1-j_2)+i_2]!} \\
&\times\frac{(2t_2+2j_2-1)!!(1-\rho^2)^{i_1+j_1}\bar{\gamma}_{1,s}^{n_1}\bar{\gamma}_{1,s}^{n_2}}{i_1!i_2!j_1!(2j_2-i_2)!\rho^{2(i_1+j_1)}}.
\end{aligned}
\tag{A.14}
$$

A.4 Derivation of Joint Moments of GG RVs

Let us consider the joint moment expression $\mathrm{E}\left[\alpha_1^{n_1}\alpha_2^{n_2}\right]$ for the GG RVs α_1 and α_2 in [50, (8)],

$$
E\left[\alpha_1^{n_1}\alpha_2^{n_2}\right] = \frac{\left(\frac{\Omega_1}{m_1}\right)^{\frac{n_1}{\beta_1}}\left(\frac{\Omega_2}{m_2}\right)^{\frac{n_2}{\beta_2}}}{\Gamma(m_1)\Gamma(m_2)}\Gamma\left(m_1+\frac{n_1}{\beta_1}\right)\Gamma\left(m_2+\frac{n_2}{\beta_2}\right),
\tag{A.15}
$$

where $\Omega_i = \mathrm{E}\left[\alpha_i^2\right]$. Substituting α_i from the relation $\gamma_i = \frac{E_s}{N_0}\alpha_i^2$, Equation A.15 can be rewritten as

$$E\left[\left(\gamma_1^{\frac{n_1}{2}}\right)\left(\gamma_2^{\frac{n_2}{2}}\right)\right] = \frac{\left(\frac{E_s}{N_0}\left(\frac{\Omega_1}{m_1}\right)^{\frac{2}{\beta_1}}\right)^{\frac{n_1}{2}}\left(\frac{E_s}{N_0}\left(\frac{\Omega_2}{m_2}\right)^{\frac{2}{\beta_2}}\right)^{\frac{n_2}{2}}}{\Gamma(m_1)\Gamma(m_2)}\Gamma\left(m_1+\frac{n_1}{\beta_1}\right)\Gamma\left(m_2+\frac{n_2}{\beta_2}\right) \times {}_2F_1\left[-\frac{n_1}{\beta_1},-\frac{n_2}{\beta_2},m_2,\rho\right]. \quad \text{(A.16)}$$

Using the relation [8, (3)], $E\left[\alpha_i^2\right] = \frac{\left(\frac{\Omega_i}{m_i}\right)^{\frac{2}{\beta_i}}}{\Gamma(m_i)}\Gamma\left(m_i+\frac{2}{\beta_i}\right)$, we can express $\left(\frac{\Omega_1}{m_1}\right)^{\frac{2}{\beta_1}} = E\left[\alpha_1^2\right]\frac{\Gamma(m_1)}{\Gamma\left(m_1+\frac{2}{\beta_1}\right)}$.

Substituting this expressions for $\left(\frac{\Omega_1}{m_1}\right)^{\frac{2}{\beta_1}}$ and $\left(\frac{\Omega_2}{m_2}\right)^{\frac{2}{\beta_2}}$ in Equation A.16 we get

$$E\left[\left(\gamma_1^{\frac{n_1}{2}}\right)\left(\gamma_2^{\frac{n_2}{2}}\right)\right] = \frac{\left(\frac{E_s}{N_0}E\left[\alpha_1^2\right]\frac{\Gamma(m_1)}{\Gamma\left(m_1+\frac{2}{\beta_1}\right)}\right)^{\frac{n_1}{2}}\left(\frac{E_s}{N_0}E\left[\alpha_2^2\right]\frac{\Gamma(m_2)}{\Gamma\left(m_2+\frac{2}{\beta_2}\right)}\right)^{\frac{n_2}{2}}}{\Gamma(m_1)\Gamma(m_2)} \times\Gamma\left(m_1+\frac{n_1}{\beta_1}\right)\Gamma\left(m_2+\frac{n_2}{\beta_2}\right){}_2F_1\left[-\frac{n_1}{\beta_1},-\frac{n_2}{\beta_2},m_2,\rho\right]. \quad \text{(A.17)}$$

Putting $m_1 = m_2 = m_g$, $\beta_1 = \beta_2 = \beta_g$, $\bar{\gamma}_i = \frac{E_s}{N_0}E\left[\alpha_i^2\right]$, $\Delta = \frac{\Gamma(m_g)}{\Gamma\left(m_g+\frac{2}{\beta_g}\right)}$, in Equation A.17 we get,

$$E\left[\left(\gamma_1^{\frac{n_1}{2}}\right)\left(\gamma_2^{\frac{n_2}{2}}\right)\right] = \frac{\bar{\gamma}_1^{\frac{n_1}{2}}\bar{\gamma}_2^{\frac{n_2}{2}}\Delta^{\frac{n_1+n_2}{2}}}{\Gamma(m_g)\Gamma(m_g)}\Gamma\left(m_g+\frac{n_1}{\beta_g}\right)\Gamma\left(m_g+\frac{n_2}{\beta_g}\right){}_2F_1\left[-\frac{n_1}{\beta_g},-\frac{n_2}{\beta_g},m_g,\rho\right] . \quad \text{(A.18)}$$

A.5 Derivation of Joint Moments of Generalized-K RVs

Let us consider the joint moment expression $\mathrm{E}\left[\alpha_1^{n_1}\alpha_2^{n_2}\right]$ for KG RVs α_1 and α_2 given below [5, (6)]

$$E[\alpha_1^{n_1}\alpha_2^{n_2}] = \left(\prod_{l=1}^{2}\frac{\Gamma\left(m+\frac{n_l}{2}\right)\Gamma\left(\beta+\frac{n_l}{2}\right)\Omega_l{}^{\frac{n_l}{2}}}{\Gamma(m)\Gamma(\beta)m^{\frac{n_l}{2}}}\right){}_2F_1\left[-\frac{n_1}{2},-\frac{n_2}{2},m,\rho\right]{}_2F_1\left[-\frac{n_1}{2},-\frac{n_2}{2},\beta,\rho\right]. \quad \text{(A.19)}$$

Substituting $\gamma_i = \frac{E_s}{N_0}\left[\alpha_i^2\right]$ in Equation A.19

$$E[\gamma_1^{\frac{n_1}{2}}\gamma_2^{\frac{n_2}{2}}] = \left(\prod_{l=1}^{2}\frac{\Gamma\left(m+\frac{n_l}{2}\right)\Gamma\left(\beta+\frac{n_l}{2}\right)\left(\frac{E_s}{N_0}\Omega_l\right)^{\frac{n_l}{2}}}{\Gamma(m)\Gamma(\beta)m^{\frac{n_l}{2}}}\right) {}_2F_1\left[-\frac{n_1}{2},-\frac{n_2}{2},m,\rho\right] {}_2F_1\left[-\frac{n_1}{2},-\frac{n_2}{2},\beta,\rho\right]. \tag{A.20}$$

Using $\frac{\bar{\gamma}_l}{\beta} = \frac{E_s}{N_0}\mathrm{E}[\alpha^2] = \frac{E_s}{N_0}\Omega_l$ [5, (15b)] and putting $m = m_k$, $\beta = \beta_k$ in Equation A.20 we get

$$E[\gamma_1^{\frac{n_1}{2}}\gamma_2^{\frac{n_2}{2}}] = \left(\prod_{l=1}^{2}\frac{\Gamma\left(m_k+\frac{n_l}{2}\right)\Gamma\left(\beta_k+\frac{n_l}{2}\right)(\bar{\gamma}_l)^{\frac{n_l}{2}}}{\Gamma(m_k)\Gamma(\beta_k)m_k^{\frac{n_l}{2}}\beta_k^{\frac{n_l}{2}}}\right) {}_2F_1\left[-\frac{n_1}{2},-\frac{n_2}{2},m_k,\rho\right] {}_2F_1\left[-\frac{n_1}{2},-\frac{n_2}{2},\beta_k,\rho\right]. \tag{A.21}$$

A.6 Derivation of EGC Output SINR in Asynchronous Case

The EGC instantaneous output SINR can be given from Equation 3.20 as

$$\gamma_{egc} = \frac{1}{2}\frac{\frac{E_s}{N_0}\left[\sum_{l=1}^{2}\alpha_{l,s}\cos\left(\psi_{l,s}\right)\right]^2}{1+\left(1-\frac{\beta}{4}\right)\frac{E_i}{2N_0}\sum_{i=1}^{N}\sum_{l=1}^{2}\left[\alpha_{l,i}^2\right]} = \frac{1}{2}\frac{\frac{E_g}{N_0}\left[\sum_{l=1}^{2}\alpha_{l,s}\cos\left(\psi_{l,s}\right)\right]^2}{1+r\frac{E_g}{N_0}\sum_{i=1}^{N}\sum_{l=1}^{2}\left[\alpha_{l,i}^2\right]} = \frac{1}{2}\frac{\left[\sum_{l=1}^{2}\sqrt{\gamma_{l,s}}\cos\left(\psi_{l,s}\right)\right]^2}{1+r\sum_{i=1}^{N}\sum_{l=1}^{2}\left[\gamma_{l,i}\right]}, \tag{A.22}$$

where $r = \frac{1-\frac{\beta}{4}}{2}$. Thus, the n^{th} moment of γ_{egc} can be given from Equation A.22 as

$$\begin{aligned} E\left[\gamma_{egc}^n\right] &= \left(\frac{1}{2}\right)^n E\left[\frac{\left[\sum_{l=1}^{2}\sqrt{\gamma_{l,s}}\cos\left(\psi_{l,s}\right)\right]^2}{\left(1+r\sum_{i=1}^{N}\sum_{l=1}^{2}\left[\gamma_{l,i}\right]\right)}\right]^n \\ &= \left(\frac{1}{2}\right)^n E\left[\sum_{l=1}^{2}\sqrt{\gamma_{l,s}}\cos\left(\psi_{l,s}\right)\right]^{2n} E\left[\left(\frac{1}{\left(1+r\sum_{i=1}^{N}\sum_{l=1}^{2}\gamma_{l,i}\right)}\right)^n\right]. \end{aligned} \tag{A.23}$$

The first expectation term in Equation A.23 is given in Equation A.7 and is reproduced below.

$$E\left[\sum_{l=1}^{2}\sqrt{\gamma_{l,s}}\cos\left(\psi_{l,s}\right)\right]^{2n} = (2n)!\sum_{\substack{k_1=0\\k_2=2n-k_1}}^{2n}\frac{E\left[\gamma_{1,s}^{k_1/2}\gamma_{2,s}^{k_2/2}\right]}{k_1!k_2!}\prod_{l=1}^{2}E\left[\cos^{k_l}\left(\psi_{l,s}\right)\right]. \tag{A.24}$$

The second expectation term in Equation A.23 can be derived by following the same procedure used for synchronous case in Equation A.8, as

$$E\left[\left(\frac{1}{\left(1+r\sum_{i=1}^{N}\sum_{l=1}^{2}\gamma_{l,i}\right)}\right)^{n}\right]=\Psi\left(2m_iN,2m_iN+1-n,\frac{m_i}{r\bar{\gamma}_i}\right). \tag{A.25}$$

Assuming $\bar{\gamma}_{l,i}$s are i.i.d, i.e., $\bar{\gamma}_{l,i}=\bar{\gamma}_i$. [3, (2.23)] and substituting Equation A.24 and Equation A.25 in Equation A.23, the nth moment of γ_{egc} can be given as

$$E\left[\gamma_{egc}^{n}\right]=\frac{(2n)!}{2^n}\sum_{\substack{k_1=0\\k_2=2n-k_1}}^{2n}\frac{E\left[\gamma_{1,s}^{k_1/2}\gamma_{2,s}^{k_2/2}\right]}{k_1!k_2!}\prod_{l=1}^{2}E\left[\cos^{k_l}\left(\psi_{l,s}\right)\right]\Psi\left(2m_iN,2m_iN+1-n,\frac{m_i}{r\bar{\gamma}_i}\right). \tag{A.26}$$

A.7 Derivation of $\mathbf{E}_U\{e^{-jn\omega_0\sqrt{\gamma_{th}U}}\}$

The integration in Equation 3.41 can be solved by applying [10, (3.462.1)] and the resulting expression can be given as

$$E_U\{e^{-jn\omega_0\sqrt{\gamma_{th}U}}\}=2^{1-\eta}\frac{\Gamma(2\eta)}{\Gamma(\eta)}e^{-\frac{n^2\omega_0{}^2\gamma_{th}}{8\left(\frac{m_i}{\Omega_i}\right)}}D_{-2\eta}\left(\frac{jn\omega_0\sqrt{\gamma_{th}}}{\sqrt{2\frac{m_i}{\Omega_i}}}\right). \tag{A.27}$$

The parabolic cylinder function $D_{-2\eta}(\cdot)$ can be expressed as [10, (9.240)]

$$\begin{aligned}D_{-2\eta}\left(\frac{jn\omega_0\sqrt{\gamma_{th}}}{\sqrt{2\frac{m_i}{\Omega_i}}}\right) &= 2^{-\eta}e^{\frac{n^2\omega_0^2\gamma_{th}\Omega_i}{8m_i}}\left[\frac{\sqrt{\pi}}{\Gamma\left(\frac{1+2\eta}{2}\right)}\right]{}_2F_1\left[\eta,\frac{1}{2},-\frac{n^2\omega_0^2\gamma_{th}\Omega_i}{4m_i}\right]\\ &\quad-\frac{\sqrt{2\pi}jn\omega_0\sqrt{\gamma_{th}}\sqrt{\frac{\Omega_i}{m_i}}}{\sqrt{2}\Gamma(\eta)}{}_2F_1\left[\frac{1}{2}+\eta,\frac{3}{2},-\frac{n^2\omega_0^2\gamma_{th}\Omega_i}{4m_i}\right].\end{aligned} \tag{A.28}$$

Substituting Equation A.28 in Equation A.27 we get

$$\begin{aligned}E_U\{e^{-jn\omega_0\sqrt{\gamma_{th}U}}\} &= \frac{\sqrt{\pi}2^{1-2\eta}\Gamma(2\eta)}{\Gamma(\eta)}\left(\left[\frac{1}{\Gamma\left(\frac{1}{2}+\eta\right)}\right]{}_2F_1\left[\eta,\frac{1}{2},-\frac{n^2\omega_0^2\gamma_{th}\Omega_i}{4m_i}\right]\right.\\ &\quad\left.-\frac{jn\omega_0\sqrt{\gamma_{th}}\sqrt{\frac{\Omega_i}{m_i}}}{\Gamma(\eta)}{}_2F_1\left[\frac{1}{2}+\eta,\frac{3}{2},-\frac{n^2\omega_0^2\gamma_{th}\Omega_i}{4m_i}\right]\right).\end{aligned} \tag{A.29}$$

Applying the identity [10, (8.335.1)] in Equation A.29 we get

$$E_U\{e^{-jn\omega_0\sqrt{\gamma_{th}U}}\} = {}_2F_1\left[\eta,\frac{1}{2},-\frac{n^2\omega_0^2\gamma_{th}\Omega_i}{4m_i}\right] - \frac{jn\omega_0\sqrt{\gamma_{th}}}{\Gamma(\eta)}\sqrt{\frac{\Omega_i}{m_i}}\Gamma\left(\eta+\frac{1}{2}\right){}_2F_1\left[\frac{1}{2}+\eta,\frac{3}{2},-\frac{n^2\omega_0^2\gamma_{th}\Omega_i}{4m_i}\right]\Bigg). \quad \text{(A.30)}$$

A.8 Derivation of PDF of $\gamma_{egc} = \left(\sum_{l=1}^{L}\sqrt{\gamma_l}\cos(\psi_l)\right)^2$

The PDF of γ_l is given in Equation 3.47. Thus, the PDF of $\sqrt{\gamma_l}$ can be obtained by applying the technique of transformation of RVs. Assuming $x=\gamma_l$, the PDF of $y=\sqrt{\gamma_l}$ can be derived using formula given in Appendix A.103 as

$$f_{\sqrt{\gamma_l}}(\sqrt{\gamma_l}) = 2(\sqrt{\gamma_l})f_x\left(\sqrt{\gamma_l}^2\right) = 2\sqrt{\gamma_l}\left(\frac{m}{\bar{\gamma}}\right)^m\frac{\sqrt{\gamma_l}^{2m-2}}{\Gamma(m)}e^{\left(-\frac{m}{\bar{\gamma}}(\sqrt{\gamma_l})^2\right)}. \quad \text{(A.31)}$$

The PDF of ψ_l is given in Equation 3.47 as

$$f_{\psi_l}(\psi_l) = \frac{\exp[\zeta_l\cos(\psi_l)]}{2\pi I_0(\zeta_l)}, |\psi_l| \le \pi. \quad \text{(A.32)}$$

Using the approximation for Bessel function of first kind [10, (8.451.5)] i.e., $I_0(\zeta_l) \approx \frac{e^{\zeta_l}}{\sqrt{2\pi\zeta_l}}$ and the Taylor series expansion of $\cos(\psi)$ i.e., $\cos(\psi_l) = 1-\frac{\psi^2}{2!}+\frac{\psi^4}{4!}-\frac{\psi^6}{6!}+\ldots$, in Equation A.32 we get

$$f_{\psi_l}(\psi_l) = \frac{e^{[\zeta\cos(\psi)]}-e^{\zeta}}{\sqrt{2\pi/\zeta}} = \frac{e^{\zeta(\cos\psi-1)}}{\sqrt{2\pi/\zeta}} = \frac{e^{\zeta\left(\left[1-\frac{\psi^2}{2!}+\frac{\psi^4}{4!}-\frac{\psi^6}{6!}+\ldots\right]-1\right)}}{\sqrt{2\pi/\zeta}} = \frac{e^{\left(\left[\zeta-\frac{\zeta\psi^2}{2!}+\frac{\zeta\psi^4}{4!}-\frac{\zeta\psi^6}{6!}+\ldots\right]-\zeta\right)}}{\sqrt{2\pi/\zeta}} \approx \frac{e^{-\frac{\zeta\psi^2}{2!}}}{\sqrt{2\pi/\zeta}}. \quad \text{(A.33)}$$

Using the approximate PDF expression for ψ_l in Equation A.33, an expression for the PDF of $\cos(\psi_l)$ can be derived using formula shown in Appendix A.104. An expression for the PDF can be obtained as

$$f_{\cos(\psi)}(\cos(\psi) = \frac{2e^{-\frac{\zeta\psi^2}{2!}}}{\sqrt{2\pi/\zeta}\sqrt{1-\cos^2(\psi)}} = \frac{2e^{-\frac{\zeta\psi^2}{2!}}}{\sqrt{2\pi/\zeta}\sqrt{1-\cos^2(\psi)}} = \frac{2e^{-\frac{\zeta\psi^2}{2!}}}{\sqrt{2\pi/\zeta}\sin(\psi)}. \quad \text{(A.34)}$$

For small values of phase estimation error $\sin\psi \approx \psi$. So, putting in Equation A.34, the PDF can be expressed as

$$f_{\cos(\psi_l)}(\cos(\psi_l) \approx \sqrt{\frac{2\zeta_l}{\pi}} \frac{e^{-\frac{\zeta_l {\psi_l}^2}{2}}}{\psi_l}. \tag{A.35}$$

Using the PDFs of $\sqrt{\gamma_l}$ and $\cos\psi_l$, in Equations A.31 and A.35, respectively, the PDF of $z = \sqrt{\gamma_l}\cos(\psi_l)$ can be derived as follows:

Let $z = xy$, where $x = \sqrt{\gamma_l}$ and $y = \cos(\psi_l)$, then the PDF of z can be derived from formula [55]

$$f_z(z) = \int_0^\infty \frac{1}{x} f_x(x) f_y(z/x)\, dx. \tag{A.36}$$

Substituting the PDF of x and z in Equation A.36 we get

$$f_z(z) = \left(\frac{m}{\bar{\gamma}}\right)^m \frac{4\sqrt{\zeta_l}}{\Gamma(m) z\sqrt{2\pi}} \int_0^\infty \sqrt{\gamma_l}^{2m-1} e^{-\frac{m}{\bar{\gamma}}\left(\sqrt{\gamma_l}\right)^2} e^{-\frac{{\zeta_z}^2}{2\left(\sqrt{\gamma_l}\right)^2}} d\sqrt{\gamma_l}. \tag{A.37}$$

Solving the integral in Equation A.37 using [10, (3.478.4)] we get

$$\begin{aligned} f_z(z) &= \left(\frac{m}{\bar{\gamma}}\right)^m \frac{\left(\sqrt{\zeta_l}\right)^{\frac{m}{2}+\frac{1}{2}}}{\Gamma(m)\sqrt{2\pi}} \frac{z^{m-1}}{2^{m/2}} K_m\left(\sqrt{\frac{2m\zeta_l}{\bar{\gamma}}} z\right) \\ &= \left(\sqrt{\frac{m}{\bar{\gamma}}}\right)^{m-\frac{1}{2}} \frac{\left(\sqrt{\zeta_l}\right)^{m+\frac{1}{2}}}{\left(\sqrt{2}\right)^{m-\frac{3}{2}}} \frac{z^{m-\frac{3}{2}}}{\Gamma(m)} e^{-\sqrt{\frac{2m\zeta_l}{\bar{\gamma}}} z}. \end{aligned} \tag{A.38}$$

where $K_m(\cdot)$ is the modified Bessel function of second kind defined as $K_m(x) = \sqrt{\frac{\pi}{2x}} e^{-x}$.

Integrating Equation A.38 and equating to unity, we get

$$\int_0^\infty f_z(z)\, dz = \left(\sqrt{\frac{m}{\bar{\gamma}}}\right)^{m-\frac{1}{2}} \frac{\left(\sqrt{\zeta_l}\right)^{m+\frac{1}{2}}}{\left(\sqrt{2}\right)^{m-\frac{3}{2}}\Gamma(m)} \int_0^\infty z^{m-\frac{1}{2}-1} e^{-\sqrt{\frac{2m\zeta_l}{\bar{\gamma}}} z} dz = 1.$$

Applying [10, (3.381.1)] the integration in L.H.S. of Equation A.39 can be solved as

$$\left(\sqrt{\frac{m}{\bar{\gamma}}}\right)^{m-\frac{1}{2}} \frac{\left(\sqrt{\zeta_l}\right)^{m+\frac{1}{2}}}{\left(\sqrt{2}\right)^{m-\frac{3}{2}}\Gamma(m)} \Gamma\left(m-\frac{1}{2}\right) \left(\sqrt{\frac{2m\zeta_l}{\bar{\gamma}}}\right)^{-\left(m-\frac{1}{2}\right)} = 1. \tag{A.39}$$

From Equation A.39, ζ_l can be determined as $\zeta_l = \frac{\left[\Gamma\left(m-\frac{1}{2}\right)\right]^2}{2^{2(m-1)}\left[\Gamma(m)\right]^2}$.

From Equation A.38, the PDF of $\gamma_{egc} = \left(\sum_{l=1}^{L}\sqrt{\gamma_l}\cos(\psi_l)\right)^2 = (z_1+z_2+\ldots+z_L)^2 = y^2$ can be derived in two steps. First, we have to obtain the PDF of $Y = z_1+z_2+\ldots+z_L$, which is the sum of L RVs, using the characteristic function approach followed in [15, Sec. 14.4, Equations (14-4-9)-(14-4-13)]. Then, the PDF of $\gamma_{egc} = y^2$ can be obtained by transformation of RV method. These two steps are used as below:

Characteristic function of z_1 can be given as [55]

$$\begin{aligned}\varphi_{z_1}(\omega) &= \int_0^\infty f_{z_1}(z_1)\, e^{j\omega z_1} dz_1 \\ &= \left(\sqrt{\frac{m}{\bar{\gamma}}}\right)^{m-\frac{1}{2}} \frac{\left(\sqrt{\zeta_l}\right)^{m+\frac{1}{2}}}{\left(\sqrt{2}\right)^{m-\frac{3}{2}}\Gamma(m)} \int_0^\infty z_1^{\left(m-\frac{1}{2}\right)-1} e^{-\left(\sqrt{\frac{2m\zeta_l}{\bar{\gamma}}}-j\omega\right)z_1} dz_1. \end{aligned} \quad \text{(A.40)}$$

The integration in Equation A.40 can be solved by applying [10, (3.381.1)]. Thus, $\phi_{z_1}(\omega)$ can be expressed as

$$\varphi_{z_1}(\omega) = \left(\sqrt{\frac{m}{\bar{\gamma}}}\right)^{m-\frac{1}{2}} \frac{\left(\sqrt{\zeta_l}\right)^{m+\frac{1}{2}}}{\left(\sqrt{2}\right)^{m-\frac{3}{2}}\Gamma(m)} \Gamma\left(m-\frac{1}{2}\right)\left(\sqrt{\frac{2m\zeta_l}{\bar{\gamma}}}-j\omega\right)^{-\left(m-\frac{1}{2}\right)}. \quad \text{(A.41)}$$

Since, z_ls are statistically independent, the characteristic function of $y = z_1+z_2+\ldots+z_L = [\varphi_{z_1}(\omega)]^L$. Hence,

$$\varphi_Y(\omega) = \left(\sqrt{\frac{m}{\bar{\gamma}}}\right)^{L\left(m-\frac{1}{2}\right)} \frac{\left(\sqrt{\zeta_l}\right)^{L\left(m+\frac{1}{2}\right)}\left[\Gamma\left(m-\frac{1}{2}\right)\right]^L}{\Gamma(m)^L\left(\sqrt{2}\right)^{L\left(m-\frac{3}{2}\right)}} \left(\sqrt{\frac{2m\zeta_l}{\bar{\gamma}}}-j\omega\right)^{-L(m-1/2)}. \quad \text{(A.42)}$$

Using the inverse Fourier transform, the PDF of y can be given from formula as

$$f_Y(y) = \frac{1}{2\pi}\int_0^\infty \varphi_y(y)\, e^{-j\omega y} d\omega. \quad \text{(A.43)}$$

Substituting Equation A.42 in Equation A.43 and applying [10, (3.382.7)] to solve the integration

we get

$$f_Y(y) = \left(\sqrt{\frac{m}{\bar{\gamma}}}\right)^{L\left(m-\frac{1}{2}\right)} \frac{\left(\sqrt{\zeta_l}\right)^{L\left(m+\frac{1}{2}\right)}\left[\Gamma\left(m-\frac{1}{2}\right)\right]^L}{\Gamma(m)^L\left(\sqrt{2}\right)^{L\left(m-\frac{3}{2}\right)}} \frac{1}{2\pi}\int_0^\infty e^{-j\omega y}\left(\sqrt{\frac{2m\zeta_l}{\bar{\gamma}}}-j\omega\right)^{-L(m-1/2)} d\omega.$$

$$= \left(\sqrt{\frac{m}{\bar{\gamma}}}\right)^{L\left(m-\frac{1}{2}\right)} \frac{\left(\sqrt{\zeta_l}\right)^{L\left(m+\frac{1}{2}\right)}\left[\Gamma\left(m-\frac{1}{2}\right)\right]^L}{\Gamma(m)^L\left(\sqrt{2}\right)^{L\left(m-\frac{3}{2}\right)}} \frac{y^{L(m-1/2)-1}e^{-\sqrt{\frac{2m\zeta_l}{\bar{\gamma}}}y}}{\Gamma\left[L\left(m-1/2\right)\right]}.$$

The PDF of $\gamma_{egc} = y^2$ can be derived from $f_y(y)$ using transformation of RVs technique as

$$f_{\gamma_{egc}}(\gamma_{egc}) = \left(\sqrt{\frac{m}{\bar{\gamma}}}\right)^{L\left(m-\frac{1}{2}\right)} \frac{\left(\sqrt{\zeta_l}\right)^{L\left(m+\frac{1}{2}\right)}\left[\Gamma\left(m-\frac{1}{2}\right)\right]^L}{(2)^{L\left(\frac{m}{2}-\frac{3}{4}\right)+1}[\Gamma(m)]^L\Gamma\left[L\left(m-1/2\right)\right]} \times \gamma_{egc}^{\frac{L(m-1/2)-2}{2}} e^{-\sqrt{\frac{2m\zeta_l}{\bar{\gamma}}}\gamma_{egc}}. \quad \text{(A.44)}$$

A.8.1 Derivation of Outage Probability of EGC

The outage probability of γ_{egc} can be derived by substituting $f_{\gamma_{egc}}(\gamma_{egc})$ in Equation 2.4

$$P_{out} = \left(\sqrt{\frac{m}{\bar{\gamma}}}\right)^{L\left(m-\frac{1}{2}\right)} \frac{\left(\sqrt{\zeta_l}\right)^{L\left(m+\frac{1}{2}\right)}\left[\Gamma\left(m-\frac{1}{2}\right)\right]^L}{(2)^{L\left(\frac{m}{2}-\frac{3}{4}\right)+1}[\Gamma(m)]^L\Gamma\left[L\left(m-1/2\right)\right]} \times \int_0^{\gamma_{th}} \sqrt{\gamma_{egc}}^{L(m-1/2)-2} e^{-\sqrt{\frac{2m\zeta_l}{\bar{\gamma}}}\sqrt{\gamma_{egc}}} d\gamma_{egc}. \quad \text{(A.45)}$$

Substituting $\sqrt{\gamma_{egc}} = u$, $d\gamma_{egc} = 2udu$ and applying [10, (3.381.1)], the integration in Equation A.45 can be solved. Thus, P_{out} can be given as

$$P_{out} = \left(\sqrt{\frac{m}{\bar{\gamma}}}\right)^{L\left(m-\frac{1}{2}\right)} \frac{\left(\sqrt{\zeta_l}\right)^{L\left(m+\frac{1}{2}\right)}\left[\Gamma\left(m-\frac{1}{2}\right)\right]^L}{(2)^{L\left(\frac{m}{2}-\frac{3}{4}\right)+1}[\Gamma(m)]^L\Gamma\left[L\left(m-1/2\right)\right]} \times \left(\sqrt{\frac{2m\zeta_l}{\bar{\gamma}}}\right)^{-[L(m-1/2)]} \nu\left(mL-1, \sqrt{\frac{2m\zeta_l}{\bar{\gamma}}}\gamma_{th}\right). \quad \text{(A.46)}$$

Applying formula [10, (8.352.1)] to the above equation and simplifying the terms, the outage probability can be expressed as

$$P_{out} = \left[1 - e^{-\sqrt{\frac{2m\zeta_l}{\bar{\gamma}}}\gamma_{th}} \sum_{k=0}^{mL-1} \frac{\left(\sqrt{\frac{2m\zeta_l}{\bar{\gamma}}}\gamma_{th}\right)^k}{k!}\right]. \tag{A.47}$$

A.8.2 Derivation of Average Bit Error Probability

Substituting the obtained PDF of γ_{egc} from Equation A.44 in Equation 3.51, the ABEP can be expressed as

$$\begin{aligned}\bar{P}_e &= \left(\sqrt{\frac{m}{\bar{\gamma}}}\right)^{L\left(m-\frac{1}{2}\right)} \frac{\left(\sqrt{\zeta_l}\right)^{L\left(m+\frac{1}{2}\right)}\left[\Gamma\left(m-\frac{1}{2}\right)\right]^L}{(2)^{L\left(\frac{m}{2}-\frac{3}{4}\right)+1}[\Gamma(m)]^L\Gamma[L(m-1/2)]} \\ &\quad \times \int_0^\infty Q(\sqrt{2\gamma_{egc}})\sqrt{\gamma_{egc}}^{L(m-1/2)-2} e^{\sqrt{\frac{2m\zeta_l}{\bar{\gamma}}}\sqrt{\gamma_{egc}}} d\gamma_{egc}.\end{aligned} \tag{A.48}$$

Substituting $\sqrt{\gamma_{egc}} = u, d\gamma_{egc} = 2udu$ and putting $Q(\sqrt{2\gamma_{egc}}) = \frac{1}{2}\left(1 - \frac{2}{\sqrt{\pi}}\sum_{n=0}^{\infty}\frac{(-1)^n\left(\sqrt{\gamma_{egc}}\right)^{2n+1}}{n!(2n+1)}\right)$, in Equation A.48, we get

$$\begin{aligned}\bar{P}_e &= \left(\sqrt{\frac{m}{\bar{\gamma}}}\right)^{L\left(m-\frac{1}{2}\right)} \frac{\left(\sqrt{\zeta_l}\right)^{L\left(m+\frac{1}{2}\right)}\left[\Gamma\left(m-\frac{1}{2}\right)\right]^L}{(2)^{L\left(\frac{m}{2}-\frac{3}{4}\right)+1}[\Gamma(m)]^L\Gamma[L(m-1/2)]} \\ &\quad \times \int_0^\infty \frac{1}{2}\left(1 - \frac{2}{\sqrt{\pi}}\sum_{n=0}^{\infty}\frac{(-1)^n}{n!(2n+1)}\right) u^{L(m-1/2)+(2n+1)-1} e^{-\sqrt{\frac{2m\zeta_l}{\bar{\gamma}}}u} du.\end{aligned} \tag{A.49}$$

Applying [10, (8.381.4)] to solve the integration in Equation A.49, ABEP can be expressed as

$$\bar{P}_e = \frac{1}{2} - \frac{1}{\sqrt{\pi}}\sum_{n=0}^{\infty}\frac{(-1)^n}{n!(2n+1)}\Gamma(L(m-1/2)+(2n+1))\left(\sqrt{\frac{2m\zeta_l}{\bar{\gamma}}}\right)^{-(2n+1)}.$$

A.9 Derivation of γ_{egc} with Phase Error and CCI - PDF Based Approach

In Equation 3.45, the signal power at the combiner output is given by $E_g^2\left[\sum_{l=1}^{L}\alpha_{l,s}\cos\psi_{l,s}\right]^2$ as shown in Appendix A.2. Total Noise power = N_0E_g as shown in Appendix A.2. Interference signal power at the combiner output is given by $E_g^2\left[\sum_{l=1}^{L}\alpha_{l,s}\cos\psi_{l,i}\right]^2$. Output SINR can be expressed as

$$\gamma_{egc}=\frac{\left[\sum_{l=1}^{2}\sqrt{\gamma}_{l,s}\cos\psi_{l,s}\right]^2}{1+\sum_{i=1}^{N}[\sum_{l=1}^{2}\sqrt{\gamma}_{l,i}\cos\psi_{l,i}]^2}. \tag{A.50}$$

A.9.1 Derivation of PDF of γ_{egc}

From Equation A.50, γ_{egc} can be written as $\gamma_{egc}=\frac{x}{1+z}$. The PDF of γ_{egc} can be derived using formula [25, (8)]

$$f_{\gamma_{egc}}(\gamma_{egc}) = \int_0^{\infty}(1+z)f_x[(1+z)\gamma]f_z(z)dz. \tag{A.51}$$

The PDF of x and z are given by Equation 3.29, Equation 3.30 respectively. Substituting the PDF of x and z in Equation A.51 we get,

$$\begin{aligned}f_{\gamma_{egc}}(\gamma_{egc}) &= \left(\frac{m_i}{N\bar{\gamma}_i}\right)^{m_i-\frac{1}{2}}\frac{\zeta_i^{m_i+\frac{1}{2}}\left[\Gamma\left(m_i-\frac{1}{2}\right)\right]^2}{2^{m_i-\frac{1}{2}}\Gamma(2m_i-1)\left[\Gamma(m_i)\right]^2}\left(\frac{m}{\bar{\gamma}}\right)^{m-\frac{1}{2}}\frac{\zeta^{m+\frac{1}{2}}\left[\Gamma\left(m-\frac{1}{2}\right)\right]^2}{2^{m-\frac{1}{2}}\Gamma(2m-1)\left[\Gamma(m)\right]^2}\\ &\times\int_0^{\infty}(1+z)\left(\sqrt{z}\right)^{2(m_i-1)-1}e^{-\sqrt{\frac{2m_i\zeta_i}{N\bar{\gamma}_i}}\sqrt{z}}\left(\sqrt{(1+z)\gamma_{egc}}\right)^{2(m-1)-1}e^{-\sqrt{\frac{2m\zeta}{\bar{\gamma}}}\sqrt{(1+z)\gamma_{egc}}}dz.\end{aligned} \tag{A.52}$$

Rearranging the terms in A.52,

$$\begin{aligned}f_{\gamma_{egc}}(\gamma_{egc}) &= \left(\frac{m_i}{N\bar{\gamma}_i}\right)^{m_i-\frac{1}{2}}\frac{\zeta_i^{m_i+\frac{1}{2}}\left[\Gamma\left(m_i-\frac{1}{2}\right)\right]^2}{2^{m_i-\frac{1}{2}}\Gamma(2m_i-1)\left[\Gamma(m_i)\right]^2}\\ &\times\left(\frac{m}{\bar{\gamma}}\right)^{m-\frac{1}{2}}\frac{\zeta^{m+\frac{1}{2}}\left[\Gamma\left(m-\frac{1}{2}\right)\right]^2}{2^{m-\frac{1}{2}}\Gamma(2m-1)\left[\Gamma(m)\right]^2}\left(\sqrt{\gamma_{egc}}\right)^{2(m-1)-1}e^{-\sqrt{\frac{2m\zeta}{\bar{\gamma}}}\left(\sqrt{\gamma_{egc}}\right)}\end{aligned}$$

$$\times \int_0^{\infty} (1+z)^{2m-1} \left(\sqrt{z}\right)^{2(m_i-1)-1} e^{-\sqrt{\frac{2m_i\zeta_i}{N\bar{\gamma}_i}}\sqrt{z}} e^{-\sqrt{\frac{2m\zeta\gamma_{egc}}{\bar{\gamma}}}\sqrt{z}} dz. \tag{A.53}$$

Applying Binomial theorem [10, (1.111)], for the term $(1+z)^{2m-1}$ in Equation A.53

$$\begin{aligned} f_{\gamma_{egc}}(\gamma_{egc}) &= \left(\frac{m_i}{N\bar{\gamma}_i}\right)^{m_i-\frac{1}{2}} \frac{{\zeta_i}^{m_i+\frac{1}{2}}\left[\Gamma\left(m_i-\frac{1}{2}\right)\right]^2}{2^{m_i-\frac{1}{2}}\Gamma(2m_i-1)\left[\Gamma(m_i)\right]^2} \\ &\times \left(\frac{m}{\bar{\gamma}}\right)^{m-\frac{1}{2}} \frac{\zeta^{m+\frac{1}{2}}\left[\Gamma\left(m-\frac{1}{2}\right)\right]^2}{2^{m-\frac{1}{2}}\Gamma(2m-1)\left[\Gamma(m)\right]^2} \left(\sqrt{\gamma_{egc}}\right)^{2(m-1)-1} e^{-\sqrt{\frac{2m\zeta}{\bar{\gamma}}}\left(\sqrt{\gamma_{egc}}\right)} \\ &\times \int_0^{\infty} \sum_{k=0}^{2m-1} \binom{2m-1}{k} \left(\sqrt{z}\right)^{2k} \left(\sqrt{z}\right)^{2(m_i-1)-1} e^{-\left(\sqrt{\frac{2m_i\zeta_i}{N\bar{\gamma}_i}}+\sqrt{\frac{2m\zeta\gamma_{egc}}{\bar{\gamma}}}\right)\sqrt{z}} dz. \end{aligned} \tag{A.54}$$

Taking $\sqrt{z}=u$, $dz=2udu$ and applying the integration formula, [10, (3.381.4)] in Equation A.54 we get,

$$\begin{aligned} f_{\gamma_{egc}}(\gamma_{egc}) &= \left(\frac{m_i}{N\bar{\gamma}_i}\right)^{m_i-\frac{1}{2}} \frac{{\zeta_i}^{m_i+\frac{1}{2}}\left[\Gamma\left(m_i-\frac{1}{2}\right)\right]^2}{2^{m_i-\frac{1}{2}}\Gamma(2m_i-1)\left[\Gamma(m_i)\right]^2} \\ &\times \left(\frac{m}{\bar{\gamma}}\right)^{m-\frac{1}{2}} \frac{\zeta^{m+\frac{1}{2}}\left[\Gamma\left(m-\frac{1}{2}\right)\right]^2}{2^{m-\frac{1}{2}}\Gamma(2m-1)\left[\Gamma(m)\right]^2} \left(\sqrt{\gamma_{egc}}\right)^{2(m-1)-1} e^{-\sqrt{\frac{2m\zeta}{\bar{\gamma}}}\left(\sqrt{\gamma_{egc}}\right)} \\ &\times \sum_{k=0}^{2m-1} \binom{2m-1}{k} \Gamma(2(m_i+k)-1) \left(\sqrt{\frac{2m\zeta\gamma_{egc}}{\bar{\gamma}}}+\sqrt{\frac{2m_i\zeta_i}{N\bar{\gamma}_i}}\right)^{-(2(m_i+k)-1)}. \end{aligned}$$

A.9.2 Derivation of Outage Probability of EGC

The outage probability of γ_{egc} can be derived as [25, (8)]

$$P_{out}(\gamma_{th}) = \int_0^{\gamma_{th}} \int_0^{\infty} (1+z) f_x\left[(1+z)\gamma_{egc}\right] f_z(z) dz d\gamma_{egc}. \tag{A.55}$$

The PDF of x and z is given by Equation 3.29, Equation 3.30, respectively. Substituting the PDF of x and z in A.55 we get,

$$P_{out} = \left(\frac{m_i}{N\bar{\gamma}_i}\right)^{m_i-\frac{1}{2}} \frac{{\zeta_i}^{m_i+\frac{1}{2}}\left[\Gamma\left(m_i-\frac{1}{2}\right)\right]^2}{2^{m_i-\frac{1}{2}}\Gamma(2m_i-1)\left[\Gamma(m_i)\right]^2} \left(\frac{m}{\bar{\gamma}}\right)^{m-\frac{1}{2}} \frac{\zeta^{m+\frac{1}{2}}\left[\Gamma\left(m-\frac{1}{2}\right)\right]^2}{2^{m-\frac{1}{2}}\Gamma(2m-1)\left[\Gamma(m)\right]^2}$$

$$\times \int_0^{\infty}\int_0^{\gamma_{th}} (1+z)\left(\sqrt{z}\right)^{2(m_i-1)-1} e^{-\sqrt{\frac{2m_i\zeta_i}{N\bar{\gamma}_i}}\sqrt{z}} \left(\sqrt{(1+z)\gamma_{egc}}\right)^{2(m-1)-1} e^{-\sqrt{\frac{2m\zeta}{\bar{\gamma}}}\sqrt{(1+z)\gamma_{egc}}} dz d\gamma_{egc}. \tag{A.56}$$

Taking the integration part alone in A.56 we have,

$$\int_0^{\infty} (1+z)^{m-\frac{1}{2}} \left(\sqrt{z}\right)^{2(m_i-1)-1} e^{-\sqrt{\frac{2m_i\zeta_i}{N\bar{\gamma}_i}}\sqrt{z}} \int_0^{\gamma_{th}} \left(\sqrt{\gamma_{egc}}\right)^{2(m-1)-1} e^{-\sqrt{\frac{2m\zeta}{\bar{\gamma}}}\sqrt{(1+z)\gamma_{egc}}} d\gamma_{egc} dz. \tag{A.57}$$

Let $\sqrt{\gamma_{egc}} = u, d\gamma_{egc} = 2udu$ and applying [10, (3.381.1)] the integration in Equation A.57 can be solved as

$$\int_0^{\infty} (1+z)^{m-\frac{1}{2}} \left(\sqrt{z}\right)^{2(m_i-1)-1} e^{-\sqrt{\frac{2m_i\zeta_i}{N\bar{\gamma}_i}}\sqrt{z}} \left(\sqrt{\frac{2m\zeta}{\bar{\gamma}}}\right)^{-(2m-1)} \nu\left(2m-1, \sqrt{\frac{2m\zeta(1+z)}{\bar{\gamma}}}\gamma_{th}\right).$$

Applying [10, (8.352.1)] and rearranging the terms outage probability can be expressed as,

$$\begin{aligned} P_{out} &= \left(\frac{m_i}{N\bar{\gamma}_i}\right)^{m_i-\frac{1}{2}} \frac{{\zeta_i}^{m_i+\frac{1}{2}}\left[\Gamma\left(m_i-\frac{1}{2}\right)\right]^2}{2^{m_i-\frac{1}{2}}\Gamma(2m_i-1)\left[\Gamma(m_i)\right]^2} \\ &\times \int_0^{\infty} \left(\sqrt{z}\right)^{2(m_i-1)-1} e^{-\sqrt{\frac{2m_i\zeta_i}{N\bar{\gamma}_i}}\sqrt{z}} \left[1 - e^{-\sqrt{\frac{2m\zeta}{\bar{\gamma}}}\gamma_{th}} \sum_{k=0}^{2m-1} e^{-\sqrt{\frac{2m\zeta z}{\bar{\gamma}}}\gamma_{th}} \frac{\left(\sqrt{\frac{2m\zeta}{\bar{\gamma}}}\sqrt{(1+z)}\gamma_{th}\right)^k}{k!}\right]. \end{aligned} \tag{A.58}$$

Applying the binomial theorem [10, (1.111)] in A.58 we get,

$$\begin{aligned} P_{out} &= \left(\frac{m_i}{N\bar{\gamma}_i}\right)^{m_i-\frac{1}{2}} \frac{{\zeta_i}^{m_i+\frac{1}{2}}\left[\Gamma\left(m_i-\frac{1}{2}\right)\right]^2}{2^{m_i-\frac{1}{2}}\Gamma(2m_i-1)\left[\Gamma(m_i)\right]^2} \int_0^{\infty} \left(\sqrt{z}\right)^{2(m_i-1)-1} e^{-\sqrt{\frac{2m_i\zeta_i}{N\bar{\gamma}_i}}\sqrt{z}} dz \\ &- \int_0^{\infty} e^{-\sqrt{\frac{2m\zeta}{\bar{\gamma}}}\gamma_{th}} \sum_{k=0}^{2m-1} \frac{\left(\sqrt{\frac{2m\zeta}{\bar{\gamma}}}\gamma_{th}\right)^k}{k!} \sum_{l=0}^{k} \binom{k}{l} \left(\sqrt{z}\right)^{2(m_i-1)+2l-1} e^{-\left(\sqrt{\frac{2m_i\zeta_i}{N\bar{\gamma}_i}}+\sqrt{\frac{2m\zeta}{\bar{\gamma}}}\gamma_{th}\right)\sqrt{z}} dz. \end{aligned}$$

Taking $\sqrt{z} = u$, $dz = 2udu$ and applying [10, (3.381.4)] for solving the integration, and rearranging the terms in (A.59) we get,

$$P_{out} = 1 - \left(\frac{m_i}{N\bar{\gamma}_i}\right)^{m_i-\frac{1}{2}} \frac{{\zeta_i}^{m_i+\frac{1}{2}}\left[\Gamma\left(m_i-\frac{1}{2}\right)\right]^2}{2^{m_i-\frac{3}{2}}\Gamma(2m_i-1)\left[\Gamma(m_i)\right]^2}$$

$$\times \sum_{k=0}^{2m-1}\sum_{l=0}^{k}\binom{k}{l}\frac{\left(\sqrt{\frac{2m\zeta}{\bar{\gamma}}}\gamma_{th}\right)^{k}}{k!}e^{-\sqrt{\frac{2m\zeta}{\bar{\gamma}}}\gamma_{th}}\Gamma\left(2\left(m_i+l\right)-1\right)$$
$$\times \left(\sqrt{\frac{2m_i\zeta_i}{N\bar{\gamma}_i}}+\sqrt{\frac{2m\zeta}{\bar{\gamma}}}\gamma_{th}\right)^{-(2(m_i+l)-1)}.$$

A.10 Output SINR of MRC Receiver

On rearranging the terms Equation 4.3 can be rewritten as

$$\begin{aligned} y &= a_s E_g\sqrt{1-\varepsilon^2}\sum_{l=1}^{L}\hat{\alpha}_{l,s}^2 + a_s E_g\sum_{l=1}^{L}\varepsilon\nu\hat{\alpha}_{l,s}^{*}e^{-j\hat{\phi}_{l,s}} \\ &\quad + \sum_{l=1}^{L}n_{0,l}\hat{\alpha}_{l,s}^{*}e^{-j\hat{\phi}_{l,s}} + E_g\sum_{i=1}^{N}\sum_{l=1}^{L}a_i\alpha_{l,i}e^{j\phi_{l,i}}\hat{\alpha}_{l,s}^{*}e^{-j\hat{\phi}_{l,s}}. \end{aligned} \tag{A.59}$$

From Equation (A.59), signal power at the output of MRC can be given as $E_g^2(1-\varepsilon^2)\left(\sum_{l=1}^{L}\hat{\alpha}_{l,s}^2\right)^2$. Since, ν is complex Gaussian with zero mean and unit variance, the total power due to error component is $E_g^2\varepsilon^2\sum_{l=1}^{L}\hat{\alpha}_{l,s}^2$.

Total noise power at the combiner output can be derived as below:

Since, $n_{0,l}$ and $\alpha_{l,s}$ are statistically independent, the total noise power can be given as

$$\begin{aligned} E\left[\left(\int_0^T n_{l,s}(\tau)g_T(\tau)d\tau\right)^2\right] &= E\left[\left(\int_0^T n_{l,s}(\tau)g_T(\tau)d\tau\right)\left(\int_0^T n_{l,s}(t)g_T(t)dt\right)^{*}\right] \\ &= \int_0^T\int_0^T E\left[n_{l,s}(\tau)n_{l,s}^{*}(t)\right]g_T(\tau)\,g_T(t)\,d\tau dt \\ &= N_0\int_0^T g_T^2(t)dt = E_g N_0. \end{aligned} \tag{A.60}$$

Total power due to noise component can be derived as $\sum_{l=1}^{L}\hat{\alpha}_{l,s}^2 N_0 E_g$. Total power due to the interference component is $E_g^2\sum_{i=1}^{N}\sum_{l=1}^{L}\alpha_{l,i}^2\hat{\alpha}_{l,s}^2$.

Instantaneous output SINR can be written as

$$\gamma_{mrc} = \frac{E_g^2\left(1-\varepsilon^2\right)\left(\sum_{l=1}^{L}\hat{\alpha}_{l,s}^2\right)^2}{\varepsilon^2 E_g^2\sum_{l=1}^{L}\hat{\alpha}_{l,s}^2 + \sum_{l=1}^{L}\hat{\alpha}_{l,s}^2 N_0 E_g + E_g^2\sum_{i=1}^{N}\sum_{l=1}^{L}\alpha_{l,i}^2\hat{\alpha}_{l,s}^2}. \tag{A.61}$$

Dividing Equation A.61 by $\sum_{l=1}^{L}\hat{\alpha}_{l,s}^2 N_0 E_g$ the output SINR of MRC receiver is given by

$$\gamma_{mrc} = \frac{\frac{\left(1-\varepsilon^2\right)}{\left(1+\varepsilon^2\right)}\left(\sum_{l=1}^{L}\gamma_{l,s}\right)}{1+\frac{1}{\left(1+\varepsilon^2\right)}\sum_{i=1}^{N}\gamma_{l,i}} = \frac{\eta\left(\sum_{l=1}^{L}\gamma_{l,s}\right)}{1+\beta\sum_{i=1}^{N}\gamma_{l,i}} = \frac{x}{1+z}.$$

where $\eta = \frac{1-\varepsilon^2}{1+\varepsilon^2}$, $\beta = \frac{1}{1+\varepsilon^2}$, $x = \eta\sum_{l=1}^{L}\gamma_{l,s}$ and $z = \eta\sum_{i=1}^{N}\gamma_{l,i}$

A.10.1 Derivation of PDF of x in Section 4.1

Consider $x = \eta\sum_{l=1}^{L}\gamma_{l,s}$. The PDF of x can be derived following the procedure given in [15, (14-4-9)-(14-4-13)]. It is as given below.

The PDF of $\gamma_{l,s}$ can be given as [3, (2.21)]

$$p_{\gamma_{l,s}}\left(\gamma_{l,s}\right) = \left(\frac{m}{\bar{\gamma}_{l,s}}\right)^m \frac{\gamma_{l,s}^{m-1}}{\Gamma(m)}\exp\left(-\frac{m}{\bar{\gamma}}\gamma_{l,s}\right), \gamma \geq 0 \tag{A.62}$$

where $\bar{\gamma}$ is the average SNR. The characteristic function of $\gamma_{l,s}$ can be obtained as below.

$$\begin{aligned}\phi_{\gamma_{l,s}}(j\omega) &= \int_0^\infty \left(\frac{m}{\bar{\gamma}}\right)^m \frac{\gamma_{l,s}^{m-1}}{\Gamma(m)}\exp\left(-\frac{m}{\bar{\gamma}}\gamma_{l,s}\right)e^{j\omega\gamma}d\gamma \\ &= \left(\frac{m}{\bar{\gamma}}\right)^m \frac{1}{\Gamma(m)}\int_0^\infty {\gamma_{l,s}}^{m-1}\exp\left(-\left(\frac{m}{\bar{\gamma}}-j\omega\right)\gamma_{l,s}\right)d\gamma_{l,s} = \frac{\left(\frac{m}{\bar{\gamma}}\right)^m}{\left(\frac{m}{\bar{\gamma}}-j\omega\right)^m},\end{aligned} \tag{A.63}$$

where we used Equation [10, (3.381.4)], to solve the above integration. Using Equation A.63, an expression for characteristic function of $\sum_{l=1}^{L}\phi_{\gamma_{l,s}}(j\omega)$ can be given as

$$\prod_{l=1}^{L}\phi_{\gamma_{l,s}}(j\omega) = \frac{\left(\frac{m}{\bar{\gamma}}\right)^{mL}}{\left(\frac{m}{\bar{\gamma}}-j\omega\right)^{mL}}. \tag{A.64}$$

The PDF of $\sum_{l=1}^{L} \gamma_{l,s}$ can be derived by taking inverse Fourier transform of Equation A.64 as

$$\begin{aligned} f_x(x) &= \frac{1}{2\pi}\int_{-\infty}^{\infty} \phi_{\gamma_{l,s}}(j\omega)\, e^{-j\omega\gamma} d\omega \left(\frac{m}{\bar{\gamma}}\right)^{mL} \int_{-\infty}^{\infty} \left(\frac{m}{\bar{\gamma}} - j\omega\right)^{-mL} e^{-j\omega\gamma} d\omega \\ &= \left(\frac{m}{\bar{\gamma}}\right)^{mL} \frac{\gamma^{mL-1}}{\Gamma(mL)} e^{-\frac{m}{\bar{\gamma}}\gamma}, \end{aligned} \tag{A.65}$$

where we have used the formula [10, (3.382.7)] to evaluate the above integration. Thus, the PDF of $x = \eta \sum_{l=1}^{L} \gamma_{l,s}$ can be derived from A.65 using functions of random variables method [55] and it can be given as

$$f_x(x) = \left(\frac{m}{\bar{\gamma}}\right)^{mL} \left(\frac{1}{\eta}\right)^{mL} \frac{\gamma^{mL-1}}{\Gamma(mL)} e^{-\frac{m}{\bar{\gamma}}\frac{\gamma}{\eta}}. \tag{A.66}$$

A.10.2 Derivation of PDF of γ_{mrc}

Substituting the PDF of x and z from Equations 4.6 and 4.7 in Equation 4.5, the PDF of γ_{mrc} can be expressed as

$$\begin{aligned} f_{\gamma_{mrc}}(\gamma_{mrc}) &= \int_0^{\infty} (1+z) f_x((1+z)\gamma_{mrc}) f_z(z) dz \\ &= \int_0^{\infty} (1+z) \frac{[(1+z)\gamma_{mrc}]^{mL-1}}{\Gamma(mL)} e^{-\left(\frac{m}{\bar{\gamma}}\frac{(1+z)\gamma_{mrc}}{\eta}\right)} \frac{z^{m_i N-1}}{\Gamma(m_i N)} e^{-\left(\frac{m_i}{\bar{\gamma}_i}\frac{z}{\beta}\right)} dz \\ &= \frac{\left(\frac{m}{\eta\bar{\gamma}}\right)^{mL}\left(\frac{m_i}{\beta\bar{\gamma}_i}\right)^{mN}}{\Gamma(mL)\Gamma(m_i N)} \gamma_{mrc}^{mL-1} e^{-\frac{m\gamma_{mrc}}{\bar{\gamma}\eta}} \int_0^{\infty} (1+z)^{mL} z^{m_i N-1} e^{-\left(\frac{m\gamma_{mrc}}{\bar{\gamma}\eta} + \frac{m_i}{\bar{\gamma}_i}\frac{1}{\beta}\right)z} dz. \end{aligned} \tag{A.67}$$

Applying Binomial theorem [10, (1.111)], (reproduced in Equation A.88) to $(1+z)^{mL}$ in Equation A.67 we get

$$f_{\gamma_{mrc}}(\gamma_{mrc}) = \frac{\left(\frac{m}{\eta\bar{\gamma}}\right)^{mL}\left(\frac{m_i}{\beta\bar{\gamma}_i}\right)^{mN}}{\Gamma(mL)\Gamma(m_i N)} \gamma_{mrc}^{mL-1} e^{-\frac{m\gamma_{mrc}}{\bar{\gamma}\eta}} \sum_{k=0}^{mL} \frac{mL!}{k!(mL-k)!} \int_0^{\infty} z^{k+m_i N-1} e^{-\left(\frac{m\gamma_{mrc}}{\bar{\gamma}\eta} + \frac{m_i}{\bar{\gamma}_i}\frac{1}{\beta}\right)z} dz. \tag{A.68}$$

Applying [10, (3.381.4)] in Equation A.68 to solve the integration we get

$$f_{\gamma_{mrc}}(\gamma_{mrc}) = \left(\frac{m}{\eta\bar{\gamma}}\right)^{mL}\left(\frac{m_i}{\beta\bar{\gamma}_i}\right)^{mN} \gamma_{mrc}^{mL-1} e^{-\frac{m\gamma_{mrc}}{\bar{\gamma}\eta}} \sum_{k=0}^{mL} \frac{mL}{(mL-k)!} \binom{k+m_i N}{k} \left(\frac{m\gamma_{mrc}}{\bar{\gamma}\eta} + \frac{m_i}{\bar{\gamma}_i}\frac{1}{\beta}\right)^{k+m_i N}. \tag{A.69}$$

A.10.3 Derivation of Outage Probability of MRC

Rearranging the terms, Equation 4.11 can be rewritten as

$$P_{out}(\gamma_{th}) = \left(\frac{m_i}{\beta\bar{\gamma}_i}\right)^{m_iN}\left(\frac{m}{\eta\bar{\gamma}}\right)^{mL}\frac{1}{\Gamma(m_iN)\Gamma(mL)}\int_0^{\infty}(1+z)^{mL}z^{m_iN-1}e^{-\frac{m_i}{\bar{\gamma}_i}\frac{z}{\beta}}\int_0^{\gamma_{th}}\gamma_{mrc}^{mL-1}e^{-\frac{(1+z)\gamma_{mrc}m}{\eta\bar{\gamma}}}d\gamma_{mrc}dz. \tag{A.70}$$

The integration w.r.t. γ_{mrc} in Equation A.70 can be solved by applying the identity in [10, (3.381.1)]. The resulting expression becomes

$$\begin{aligned}P_{out}(\gamma_{th}) &= \left(\frac{m_i}{\beta\bar{\gamma}_i}\right)^{m_iN}\left(\frac{m}{\eta\bar{\gamma}}\right)^{mL}\frac{1}{\Gamma(m_iN)\Gamma(mL)}\\ &\times\int_0^{\infty}(1+z)^{mL}z^{m_iN-1}e^{-\frac{m_i}{\bar{\gamma}_i}\frac{z}{\beta}}\left[\left(\frac{(1+z)m}{\eta\bar{\gamma}}\right)^{-mL}\nu\left(mL,\frac{(1+z)\gamma_{th}m}{\eta\bar{\gamma}}\right)\right]dz.\end{aligned} \tag{A.71}$$

Applying formula [10, (8.352.1)] (reproduced in Equation A.97), Equation A.71 can be rewritten as

$$P_{out}(\gamma_{th}) = \left(\frac{m_i}{\beta\bar{\gamma}_i}\right)^{m_iN}\frac{1}{\Gamma(m_iN)}\int_0^{\infty}z^{m_iN-1}e^{-\frac{m_i}{\bar{\gamma}_i}\frac{z}{\beta}}\left[1-e^{-\frac{(1+z)\gamma_{th}m}{\eta\bar{\gamma}}}\sum_{k=0}^{mL-1}\frac{\left(\frac{(1+z)\gamma_{th}m}{\eta\bar{\gamma}}\right)^k}{k!}\right]dz. \tag{A.72}$$

Equation A.97 is valid for integer value of mL and L takes only integer values. Hence, Equation A.72 is valid only for integer values of m. Rearranging the terms in Equation A.72, we get

$$\begin{aligned}P_{out}(\gamma_{th}) &= \left(\frac{m_i}{\beta\bar{\gamma}_i}\right)^{m_iN}\frac{1}{\Gamma(m_iN)}\int_0^{\infty}z^{m_iN-1}e^{-\frac{m_i}{\bar{\gamma}_i}\frac{z}{\beta}}dz\\ &-\left(\frac{m_i}{\beta\bar{\gamma}_i}\right)^{m_iN}\frac{1}{\Gamma(m_iN)}\int_0^{\infty}z^{m_iN-1}e^{-\frac{m_i}{\bar{\gamma}_i}\frac{z}{\beta}}e^{-\frac{(1+z)\gamma_{th}m}{\eta\bar{\gamma}}}\sum_{k=0}^{mL-1}\frac{\left(\frac{(1+z)\gamma_{th}m}{\eta\bar{\gamma}}\right)^k}{k!}dz.\end{aligned} \tag{A.73}$$

Applying formula [10, (3.381.1)] (reproduced in Equation A.95) to the first integration and binomial expansion (Equation A.88) to the second integration of Equation A.73, an expression for $P_{out}(\gamma_{th})$ can be given as

$$P_{out}(\gamma_{th}) = 1-\left(\frac{m_i}{\beta\bar{\gamma}_i}\right)^{m_iN}\frac{e^{-\frac{\gamma_{th}m}{\eta\bar{\gamma}}}}{\Gamma(m_iN)}\sum_{k=0}^{mL-1}\sum_{l=0}^{k}\frac{l!\left(\frac{\gamma_{th}m}{\eta\bar{\gamma}}\right)^k}{(k!)^2(l-k)!}\int_0^{\infty}z^{m_iN+l-1}e^{-\left(\frac{m_i}{\beta\bar{\gamma}_i}+\frac{\gamma_{th}m}{\eta\bar{\gamma}}\right)z}dz. \tag{A.74}$$

Applying formula [10, (3.381.1)] (reproduced in Equation A.95) to evaluate the integration in Equation A.74 and rearranging the terms, the closed from expression for P_{out} can be given as

$$P_{out}(\gamma_{th}) = 1-\left(\frac{m_i}{\beta\bar{\gamma}_i}\right)^{m_iN} e^{-\frac{\gamma_{th}m}{\eta\bar{\gamma}}} \sum_{k=0}^{mL-1}\sum_{l=0}^{k}\frac{1}{(k-l)!}\left(\frac{\gamma_{th}m}{\eta\bar{\gamma}}\right)^{k}\binom{m_iN+l-1}{l}\left(\frac{m_i}{\beta\bar{\gamma}_i}+\frac{\gamma_{th}m}{\eta\bar{\gamma}}\right)^{-(m_iN+l)}. \tag{A.75}$$

A.10.4 Derivation of ASEP of MRC

Substituting the pdf of x and z from Equations 4.6 and 4.7 and $Q(\sqrt{2g\gamma_{mrc}}) = \frac{1}{\pi}\int_0^{\frac{\pi}{2}} \exp\left(-\frac{g\gamma_{mrc}}{\sin^2\theta}\right)d\theta$ where a and g are modulation specifying parameters, in Equation 4.14 and rearranging the terms we get

$$\bar{P}_e = \frac{\left(\frac{m}{\eta\bar{\gamma}}\right)^{mL}\left(\frac{m_i}{\beta\bar{\gamma}_i}\right)^{mN}}{\Gamma(mL)\Gamma(m_iN)}\frac{a}{\pi}\int_0^{\infty}\int_0^{\frac{\pi}{2}}(1+z)^{mL}z^{m_iN-1}e^{-\left(\frac{m_i}{\bar{\gamma}_i}\frac{z}{\beta}\right)}\int_0^{\infty}(\gamma_{mrc})^{mL-1}e^{-\left(\frac{g}{\sin^2\theta}+\frac{m}{\bar{\gamma}}\frac{(1+z)}{\eta}\right)\gamma_{mrc}}d\gamma_{mrc}dzd\theta. \tag{A.76}$$

Applying formula [10, (3.381.1)] to solve the integration Equation A.76 and rearranging the terms we get,

$$\bar{P}_e = \frac{\left(\frac{m_i}{\beta\bar{\gamma}_i}\right)^{mN}}{\Gamma(m_iN)}\frac{a}{\pi}\int_0^{\infty}\int_0^{\frac{\pi}{2}} z^{m_iN-1}e^{-\left(\frac{m_i}{\bar{\gamma}_i}\frac{z}{\beta}\right)}\left(\frac{\sin^2\theta}{\sin^2\theta+\frac{g}{c}}\right)^{mL}dzd\theta, \tag{A.77}$$

where $\frac{m}{\bar{\gamma}}\frac{(1+z)}{\eta} = c$. Applying identity $\frac{1}{\pi}\int_0^{\phi}\left(\frac{\sin^2\theta}{\sin^2\theta+\frac{g}{c}}\right)^{mL}d\theta = I\left(\phi,\frac{g}{c},mL\right), -\pi\le\phi\le\pi$ [25], Equation A.77 can be written as

$$\bar{P}_e = \frac{\left(\frac{m_i}{\beta\bar{\gamma}_i}\right)^{mN}a}{\Gamma(m_iN)}\int_0^{\infty} z^{m_iN-1}e^{-\left(\frac{m_i}{\bar{\gamma}_i}\frac{z}{\beta}\right)}I\left(\frac{\pi}{2},\frac{\frac{g\eta\bar{\gamma}}{m}}{(1+z)},mL\right)dz. \tag{A.78}$$

Applying Equations 11, 12 and 13 of [25] the integral in Equation A.78 can be evaluated and the expression for p_e can be obtained as

$$\bar{P}_e = \frac{a}{2}\left[1-\sqrt{\frac{g\eta\bar{\gamma}}{m}}\sum_{k=0}^{mL-1}\sum_{l=0}^{k}\binom{2k}{k}\binom{k}{l}\left(\frac{1}{\beta}\right)^{m_iN}\frac{\Gamma(l+m_iN)}{\Gamma(m_iN)}\left(1+\frac{g\eta\bar{\gamma}}{m}\right)^{m_iN+l-k-\frac{1}{2}}\left(\frac{m_i}{\bar{\gamma}_i}\right)^{m_iN}\right.$$
$$\left.\times\,\Psi\left(l+m_iN,l+m_iN-k+\frac{1}{2},\frac{m_i}{\bar{\gamma}_i\beta}\left(1+\frac{\eta\bar{\gamma}g}{m}\right)\right)\right]. \tag{A.79}$$

A.11 Padé Approximation

Let us consider the expression $M_{\gamma_{egc}}(s) = \sum_{n=0}^{\infty} \frac{1}{n!} E[\gamma_{egc}^n s^n] = \sum_{n=0}^{\infty} \frac{\bar{\gamma}_{egc}^n s^n}{n!}$, which requires infinite number of moments of γ_{egc} to evaluate the series. But in practice, only a finite number of moments can be used to evaluate the series. This can be done by truncating the series as $M_{\gamma_{egc}}(s) \cong \sum_{n=0}^{K} \frac{\bar{\gamma}_{egc}^n s^n}{n!}$, which requires only K number of moments of γ_{egc} for the evaluation.

To obtain the best approximation to $M_{\gamma_{egc}}(s)$, Padé approximation method can be used which is already applied in several fields to approximate series, where practically only few coefficients are known [34]. A Padé approximant is a rational function approximation of a specified order M for the denominator and N for the numerator whose power series expansion agrees with the order of the expansion of $M_{\gamma_{egc}}(s)$. The rational function

$$R_{[N,M]}(s) = \frac{\sum_{i=0}^{N} a_i s^i}{1 + \sum_{i=1}^{M} b_i s^i} \tag{A.80}$$

is said to be the Padé approximant of any series of order $N+M$ [56]. Applying it, $M_{\gamma_{egc}}(s)$ can be approximated as

$$R_{[N,M]}(s) = \frac{\sum_{i=0}^{N} a_i s^i}{1 + \sum_{i=1}^{M} b_i s^i} \cong \sum_{n=0}^{N+M} \frac{\bar{\gamma}_{egc}^n s^n}{n!} \cong \sum_{n=0}^{K} \frac{\bar{\gamma}_{egc}^n s^n}{n!} \tag{A.81}$$

To obtain the Padé approximant $R_{[N,M]}(s)$ to the series we need to find the coefficients $a_i s$ and $b_i s$. Padé approximants are available in most mathematical software packages, such as MATHEMATICA, MATLAB, and MAPLE. In the numerical evaluation of expressions in the thesis work the Padé approximants are evaluated by using MATHEMATICA software.

The manual derivation steps of Padé approximants is explained with an example as given below.

Let us consider the expression

$$g(x) = Cos(x) = 1 - \frac{x^2}{2!} + \frac{x^4}{4!} + \frac{x^6}{6!} + \ldots \tag{A.82}$$

The Padé rational function for $g(x)$ can be given as

$$g(x) \approx R_{[N,M]}(x) = \frac{\sum_{i=0}^{N} p_i x^i}{1 + \sum_{i=1}^{M} q_i x^i} = \frac{P_N(x)}{Q_M(x)} \tag{A.83}$$

where $P_N(x) = \sum_{i=0}^{N} p_i x^i$ is the numerator polynomial and $Q_M(x) = 1 + \sum_{i=1}^{M} q_i x^i$ is the denominator polynomial. Taking $M = N = 4$, we can express $P_N(x) = p_0 + p_1 x + p_2 x^2 + p_3 x^3 + p_4 x^4$ and $Q_M(x) = 1 + q_1 x + q_2 x^2 + q_3 x^3 + q_4 x^4$. We can also write

$$g(x) = 1 - \frac{x^2}{2} + \frac{x^4}{24} - \frac{x^6}{720} + \frac{x^8}{40320} + O[x]^9, \tag{A.84}$$

neglecting all higher order terms than x^8. Further, from Equation A.83 we have

$$\begin{aligned}
& g(x)\,Q_M(x) - P_N(x) = 0 \\
\Rightarrow\ & (1 - p_0) + (-p_1 + q_1)x + \left(-\frac{1}{2} - p_2 + q_2\right)x^2 + \left(-p_3 - \frac{q_1}{2} + q_3\right)x^3 \\
+\ & \left(\frac{1}{24} - p_4 - \frac{q_2}{2} + q_4\right)x^4 + \left(\frac{q_1}{24} - \frac{q_3}{2}\right)x^5 \left(-\frac{1}{720} + \frac{q_2}{24} - \frac{q_4}{2}\right)x^6 \\
+\ & \left(-\frac{q_1}{720} + \frac{q_3}{24}\right)x^7 + \left(\frac{1}{40320} - \frac{q_2}{720} + \frac{q_4}{24}\right)x^8 + O[x]^9 = 0.
\end{aligned} \tag{A.85}$$

In Equation A.85, equating coefficients to zero and solving, we get $p_0 = 1$, $p_1 = 0$, $p_2 = \frac{-115}{252}$, $p_3 = 0$, $p_4 = \frac{-313}{15120}$, $q_1 = 0$, $q_2 = \frac{-11}{252}$, $q_3 = 0$ and $q_4 = \frac{-13}{15120}$. Hence, the Padé approximant for the series $g(x) = Cos(x)$ can be given as

$$R_{4,4}(x) = \frac{15120 - 6900x^2 + 313x^4}{15120 + 660x^2 + 13x^4}. \tag{A.86}$$

The error in the approximation over the interval [-1,1] can be obtained as

$$f(x) - R_{4,4}(x) = Cos(x) - \left(\frac{15120 - 6900x^2 + 313x^4}{15120 + 660x^2 + 13x^4}\right), \tag{A.87}$$

which results in a maximum error of $|f(x) - R_{4,4}(x)| \leq 3.5987 \times 10^{-7}$.

A.12 Padé Approximation Coefficients in the Numerical Evaluation of Equation 2.8 for GG Fading Channels

These coefficients are generated by MATHEMATICA programme.

For $N = 6$, $\rho = 0$, $\bar{\gamma}$ (dB) :

1. $\bar{\gamma} = 0$, order 4/5,

   $a_i = 1, 1.3167s, 0.488059s^2, 0.0392462s^3, 0.000163502s^4,$

   $b_i = 1, 1.93406s, 1.34351s^2, 0.398507s^3, 0.0459701s^4, 0.00151048s^5.$

2. $\bar{\gamma} = 5$, order 4/5,

   $a_i = 1, 4.16377s, 4.88059s^2, 1.24107s^3, 0.0163502s^4,$

   $b_i = 1, 6.11603s, 13.4351s^2, 12.6019s^3, 4.59701s^4, 0.477656s^5.$

3. $\bar{\gamma} = 15$, order 4/5,

   $a_i = 1, 41.6377s, 488.059s^2, 1241.07s^3, 163.502s^4,$

   $b_i = 1, 61.1603s, 1343.51s^2, 12601.9s^3, 45970.1s^4, 47765.6s^5.$

For $N = 10$, $\rho = 0$:

1. $\bar{\gamma} = 0$, order 4/5,

   $a_i = 1, 1.34168s, 0.577437s^2, 0.0807097s^3, 0.00065638s^4,$

   $b_i = 1, 1.65337s, 0.997046s^2, 0.264435s^3, 0.0284041s^4, 0.000719649s^5.$

2. $\bar{\gamma} = 5$, order 4/5,

   $a_i = 1, 4.24277s, 5.77437s^2, 2.55226s^3, 0.065638s^4,$

   $b_i = 1, 5.22842s, 9.97046s^2, 8.36217s^3, 2.84041s^4, 0.227573s^5.$

3. $\bar{\gamma} = 15$, order 4/5,

   $a_i = 1, 53.4133s, 915.175s^2, 5092.44s^3, 1648.75s^4,$

   $b_i = 1, 65.822s, 1580.21s^2, 16684.7s^3, 71347.8s^4, 71964.9s^5.$

A.13 Padé Approximation Coefficients in the Numerical Evaluation of Equation 2.8 for K_G Fading Channels

These coefficients are generated by MATHEMATICA program.

For $N = 6$, $\rho = 0$, $\bar{\gamma}$ in (dB):

1. $\bar{\gamma} = 0$, order 3/4,

   $a_i = 1, 1.19518s, 0.324495s^2, 0.0000161468s^3,$

   $b_i = 1, 1.54936s, 0.750791s^2, 0.122463s^3, 0.0036963s^4.$

2. $\bar{\gamma} = 5$, order 3/4,

   $a_i = 1, 3.77948s, 3.24495s^2, 0.000510606s^3,$

   $b_i = 1, 4.8995s, 7.50791s^2, 3.87262s^3, 0.36963s^4.$

3. $\bar{\gamma} = 15$, order 3/4,

   $a_i = 1, 37.7948s, 324.495s^2, 0.510606s^3,$

   $b_i = 1, 48.995s, 750.791s^2, 3872.62s^3, 3696.3s^4.$

For $N = 10$, $\rho = 0$:

1. $\bar{\gamma} = 0$, order 3/4,

   $a_i = 1, 0.420118s, 0.0400947s^2, 7.01310^{-7}s^3,$

   $b_i = 1, 0.544616s, 0.0927679s^2, 0.00531892s^3, 0.0000564318s^4.$

2. $\bar{\gamma} = 5$, order 3/4,

   $a_i = 1, 1.67252s, 0.635458s^2, 0.000044249s^3,$

   $b_i = 1, 2.16816s, 1.47027s^2, 0.335601s^3, 0.014175s^4.$

3. $\bar{\gamma} = 15$, order 3/4,

   $a_i = 1, 13.2853s, 40.0947s^2, 0.022177s^3,$

   $b_i = 1, 17.2223s, 92.7679s^2, 168.199s^3, 56.4318s^4.$

A.14 Padé Approximation Coefficients in the Numerical Evaluation of Eq. 2.8 for Nakagami-*m* Fading Channels

These coefficients are generated by MATHEMATICA programme.

1. $\bar{\gamma} = 0$, order 4/5,

   $a_i = 1, 0.927982s, 0.152915s^2, 0.0260852s^3, 0.000488809s^4,$

   $b_i = 1, 1.38206s, 0.58773s^2, 0.0583506s^3, 0.00927429s^4, 0.00076702s^5.$

2. $\bar{\gamma} = 5$, order 4/5,

   $a_i = 1, 3.69436s, 2.42355s^2, 1.64587s^3, 0.122783s^4,$

   $b_i = 1, 5.50209s, 9.31489s^2, 3.68167s^3, 2.3296s^4, 0.76702s^5.$

3. $\bar{\gamma} = 15$, order 4/5,

   $a_i = 1, 36.9436s, 242.355s^2, 1645.87s^3, 1227.83s^4,$

   $b_i = 1, 55.0209s, 931.489s^2, 3681.67s^3, 23296.s^4, 76702.s^5.$

A.15 List of Formulas

1.
$$(a+x)^n = \sum_{k=0}^{n} \binom{n}{k} x^k a^{n-k} \tag{A.88}$$

2.
$$\varphi_x(j\omega) = \int_0^{\infty} f_x(x)\, e^{j\omega x} dx \tag{A.89}$$

3.
$$f_x(x) = \frac{1}{2\pi} \int_{-\infty}^{\infty} \varphi_x(j\omega)\, e^{-j\omega x} d\omega \tag{A.90}$$

4.

$$\int_0^\infty x^{n-1}e^{-\beta x}dx = \Gamma(m)\beta^{-n}, n > 0 \tag{A.91}$$

5.

$$\int_{-\infty}^{\infty}(\beta - ix)^{-v}e^{-ipx}dx = \frac{2\pi p^{v-1}e^{-\beta p}}{\Gamma(v)}, p > 0 \tag{A.92}$$

6.

$$y = ax, f_y(y) = \frac{1}{a}f_x\left(\frac{y}{a}\right) \tag{A.93}$$

7.

$$\Gamma(z) = \int_0^\infty e^{-t}t^{z-1}dt \tag{A.94}$$

8.

$$\int_0^u x^{\beta-1}e^{-\mu x}dx = \mu^{-\beta}\nu(\beta,\mu u), \beta > 0 \tag{A.95}$$

9.

$$\nu(\alpha,x) = \int_0^x e^{-t}t^{\alpha-1}dt, \alpha > 1 \tag{A.96}$$

10.

$$\nu(1+n,x) = n!\left[1 - e^x\sum_{m=0}^{n}\frac{x^m}{m!}\right], n = [0,1,\ldots] \tag{A.97}$$

11.

$$\Gamma(x) = (x-1)! \tag{A.98}$$

12.

$$Q(\sqrt{2g\gamma}) = \frac{1}{\pi}\int_0^{\frac{\pi}{2}}\exp\left(-\frac{g\gamma}{\sin^2\theta}\right)d\theta \tag{A.99}$$

13.

$$I_v(z) = \left(\frac{z}{2}\right)^v \sum_{k=0}^{\infty} \frac{\left(z^2/2\right)^k}{k!\Gamma(v+k+1)} \tag{A.100}$$

14.

$$\int_0^{\infty} x^{v-1} e^{-\beta x^2 - \gamma x} dx = (2\beta)^{-v/2} \Gamma(v) \exp\left(\frac{\gamma^2}{8\beta}\right) D_{-v}\left(\frac{\gamma}{\sqrt{2\beta}}\right) [\mathrm{Re}\{\beta\} > 0, \mathrm{Re}\{v\} > 0] \tag{A.101}$$

15.

$$D_p(z) = 2^{\frac{p}{2}} e^{-\frac{z^2}{4}} \left\{ \frac{\sqrt{\pi}}{\Gamma\left(\frac{1-p}{2}\right)} \Phi\left[-\frac{p}{2}, \frac{1}{2}, \frac{z^2}{2}\right] - \frac{\sqrt{2\pi} z}{\Gamma\left(-\frac{p}{2}\right)} \Phi\left[\frac{1-p}{2}, \frac{3}{2}, \frac{z^2}{2}\right] \right\} \tag{A.102}$$

16.

$$y = x^n, f_y(y) = \frac{1}{n} y^{\left(\frac{1-n}{n}\right)} f_x\left(y^{\frac{1}{n}}\right) \quad y > 0 \tag{A.103}$$

17.

$$y = \cos x, f_y(y) = \frac{2}{\sqrt{1-y^2}} f_x(x) \tag{A.104}$$

18.

$$z = xy, f_z(z) = \int_0^{\infty} \frac{1}{x} f_x(x) f_y(z/x) dx \tag{A.105}$$

19.

$$\Gamma(nx) = (2\pi)^{\frac{1-n}{2}} n^{nx-\frac{1}{2}} \prod_{k=0}^{n-1} \Gamma\left(x + \frac{k}{n}\right) \tag{A.106}$$

Bibliography

[1] T. S. Rappaport, *Wireless Communications Principles and Practice*. Prentice Hall, 2007.

[2] G. L. Stuber, *Principles of Mobile Communications*, 2nd ed. Norwell MA: Kluwer Academic Publishers, 2001.

[3] M. K. Simon and M. S. Alouni, *Digital Communication Over Fading Channels: A Unified Approach*. 2nd ed., Wiley, 2005.

[4] M. Nakagami, "The *m*-distribution: A general formula of intensity distribution of rapid fading," *Statistical Methods of Radio Wave Propagation*, pp. 3–36, 1960.

[5] P. S. Bithas, N. C. Sagias, and P. T. Mathiopoulos, "The bivariate generalized-KK_G distribution and its application to diversity receivers," *IEEE Trans. on Commun.*, vol. 57, no. 9, pp. 2655–2662, Sep. 2009.

[6] P. Bithas, N. Sagias, and T. Tsiftsis, "Performance analysis of dual-diversity receivers over correlated generalised Gamma fading channels," *IET Commun.*, vol. 2, no. 1, pp. 174–178, 2008.

[7] E. W. Stacy, "A generalization of the gamma distribution," *Ann. Math. Stat.*, vol. 33, no. 3, p. 1187?1192, Sep. 1962.

[8] N. C. Sagias, G. K. Karagiannidis, P. T. Mathiopoulos, and T. A. Tsiftsis, "On the performance analysis of equal-gain diversity receivers over Generalized Gamma fading channels," *IEEE Trans. Wirel. Commun.*, vol. 5, no. 18, pp. 2967–2975, Oct. 2006.

[9] P. S. Bithas, N. C. Sagias, P. T. Mathiopoulos, G. K. Karagiannidis, and A. A. Rontogiannis, "On the performance analysis of digital communications over Generalized-K fading channels," *IEEE Commun. Lett.*, vol. 10, no. 5, pp. 353–355, Oct. 2006.

[10] I. S. Gradshteyn and I. M. Rhyzik, *Table of Integrals, Series and Products*. San Diego, CA: Academic, 2000.

[11] M. D. Yacoub, "The $\kappa-\mu$ distribution: A general fading distribution," *IEEE Atlantic City Fall Vehicular Technology Conf.*, pp. 1427–1432, Oct. 2001.

[12] ——, "The $\kappa-\mu$ distribution and the $\eta-\mu$ distribution," *IEEE Ant. Prop. Mag.*, vol. 49, no. 1, pp. 68–81, Feb. 2007.

[13] ——, "The $\eta-\mu$ distribution: A general fading distribution," *IEEE Boston Fall Vehicular Technology Conf.*, pp. 872–877, Sep. 2000.

[14] D. G. Bernnan, "Linear diversity combining techniques," *IRE*, vol. 47, pp. 1075–1102, 1959.

[15] J. G. Proakis, *Digital Communications*. Mc-Graw-Hill, 2005.

[16] M. A. Najib and V. K. Prabhu, "Analysis of EGC with partially coherent fading signals," *IEEE Trans. on Veh. Tech.*, vol. 49, no. 3, pp. 783–791, May 2000.

[17] W. Lindsey and C. Chie, *Phase Locked Loops*. IEEE Press, 1986.

[18] A. J. Viterbi, *Principles of Coherent Communication*. Mc-Graw-Hill, 1966.

[19] N. C. Sagias and G. K. Karagiannidis, "Effects of phase error on EGC receivers in correlated Nakagami-*m* fading," *IEEE Commun. Lett.*, vol. 9, no. 7, pp. 580–582, July 2005.

[20] S. A. Rhodes, "Effect of noisy phase reference on coherent detection of offset-QPSK signals," *IEEE Trans. on Commun.*, vol. 22, pp. 1046–1055, Aug. 1974.

[21] M. A. Smadi and V. K. Prabhu, "Performance analysis of generalized-faded coherent PSK channels with equal-gain combining and carrier phase error," *IEEE Trans. on Wireless Commun.*, vol. 5, no. 3, pp. 509–513, Mar. 2006.

[22] N. C. Beaulieu and A. A. Abu-Dayya, "Bandwidth efficient QPSK in cochannel interference and fading," *IEEE Trans. on Commun.*, vol. 43, no. 9, pp. 2464–2474, Sep. 1995.

[23] A. A. Abu-Dayya and N. C. Beaulieu, "Outage probabilities of diversity cellular systems with cochannel interference in Nakagami fading," *IEEE Trans. Veh. Technol.*, vol. 41, no. 4, pp. 343–355, Nov. 1992.

[24] Y. Song, S. D. Blostein, and J. Cheng, "Exact outage probability for equal gain combining with cochannel interference in rayleigh fading," *IEEE Trans. on Wireless. Commun.*, vol. 2, no. 5, pp. 865–870, Sep. 2003.

[25] K. S. Ahn and R. W. Heath, "Performance analysis of maximum ratio combining with imperfect channel estimation in the presence of cochannel interferences," *IEEE Trans. on Wireless Commun.*, vol. 8, no. 3, pp. 1080–1085, Mar. 2009.

[26] Y. Tokgoz and B. D. Rao, "The effect of imperfect channel estimation on the performance of maximum ratio combining in the presence of cochannel interference," *IEEE Trans. on Veh. Tech.*, vol. 55, no. 5, pp. 1527–1534, Sep. 2006.

[27] Z. Hadzi-Velkov, "Level crossing rate and average fade duration of EGC systems with cochannel interference in Rayleigh fading," *IEEE Trans. on Commun.*, vol. 55, no. 11, pp. 2104–2113, Nov. 2007.

[28] A. Shah and A. M. Haimovich, "Performance analysis of maximal ratio combining and comparison with optimum combining for mobile radio communications with cochannel interference," *IEEE Trans. on Veh. Tech.*, vol. 49, no. 4, pp. 1454–1463, Jul. 2000.

[29] P. D. Rahimzadeh and N. C. Beaulieu, "Novel simpler expressions for the BER of MRC BPSK in correlated rayleigh fading and CCI," *IEEE Int. Conf. on Commun.*, pp. 1370 – 1376, May 2008.

[30] J. F. Paris and D. M. Jimenez, "Outage probability analysis for Nakagami-q (Hoyt) fading channels under Rayleigh interference," *IEEE Trans. on Wireless Commun.*, vol. 9, no. 4, pp. 1272–1276, April 2010.

[31] D. M. Jimenez, J. F. Paris, and A. Lozano, "Outage probability analysis for MRC in η-μ fading channels with co-channel interference," *IEEE Commun. Lett.*, vol. 16, no. 5, pp. 674–677, May 2012.

[32] H. Leib and S. Pasupathy, "The phase of a vector perturbed by Gaussian noise and differentially constant receivers," *IEEE Trans. on Information Theory.*, vol. 34, pp. 1491–1501, Nov. 1988.

[33] N. C. Beaulieu and C. Julian, "Precise error rate analysis of bandwidth efficient BPSK to Nakagami fading and co-channel interference," *IEEE Trans. on Wirel. Commun.*, vol. 52, pp. 149–188, jan 2004.

[34] G. K. Karagiannidis, "Moment based approach to the performance analysis of equal gain diversity in Nakagami-*m* fading," *IEEE Trans. on Commun.*, vol. 52, no. 5, pp. 685 – 690, May 2004.

[35] J. R. Mendes, M. D. Yacoub, and G. Fraidenraich, "Closed-form generalized power correlation coefficient of the Hoyt fading signal," *IEEE Commun. Lett.*, vol. 10, no. 2, pp. 94–96, Feb. 2006.

[36] P. Patel, P. R. Sahu, and A. K. Chaturvedi, "ABER of dual predetection EGC in correlated Nakagami-*m* fading channels with arbitrary *m*." *IEEE Commun. Letters*, vol. 12, no. 7, pp. 487–489, Jul. 2008.

[37] D. A. Zogas, G. K. Karagiannidis, and S. A. Kotsopoulos, "Equal gain combining over Nakagami-*n* (Rice) and Nakagami-*q* (Hoyt) generalized fading channels," *IEEE Trans. on Wireless Commun.*, vol. 4, pp. 374–379, Mar. 2005.

[38] G. K. Karagiannidis, D. A. Zogas, , and S. A. Kotsopoulos, "BER performance of dual predetection EGC in correlative Nakagami-*m* fading," *IEEE Trans. on Commun.*, vol. 52, no. 1, pp. 50–53, Jan. 2004.

[39] R. Hoyt, "Probability functions for the modulus and angle of the normal complex variate," *Bell Syst. Tech. J.*, vol. 26, pp. 318–359, 1947.

[40] A. A. Abu-Dayya and N. C. Beaulieu, "Diversity $\pi/4$-dqpsk on microcellular interference channels," *IEEE Trans. on Commun.*, vol. 44, no. 10, pp. 1289–1297, Nov. 1996.

[41] S. Zhang, P. Y. Kam, and P. Ho, "Performance of differentially detected dpsk over nonselective Rayleigh fading channels with maximal ratio combining and multiple cochannel interferers," *IEEE Trans. on Commun.*, vol. 55, no. 1, pp. 133–141, Jan. 2007.

[42] K. Sivanesan and N. C. Beaulieu, "Exact BER analyses of Nakagami/Nakagami CCI BPSK and Nakagami/Rayleigh CCI QPSK systems in slow fading," *IEEE Commun. Lett.*, vol. 8, no. 1, pp. 45–47, 2004.

[43] ——, "Precise bit error rate analysis of bandlimited BPSK with EGC and SC diversity in CCI and Nakagami fading," *Vehicular Technology Conference, 2004. VTC2004-Fall.*, vol. 3, pp. 1811 – 1814, Sept. 2004.

[44] V. A. Aalo and J. Zhang, "Performance analysis of maximal ratio combining in the presence of multiple equal-power cochannel interferers in a Nakagami fading channel," *IEEE Trans. on Veh. Tech.*, vol. 50, no. 2, pp. 497–503, Mar. 2001.

[45] C. Chayawan and V. A. Aalo, "Average error probability of digital cellular radio systems using MRC diversity in the presence of multiple interferers," *IEEE Trans. on Wireless Commun.*, vol. 2, no. 5, pp. 860–864, Sep. 2003.

[46] H. Cramer, *Random Variables and Probability Distributions*. Cambridge: Cambridge Univ. Press, 1970.

[47] A. Goldsmith, *Wireless Communication*. Cambridge Univ. Press, 2005.

[48] P. S. Bithas, P. T. Mathiopoulos, and S. A. Kotsopoulos, "Diversity reception over generalized-k (kg) fading channels," *IEEE Trans. on Wireless Commun.*, vol. 6, no. 12, pp. 4238–4243, December 2007.

[49] A. Annamalai, C. Tellambura, and V. Bhargava, "Equal-gain diversity receiver performance in wireless channels," *IEEE Trans. Commun.*, vol. 48, no. 10, pp. 1732–1745, Oct. 2000.

[50] T. Piboongungon, V. Aalo, C. Iskander, and G. Efthymoglou, "Bivariate generalised gamma distribution with arbitrary fading parameters," *IEE Electronics Lett.*, vol. 41, no. 12, 9th June 2005.

[51] P. S. Bithas, N. C. Sagias, P. T. Mathiopoulos, S. A. Kotsopoulos, and A. M. Maras, "On the correlated K-distribution with arbitrary fading parameters," *IEEE Sig. Proc. Lett.*, vol. 15, pp. 541 – 544, 2008.

[52] A. M. Rabiei, N. C. Beaulieu, and K. Sivanesan, "Cochannel interference whitening receiver designs for BPSK in Nakagami-*m*/Rayleigh fading," *IEEE International Conference on Communication, ICC '07.*, pp. 803 – 808, June 2007.

[53] S. Souissi and E. F. Meihofer, "Performance evaluation of a bluetooth network in the presence of adjacent and co-channel interference," *IEEE Conf. on Emerging Technologies Symposium: Wireless Internet Access Broadband.*, April 2000.

[54] S. Haykin, *Communication Systems*, 4th ed. John Wiley and Sons, India., 2001.

[55] H. Stark and J. Woods, *Probability And Random Processes With Applications To Signal Processing*, 3rd ed. Prentice-Hall, 2002.

[56] H. Amindavar and J. A. Ritcey, "Padé approximations of probability density functions," *IEEE Trans. on Aerospace and Electronic Systems*, vol. 30, no. 2, pp. 416–424, Apr. 1994.

Publications

1. G. Aruna and P. R. Sahu, "ABEP of EGC Receiver over Composite and Non-homogenous Fading Channels with Phase Error and Co-Channel Interference", IETE Journal of Research, vol. 59, no. 5, Sep-Oct 2013.

2. G. Aruna and P. R. Sahu, "Performance Analysis of MRC Receiver with Channel Estimation error and CCI in Nakagami-m Fading Channels",*National Conference on Communications, NCC 2012*, IIT Kharagpur, India.

3. G. Aruna and P. R. Sahu, "ABER of Equal Gain Combiner over Correlated Hoyt Fading Channels with Phase Error and Co-Channel Interference," *Annual IEEE India Conference, Indicon, 2012*, India.